

https://dspace.org/

Limb loading of thrinaxodon liorhinus: postural inference of non-mammaliaform cynodonts

Iqbal, Safiyyah

2019

https://hdl.handle.net/10539/27928

Downloaded from a DSpace repository. https://dspace.org/

EVOLUTIONARY STUDIES INSTITUTE AND SCHOOL OF GEOSCIENCES,
UNIVERSITY OF THE WITWATERSRAND

Limb loading of *Thrinaxodon liorhinus*: postural inference of non-mammaliaform cynodonts

---

A thesis submitted to the Faculty of Science, University of the Witwatersrand, in fulfillment of the requirements for the degree of

DOCTOR OF PHILOSOPHY

in
PALAEONTOLOGY
by

Safiyyah Iqbal

Student Number: 360821

2/5/2019

Supervisors:

Prof. Kristian J. Carlson

Prof. Fernando Abdala

Prof. Frank Kienhofer

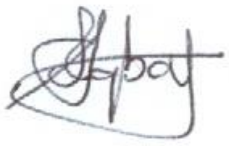
Prof. Jonah Choiniere

DECLARATION

I, Safiyyah Iqbal (Student number: 360821), am a student registered for the doctoral degree in Philosophy (SD000) in the academic year 2015 completing in February 2019 at the University of the Witwatersrand. I herewith submit the following research "Limb loading of *Thrinaxodon liorhinus*: postural inference of non-mammaliaform cynodonts" in fulfilment of the above course requirements.

I hereby declare the following:

- I am aware that plagiarism (the use of someone else's work without their permission and/or without acknowledging the original source) is wrong.
- I confirm that the work submitted for assessment for the above degree is my own unaided work except where I have explicitly indicated otherwise.
- This research has not been submitted before, either individually or jointly, for any course requirement, examination or degree at this or any other tertiary educational institution.
- I have followed the required conventions in referencing the thoughts and ideas of others.
- I understand that the University of the Witwatersrand may take disciplinary action against me if it can be shown that this task is not my own unaided work or that I failed to acknowledge the sources ideas or words in my writing in this research.



Signature: _____ Date: 05 February 2019

Dedication

This PhD is dedicated to my father and mother, who always knew I had the potential to achieve great things in life, who stood by me, motivated and encouraged me in all endeavours. I'm truly blessed to have you both as my foundation and inspiration to be here today. Thank you daddy and mommy for all your eternal support, I could not have completed this without you.

In Loving Memory of My Father

Hoosen Iqbal

13 December 1957

05 January 2018

This PhD would not have been completed if it weren't for my father. I am so grateful that he saw the process of this research through to its completion, offering the support and enthusiasm as each part was concluded. Words fail me when it comes to describing how truly wonderful of a father he was. He gave me the strength, he was the concrete pillar that held me up. He corrected me when I had made mistakes, he stood by me no matter what. He never once allowed me to be disheartened by any of my trials in life. He was always my biggest devotee when it came to my studies. He held my hand as he walked me into Wits on my first day at campus in 2009 and now as I take my final steps as I become a Doctor, he is truly missed and walks with me in heart. No matter how many times I have cried and felt like giving up, he always kept me motivated and passed on the confidence he had in me. Today, I submit this research for and because of you, my daddy. You are forever in my heart and as you look down from heaven, I hope that you are proud of your baby girl.

Because of you, I am me.

Acknowledgments

I sincerely thank my advisors, Prof. Kristian J. Carlson, Prof. Fernando Abdala, Prof. Frank Kienhofer and Prof. Jonah Choiniere for providing unlimited support, assistance, guidance and expertise. Thank you for always believing in me, mentoring and nurturing me into the researcher that I am today. This research was graciously funded by The Palaeontological Scientific Trust (PAST) and its Scatterlings of Africa programmes, Johannesburg, South Africa who has been the major African based funder for my PhD research, the Centre of Excellence (COE) in Palaeosciences and the African Origins Platform (AOP) by the National Research Foundation (NRF). My sincere gratitude goes to Dr. Josep Fortuny, Dr. Jordi Marce-Nogue, Dr. Soledad De Esteban-Trivigno, Prof. Claudia Polese and Miss Taahirah Mangera for their help and assistance with learning and understanding FEA and ANSYS.

I humbly wish to thank my family and friends for always being there during my need. A heart-warming thank you to my best friend, Mrs. Raheema Amiroodeen-Hakimjee for always being there cheering me on. Miss. Kimberleigh Tommy, Miss. Kimberley Chapelle, Miss. Tandi Scott-Turner, Miss. Bronwyn Quinn and Mr. Gerry Germishuizen, without your excitement for me, I'd have lost my mind. I gratefully wish to thank Miss. Sonia Sequeira for her assistance in resolving difficulties in reconstructing the resolution of broken bones, motivating, and encouraging me to not self-doubt my capabilities. My appreciation goes out to Dr. Christine Steininger, Dr. Bonita De Klerk, Dr. Cameron Penn-Clarke and Dr. James M. Neenan for their heartiness talks and support when I felt overwhelmed with my research.

A thank you goes to each and every colleague and friend at the Evolutionary Studies Institute who kept me pushing forward. The curators and collection managers of the following institutions are acknowledged for allowing access to their specimens: APES, DNMNH and ESI. I would also like to thank the University of the Witwatersrand and the Evolutionary Studies Institute for the opportunity to conduct this research.

TABLE OF CONTENTS:

Declaration Page 2
Dedication Page 3
Acknowledgements Page 4
Table of Contents Page 5
List of Figures and Tables Page 7
List of Abbreviations Page 10
Keywords Page 10
Abstract Page 11

CHAPTER 1:
Introduction
1.1. Cynodonts Page 12
1.2. *Thrinaxodon* Page 13
1.3. Functional Gait and Posture Page 16
1.4. Fossorialism Page 17
1.5. Bone Composition Page 18
1.6. Functional Adaptation of Bone Page 19
1.7. Finite Element Analysis Page 19
1.8. Comparative Species Page 22
1.9. Goal, Aim and Hypothesis Page 24
1.9.1. Goal Page 24
1.9.2. Aims Page 25
1.9.3. Hypothesis Page 26
1.10. Significance of Study Page 26

CHAPTER 2:
Materials and Methods
2.1. Materials Page 27
2.2. Methods Page 29
2.2.1. Cross-Sectional Properties Page 31
2.2.2. Body Mass Page 32
2.2.3. Finite Element Analysis
Pre-Process:
2.2.3.1. Model Creation Page 33
2.2.3.2. Mechanical Properties Page 34
2.2.3.3. Mesh Generation Page 35
2.2.3.4. Constraints Page 36

2.2.3.5. Boundary Conditions Page 37
FE Solver:
2.2.3.6. Model Solution Page 39
Post-Process:
2.2.3.7. Hypothesis Confirmation Page 40
2.2.4. Statistical Analysis Page 40

CHAPTER 3:
Results
3.1. FEA Results - Humerus Page 41
3.2. FEA Results - Femur Page 41
3.3. FEA Results - Humerus
3.3.1. Parasagittal Gait Page 42
3.3.2. Semi-Sprawled Gait Page 48
3.3.3. Sprawled Gait Page 54
3.3.3.1. Comparison among gaits Page 60
3.4. FEA Results - Femur
3.4.1. Parasagittal Gait Page 62
3.4.2. Semi-Sprawled Gait Page 68
3.4.3. Sprawled Gait Page 84
3.3.4.1. Comparison among gaits Page 80
3.5. Summary of overall EES and ES Page 82
3.6. Cross-Sectional Properties
3.6.1. Humerus Page 84
3.6.1. Femur Page 88

CHAPTER 4:
Discussion Page 92
4.1. Factors that affect the stress and strain of limb bones Page 93
4.1. Gait and limb posture Page 96
4.1. Hypothesis Confirmation Page 98
4.1. Research Limitations Page 99
4.1. Future Directions Page 100
Conclusion Page 101

References Page102

Appendices Page119

LIST OF FIGURES AND TABLES:

Figure 1.1: Cladogram of cynodont interrelationships Page 14

Figure 1.2: Posture of *Thrinaxodon liorhinus* Page 16

Figure 1.3: FEA diagram Page 22

Figure 1.4: Time-calibrated phylogeny of tetrapods Page 24

Figure 2.1: Cross-sectional measurements Page 32

Figure 2.2: Regions of the applied muscle forces Page 39

Figure 3.1: Strain deformation Page 42

Figure 3.2: Parasagittal humeri - *Thrinaxodon* Page 43

Figure 3.3: Parasagittal humeri - *Cynognathus* Page 44

Figure 3.4: Parasagittal humeri - *Galesaurus* Page 45

Figure 3.5: Parasagittal humeri - *Therocephalia* Page 46

Figure 3.6: Parasagittal humeri - *Tachyglossus* Page 47

Figure 3.7: Semi-sprawled humeri - *Thrinaxodon* Page 49

Figure 3.8: Semi-sprawled humeri - *Cynognathus* Page 50

Figure 3.9: Semi-sprawled humeri - *Galesaurus* Page 51

Figure 3.10: Semi-sprawled humeri – *Therocephalia* Page 52

Figure 3.11: Semi-sprawled humeri - *Tachyglossus* Page 53

Figure 3.12: Sprawled humeri - *Thrinaxodon* Page 55

Figure 3.13: Sprawled humeri - *Cynognathus* Page 56

Figure 3.14: Sprawled humeri - *Galesaurus* Page 57

Figure 3.15: Sprawled humeri - *Therocephalia* Page 58

Figure 3.16: Sprawled humeri - *Tachyglossus* Page 59

Figure 3.17: EES and ES for comparative gaits by species humeri Page 61

Figure 3.18: Parasagittal femora - *Thrinaxodon* Page 63

Figure 3.19: Parasagittal femora - *Cynognathus* Page 64

Figure 3.20: Parasagittal femora - *Galesaurus* Page 65

Figure 3.21: Parasagittal femora - *Therocephalia* Page 66

Figure 3.22: Parasagittal femora - *Tachyglossus* Page 67

Figure 3.23: Semi-sprawled femora - *Thrinaxodon* Page 69

Figure 3.24: Semi-sprawled femora - *Cynognathus* Page 70

Figure 3.25: Semi-sprawled femora - *Galesaurus* Page 71

Figure 3.26: Semi-sprawled femora – *Therocephalia* Page 72

Figure 3.27: Semi-sprawled femora - *Tachyglossus* Page 73

Figure 3.28: Sprawled femora - *Thrinaxodon* Page 75

Figure 3.29: Sprawled femora - *Cynognathus* Page 76

Figure 3.30: Sprawled femora - *Galesaurus* Page 77

Figure 3.31: Sprawled femora - *Therocephalia* Page 78

Figure 3.32: Sprawled femora - *Tachyglossus* Page 79

Figure 3.33: EES and ES comparative gaits models for each species femora Page 81

Figure 3.34: Limb differentiation EES and ES comparative gaits for each species; Humeri scaled to the maximum magnitude of 1.72e-3. Femora scaled to the maximum magnitude of 1.56e-3 Page 83

Figure 3.35: sLn I_x and sLn I_y - Humerus Page 85

Figure 3.36: I_x/I_y and I_{max}/I_{min} - Humerus Page 86

Figure 3.37: sLn J and J/2 - Humerus Page 87

Figure 3.38: sLn I_x and sLn I_y - Femur Page 89

Figure 3.39: I_x/I_y and I_{max}/I_{min} - Femur Page 90

Figure 3.40: sLn J and J/2 - Femur Page 91

Table 2.1: Sample composition and length measurements Page 28

Table 2.2: Scan parameters Page 30

Table 2.3: Species BM and bone geometry mesh of the humeri and femora Page 36

Table 2.4: Muscle forces Page 38

Table 3.1: Size-standardized cross-sectional properties of humeri at 50% region of interest Page 87

Table 3.2: Size-standardized cross-sectional properties of femora at 50% region of interest Page 91

Appendix A1: Cross-sections of species humeri at 50% diaphyseal length Page 119

Appendix A2: Cross-sections of species femora at 50% diaphyseal length Page 119

Appendix A3: Loading parameters for species humeri Page 120

Appendix A4: Loading parameters for species femora Page 120

Appendix B: Parasagittal, semi-sprawled and sprawled humerus Page 121

Appendix C: Parasagittal, semi-sprawled and sprawled femur Page 124

Appendix D: Kruskal-Wallis Page 127

LIST OF ABBREVIATIONS

.ply	–	Polygon File Format
.stl	–	Stereolithography
AD	–	*mm. Adductor Muscles*
AN	–	*m. Anconeus*
AOP	–	African Origins Platform
AP	–	Anteroposterior
APES	–	School of Animal, Plant and Environmental Sciences
BM	–	Body Mass
CAD	–	Computer-Aided Design
CSA	–	Cross-Sectional Area
DD	–	Directional Deformation
DNMNH	–	Ditsong National Museum of Natural History
EES	–	Equivalent Elastic Strain
ES	–	Equivalent Stress
ESI	–	Evolutionary Studies Institute
ESRF	–	European Synchrotron Radiation Facility
FCR	–	*m. Flexor carpi radialis*
FCU	–	*m. Flexor carpi ulnaris*
FEA	–	Finite Element Analysis
FEM	–	Finite Element Model
GM	–	*mm. Gluteal Muscles*
GRF	–	Ground Reaction Force
J	–	Polar Moment of Area
LD	–	*m. Latissimus dorsi*
microCT	–	Micro-Computed Tomography
ML	–	Mediolateral
MS	–	Mean Squares
NRF	–	National Research Foundation
PAST	–	Palaeontological Scientific Trust
PE	–	*m. Pectoralis*
SM	–	*m. Semimembranous*
SS	–	*m. Subscapularis*
S.Sq	–	Sum of Squares
TD	–	Total Deformation
v	–	Poisson's Ratio
VI	–	*m. Vastus intermedius*
VL	–	*m. Vastus lateralis*
VM	–	*m. Vastus medialis*

Keywords: Finite Element Analysis, Loading Conditions, Mechanical Properties, Posture, Stress/Strain.

Abstract

Therapsids were severely affected by the Permian-Triassic mass extinction event, resulting in the survival of only a few lineages. One of these lineages, Cynodontia, includes one of the best known non-mammaliaform transitional fossil taxa, *Thrinaxodon liorhinus*. This species is significant for understanding the evolution of the therapsids which ultimately gave rise to mammals, because of its combination of primitive and derived traits. Complete, fossilized skeletons of *Thrinaxodon* are abundant in the South African Karoo Basin, permitting accurate reconstruction of their limbs. Although much is known about posture in extant mammal groups, fundamental questions remain about the postures of their closest extinct relatives, including Cynodontia. The goal of this research is to better understand *Thrinaxodon* limb functional morphology using a combination of limb bone cross-sectional properties and finite element analyses (FEA) of limb bone structural competency. I hypothesized that, because of its transitional phylogenetic position, stylopodial elements (i.e., humeri and femora) of *Thrinaxodon* are better adapted structurally to resist loading associated with semi-sprawled postures rather than loading associated with sprawled or parasagittal postures during gait. I also tested this hypothesis in *Cynognathus*, *Galesaurus*, *Tetracynodon darti*, *Glanosuchus macrops* and *Tachyglossus*. The FEA results show that as *Thrinaxodon*'s posture is experimentally altered from sprawled to parasagittal, stress and strain increase in its humerus. Cross-sectional properties of limb bones revealed that the femora experienced higher anteroposterior (AP) stress and strain. Together, these results suggest that the humerus is structurally optimised for a sprawled to semi-sprawled posture, showing that *Thrinaxodon* retained a reptilian skeletal configuration in the forelimb, paired with a more derived, incipiently parasagittal posture in the hind limb. These *Thrinaxodon* limb loading and cross-sectional results corroborate other external morphological evidence of semi-sprawled postures in the forerunners of mammals. My results do not preclude the capacity of *Thrinaxodon* to dynamically adopt fully sprawling or parasagittal postures for a short of time, but do indicate that these postures were suboptimal and likely not habitually used. This difference in

posture between the forelimbs and the hind limbs is widespread across the therapsid lineage and may reflect shared functional demands of specific behaviours. FEA presents an independent means for palaeontologists to conduct explicit hypothesis testing in a comparative framework. Here, I were able to use it to test what postural transitions were occurring in some of the closest extinct relative of mammals.

CHAPTER 1

Introduction

Cynodonts

The Early Triassic, between 252.2 and 247.2 million years ago, represents an age of deep transformation on Earth. The Permian-Triassic extinction event killed nearly 95% of all marine genera and 70% of land species (Sues and Fraser 2010). Therapsids ('mammal-like reptiles') represented the majority of the large-bodied terrestrial vertebrate fauna during the Permian, and were severely affected by the extinction event such that only a few lineages were able to persist. Among these therapsids, were the non-mammaliaform cynodonts (Figure 1.1), that first appeared in the Late Permian and survived the Permian-Triassic mass extinction event (Botha and Smith 2006; Abdala and Ribeiro 2010). This clade underwent its main diversification during the Middle Triassic and is widely considered a transitional lineage that ultimately gave rise to mammals (Kemp 2005). Evincing their reptilian ancestry, the forelimbs and pectoral girdle in cynodonts are adapted for a semi-sprawling position (Romer 1922; Blob 2001). Several key mammalian characters, including morphological and functional aspects of the postcranium, are thought to have initially evolved in this lineage (Jenkins 1971; Liu and Olsen 2010). These modifications of the postcrania include: a gait transition from a sprawled to a parasagittal posture; the atlas-axis complex to allow movement of the cranium; expansion of the rib cage; emergence of the complete scapula with the loss of the coracoids portion of the scapulocoracoid; and functionality of four

trochanters on the femur; among other features (Broom 1903; Romer 1924; Evans 1939; Howell 1941; Boonstra 1965; Hoffstetter and Gasc 1969; Jenkins 1971; Kemp 1980, 2005; Iqbal *et al*. in prep).

In extinct taxa, behavioural patterns are generally no longer observable. In these situations, morphological correlates in living taxa are critical to testing paleobiological hypotheses of behaviour in the earliest mammals, and their forerunners. These questions are useful for understanding several aspects of the organisms: how fossil taxa survived harsh climates (e.g., their response to arid regions), diversification among species (e.g., fulfilling different types of niches), fossorialism, evolutionary aspects of key characteristics (e.g., inner-ear, postcanine dentition, secondary palate) and locomotor efficiency with changes in gait (Crompton and Jenkins 1973; Botha and Chinsamy 2005; Botha *et al*. 2005; Luo 2007; Fernandez *et al*. 2012; Oliveira and Schultz 2015; Iqbal *et al*. in prep). Many therapsids across independent lineages adopted fossorialism at this time of ecosystem upheaval, and researchers have hypothesized that it was an excellent survival strategy to cope with unfavourable habitat conditions. As burrowing is common today, even in the most primitive mammals (e.g., platypus), it seems likely that the early mammalian condition evolved from at least a semi-fossorial therapsid ancestor. Thus, studying the morphofunctional aspects of taxa associated with this transition can address this hypothesis.

Thrinaxodon

The Early Triassic cynodont *Thrinaxodon*, which is particularly abundant in the Karoo Basin, is considered as representing an intermediate stage (Crompton 1968; Crompton and Jenkins 1973; Hopson and Crompton 1969). Because of its abundance and generally good preservation in the fossil record, this taxon has been well-studied (Parrington 1936; Crompton 1963; Jenkins 1971; Gow 1985; Damiani *et al*. 2003; Botha and Chinsamy 2005; Smith and Botha 2005; Butler 2009; Abdala *et al*. 2013; Jasinoski *et al*. 2015; Iqbal *et al*. In prep). The initial postcranial description of *Thrinaxodon* was published in a monograph sixty-two years ago (Brink 1956), which remains influential on more recent assessments of the postcranium of cynodonts (such as Jenkins 1971). Accurately reconstructing limb posture in

Thrinaxodon is crucial, as the taxon appears to manifest a transitional change from a sprawling posture, as represented in basal pelycosaurs, to a more erect parasagittal posture, as represented in extant mammals (Parrington 1933; Brink 1958; Jenkins 1971; Iqbal *et al*. in prep). Integrating early descriptive techniques and current practices, will aid in accomplishing an extensive sequence that best describes the development in these prehistoric organisms.

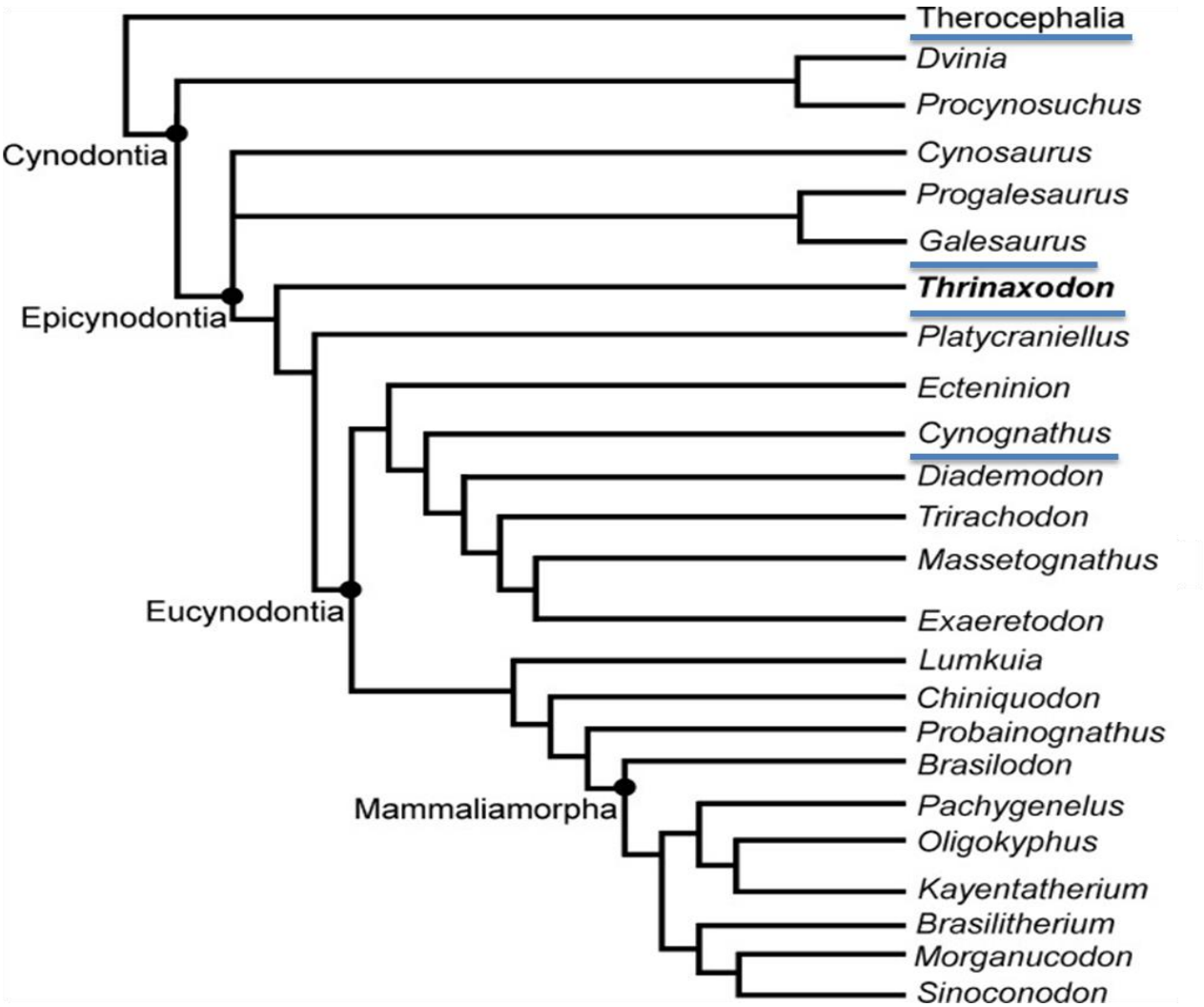


Figure 1.1: Cladogram of cynodont interrelationships. The cynodonts included in the research are underlined in blue. Two therocephalian are also part of the study. (Figure adapted from Jasinoski *et al*. 2015).

Transitional posture attributed to cynodonts is thought to include a semi-sprawled forelimb posture (Figure 1.2). Limb differentiation observed in fossil and extant animals is a response to selective functional causes. *Thrinaxodon* exhibited forelimb versus hind limb differentiation likely due to a fossorial lifestyle that required dominant usage of the forelimb in burrowing (Iqbal *et al*. In prep). For example, in cynodonts, the proximal and distal ends of the humerus are expanded laterally, which functions primarily to support and stabilise the body during locomotion (Kemp 1980). Lateral expansions of the proximal and distal ends of limb bones increase muscle attachment areas for forelimb flexors and extensors that support the body above the ground, e.g., resist gravitational forces that collapse joints (Kardong 2009; Iqbal *et al.* in prep). Hind limb modifications favour parasagittal locomotor modes with increased speed (Kemp 1978, 1980). Hip musculature of cynodonts is enlarged and accompanies a reduced angulation of the femur in order to promote hind limb adducted postures underneath the body, which is hypothesized to be a selective consequence of the change in posture from sprawling to parasagittal gait (Kemp 1980). Functional differentiation of the forelimb and hind limb appeared to be prominent in cynodonts, specifically in *Thrinaxodon*. This differentiation gave cynodonts a selective advantage by increasing mobility of the pectoral and pelvic girdles compared to girdles of other clades during the Permian-Triassic era (Lai *et al.* 2017).

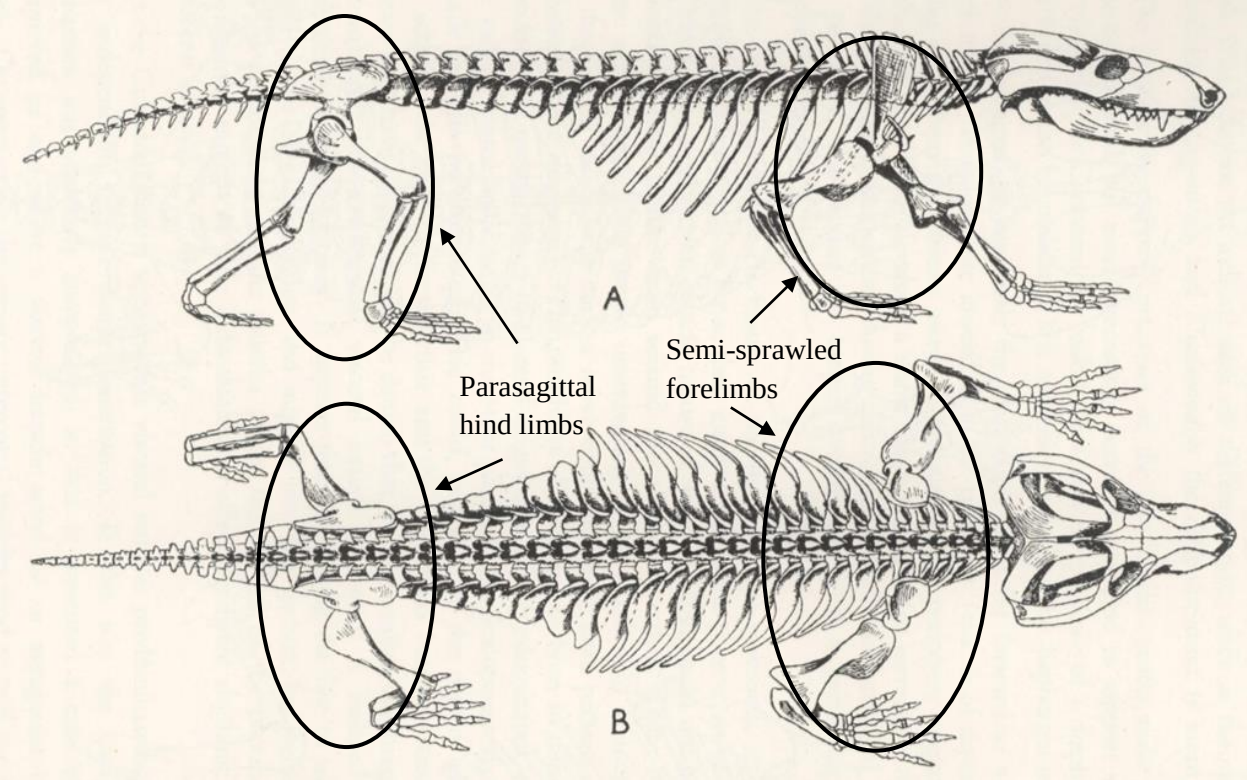


Figure 1.2: Posture of *Thrinaxodon liorhinus* A: Right lateral view and B: Dorsal view (Figure adapted from Brink 1956).

Functional Gait and Posture Variation

Functional gait and limb posture are defined by the degree of adduction and abduction of the humerus. Thus, a sprawled posture is represented by the humerus being abducted and positioned approximately in a horizontal plane during the stance phase, while in the semi-sprawled posture the humerus is only semi-abducted (i.e., oriented at an angle of 45˚ from the sagittal plane). Parasagittal posture includes the propodial of the limb positioned in an orientation relatively more beneath the body (Blob 2001), i.e., adducted into an approximately vertical plane. Sprawling and parasagittal postures have been considered by some scholars as evidence of ectothermy versus endothermy, respectively (Heath 1968; Bakker 1971; Bennett and Ruben 1986), but due to the semi-sprawled postures of therapsids, there is uncertainty as to whether they are ectothermic or endothermic (Bennett and Ruben 1986).Sprawling

gaits provide good mediolateral stability while maintaining a low-rise posture and low centre of gravity (Blob 2001). Conversely, parasagittal gaits decrease mediolateral stability and raise the centre of gravity, which increases the mechanical efficiency of the limb that allows for powerful force generation during an increase in velocity and longer distance travel, and decreases bending moments of the humerus and femur compared to those typically experienced during sprawled gaits (Biewener 1989; Christiansen and Paul 2001). There have been observations on postural variation within extant taxa dependent upon the speed and environment of the species (Reilly and Blob 2003). This postural variation among tetrapods, requires change in the limb muscle attachment angle (Reilly and Elias 1998; Reilly and Blob 2003). Research conducted by Kubo and Benton (2009), documents the change in posture from fossil trackways between the Permian and Triassic periods. Fossil trackways provide evidence of the size of footprints and the stride length that would allow for comparisons between sprawled vs. parasagittal posture (Wilson 2005), as well as offering insight into quadrupedal biomechanics related to changes in step widths.

Fossorialism

A study on burrow dimensions led previous researchers (e.g., Damiani *et al.* 2003) to infer a more parasagittal posture in *Thrinaxodon*'s hind limb. However, burrow dimensions could have been altered after their use during diagenesis of the trace fossil, for example. Thus, morphology of the limb bones and limb postural configurations, which are important in transmitting locomotor stresses (Biewener 1989),should only be cautiously based on the size of the preserved burrow that species inhabited during life (Iqbal *et al*. in prep).Morphology exhibited by *Thrinaxodon* forelimbs has been described as reflecting semi-sprawled posture (Jenkins 1971; Reilly and Delancey 1997; Damiani *et al.* 2003; Botha and Chinsamy 2005; Iqbal *et al*. in prep), while the hind limbs have been described as reflecting parasagittal posture (Jenkins 1971; Kemp 1980). Thus, the limb posture of *Thrinaxodon* suggests a combination of primitive and derived traits should be evident in the limb bones. Improving current understanding of the structural basis for inferring limb posture of *Thrinaxodon* will offer more authoritative insight into the

transition from sprawling to parasagittal gaits, particularly in the lineage that led to mammals (Jenkins 1971; Blob 2001; Van Valkenburgh and Jenkins 2002).

Bone composition

Strength of a bone is characterised by its shape, size and the material properties (Martin 1991). Mechanical loads that are applied to bone are expressed as cyclic stress (Carter 1987) namely compression, tension, and shear, while combinations of these loads are introduced during torsion and bending (Bankoff 2007). Modelling of bone becomes complicated as material properties differ within and between bones of an individual species (Saha and Hayes 1974; Abdel-Wahab *et al*. 2011; Dzialo 2012). The work of Wolff formulated the law that bone will adapt to the mechanical force that is applied to it (Prendergast and Huiskes 1995). This has become known as 'Wolff's Law", or more recently as bone functional adaptation (Ruff *et al*. 2006; Ruff and Larson 2014). Bone structural design can be divided according to the mechanical (e.g., structural support, locomotion), biological (e.g., protection), and chemical and physiological factors (e.g., homeostasis) experienced by an organism (Rho *et al*. 1998; Olesiak *et al*. 2007).

Consideration of different structural scales of bone allows a more thorough understanding of the factors influencing material properties of bone. These include macrostructure (cortical and trabecular bone), microstructure (osteons and Haversian system), sub-microstructure (lamella), nanostructure (fibrillar collagen) and the sub-nanostructure (molecular constituents) levels that makes bone heterogeneous and anisotropic (Rho *et al*. 1998). When mechanically modelling bone, simplifying assumptions, such as a homogenous continuum within material properties (i.e., isotropic material), are required.

Functional Adaptation of Bone

The structure of vertebrate bones is complex and adapts to the loading conditions to which it is subjected (Martin 1991). Functional adaptation of bone relies on its response to the external (e.g., ground reaction forces) and internal (e.g., muscle forces) loading regimes that affect morphology and in turn reflect function (Habib and Ruff 2008; Su 2011). By this modification in limb bone morphology, the locomotor signal can be inferred. Therefore, a relationship exists between bone morphology and the behaviour of species (Habib and Ruff 2008). This relationship is particularly useful in inferring behaviours to fossil taxa where behaviour can no longer be observed. Strain regimes experienced by bone in response to *in vivo* loading have been investigated on extant species (Blob and Biewener 1999, 2001; Biewener and Taylor 1986; Gills and Biewener 2001). There have been numerous studies conducted on functional adaptations in therapsid limbs that have proven to be useful for reconstructing their locomotion (Eaton 1962; Gow 1997; Kemp 2005, 2006), whereas there has been less focus on the inferred stress and strain experienced by the limb of these therapsids (Blob 2001).Bone histology has proven to be useful in understanding functional adaptation (Chinsamy 1997), however, recent studies conducted with medical-CT, micro-CT and synchrotron image data have demonstrated an effective non-invasive alternative method of analysing internal structure of limb bones. Moreover, the images provide data for a digital tool, such as finite element analysis (FEA), to successfully estimate and quantify bone loading regimes. Inference of functional adaptation of bone using evidence generated by this newly adopted approach can be used to address similar questions in complementary types of studies.

Finite Element Analysis

FEA is a computational technique that models mechanical behaviour of materials (Richmond *et al.* 2005; Kupczik 2008; Bright and Rayfield 2011; Young *et al.* 2012). The application of FEA in biological sciences was established after the technique was accepted in engineering (Brekelmans *et al*. 1972). As the practical technique of FEA proved to be a success in orthopaedic biomechanics, theoretical

research was cultivated in assessing the role of skeletal stress and development (Huiskes and Hollister 1993; Beaupre and Carter 1992). This method is regularly used in engineering disciplines, and has recently been adopted in palaeontology to assess questions about biomechanical function of organisms (Bouza-Rodrigueza and Miramontes-Sequeiros 2014). This technique allows for a broad-scale evolutionary assessment, functional and adaptive significance of skeletal morphology (Brassey 2014) and comparative analysis with extant taxa in palaeontology (Kupczik 2008; Hohn-Schulte 2010; Tamvada 2014). FEA is a non-invasive method that permits exploring different behavioural characteristics of structures, including stress and strain patterns that are experienced in the musculoskeletal system (Fortuny *et al*. 2015). Applying FEA to models of biological systems promotes a deeper understanding between the form and function of organisms because it can be used as a sufficient proxy for challenging experimental approaches (e.g., quantifying bone strain).

FEA has three integral phases that consist of the pre-process, the solution and the post-process (Figure 1.3). FEA methodology uses a numerical examination that divides the structure into discrete elements that are connected by nodes and comprise a mesh (Prendergast and Huiskes 1995; Kupczik 2008; Hodgson 2015). The pre-processing phase involves converting a computer-aided design (CAD) into a finite element model (FEM). The FEM must reflect complexity of the actual element but still be simple enough for appropriate digital manipulation (Rayfield 2007). In the pre-processing phase, complexity of the models and the computing time required to produce the most accurate results has to be considered. The defined material properties i.e., Young's modulus (elasticity of the material), Poisson's ratio and density, as well as loads and forces that are applied to the nodes of the element, produce a deformation calculated in the solution phase that in turn results in an estimate of the stress and strain of the material (Rayfield 2007; Kupczik 2008). The elastic modulus, Young's modulus, illustrates the strain a structure experiences in response to the stress loading axially onto it, while the Poisson's ratio describes the tension or compression the structure is subjected to (Blake 1990; Tamvada 2014). Material properties of bone differ depending upon the direction of assessment, permitting bone to be tested as anisotropic or

orthotropic in elasticity (Rayfield 2007). Directly testing the elasticity of bone, however, allows for the FEM to be processed as isotropic. A more comprehensive study has yet to be conducted on the effects of modelling more complex bone elasticity parameters on the resulting FEMs. Each node has x, y, and z coordinates in virtual space from which the change in position (i.e., displacement and deformation) is established (Richmond *et al.* 2005). FEA solves for the displacements at the nodes by converting stress-strain differential equations into a set of linear equations (Panagiotopoulou *et al.* 2012).The output result is von Mises stress (equivalent stress) and von Mises strain (equivalent elastic strain), which are functions of principal stresses and strains that assess the deformation (i.e., directional deformation and total deformation) a material undergoes when exposed to external and internal loads (Rayfield 2007). The most precise deduction of fracture location is possibly von Mises stress and deformations (Marce-Nogue *et al*. 2011; Fortuny *et al*. 2015). The von Mises yield criterion calculates the yield of ductile materials by conjecture that tension and compression are equal in strength. The post-process phase entails the interpretation of reconstructed stress, strain and deformation that the structure/materials experiences (Rayfield 2007; Young *et al.* 2012).

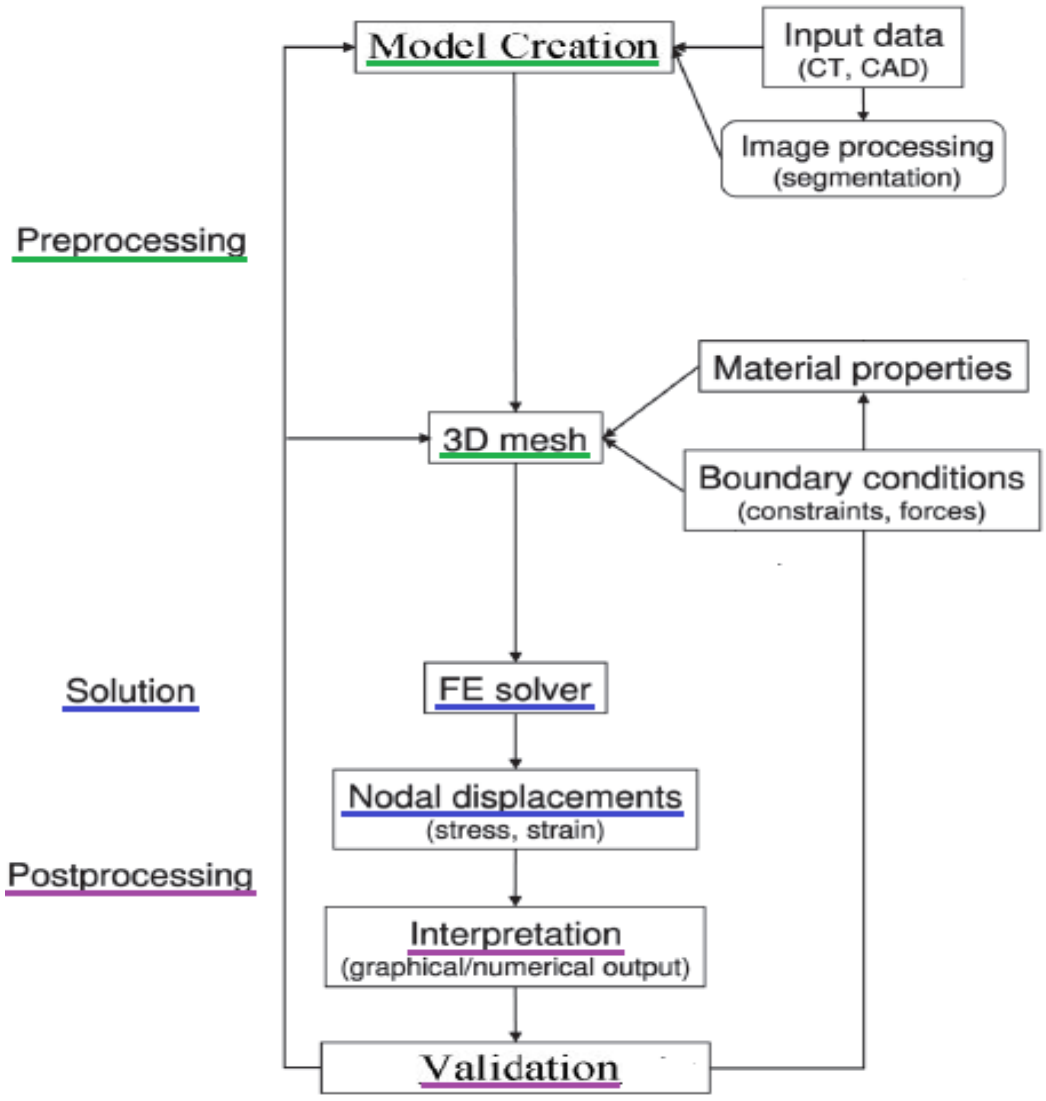


Figure 1.3: FEA diagram of the steps involved (Figure adapted from Kupczik 2008).

Comparative Species

Thrinaxodon liorhinus humeri and femora were analysed and compared with those of a basal cynodont, *Galesaurus*, and a large-bodied cynodont, *Cynognathus*, as well as multiple Therocephalia species, including the basal Therocephalia *Glanosuchus macrops* and *Tetracynodon darti* (Figure 1.4). *Galesaurus* is a common taxon in the Early Triassic that was an active burrower according to its limb morphology (Butler 2009). *Cynognathus* was a large carnivorous, cursorial cynodont that was also common during the Early Triassic (Solomon *et al*. 2011). Therocephalia species existed during the

Middle Permian to Middle Triassic (Fourie and Rubidge 2009; Sigurdsen *et al*. 2012; Huttenlocker and Botha-Brink 2014) and exhibit physical evidence of functional differentiation of forelimbs and hind limbs (Kemp 1986; Frobisch 2006). By comparison, studies emphasizing extant taxa, and conducted on long bone morphology, propose that the posture and locomotor behaviour of the monotreme *Tachyglossus* (Echidna) is roughly analogous to that of cynodonts in terms of limb postures and musculoskeletal anatomies (Peters *et al*. 1984; Erickson *et al*. 2002). Therefore, the biomechanical context (Erickson *et al*. 2002; Rowe *et al*. 2011) that establishes loading conditions of the limbs in this extant monotreme is used in the present study to serve as a living functional analog (i.e., proxy)against which the extinct taxa can be evaluated.

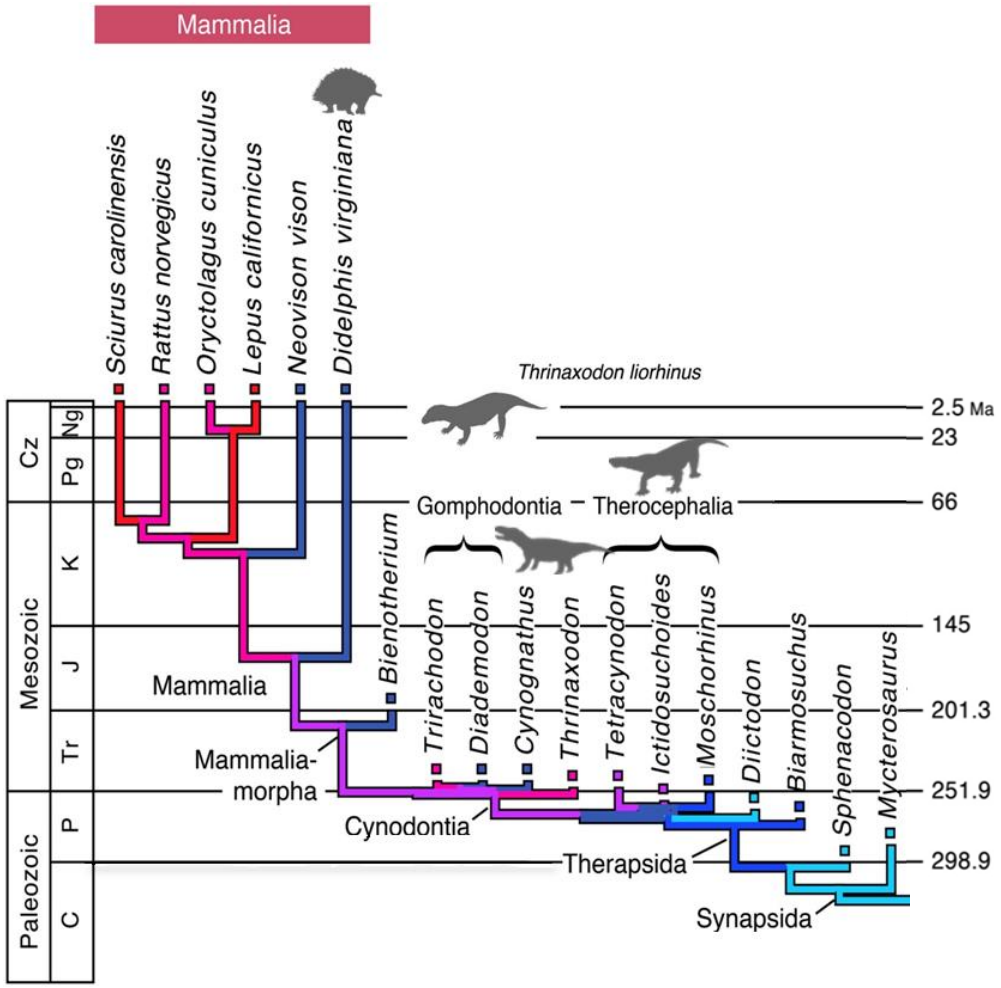


Figure 1.4: Time-calibrated phylogeny of tetrapods including: *Thrinaxodon*, *Cynognathus* and the therocephalian *Tetracynodon*. Abbreviations are as follows: C-Carboniferous, Cz-Cenozoic, J -Jurassic, K-Cretaceous, Ng-Neogene, P-Permian, Pg-Paleogene, Tr-Triassic (Figure adapted from Huttenlocker and Farmer 2017).

Goal, Aim and Hypothesis

Goal

Mechanical loads that are applied to bone diaphyses over time influence bone properties and in turn solicit bone functional adaptations. The extent to which these functional adaptations indicate structural optimization in *Thrinaxodon* limb bone diaphyses for one type of limb posture versus another

has not been documented. The main goal of this project is to test hypotheses about reconstructed limb postures in the fossil mammalian forerunner that have been based on descriptive and qualitative assessments of morphology thus far. New evidence revealing the likely postural configuration and gait of *Thrinaxodon* (or non-mammaliaform cynodonts more broadly-speaking) will help deepen current understanding of the origin of mammalian posture. The project will use FEA to quantify and assess structural optimization of humeral and femoral bones in response to different loading conditions associated with sprawling, semi-sprawling and parasagittal gaits. The proposed research will build on previous work by Iqbal *et al*. (in prep), which was the first attempt to use geometric morphometric analyses of long bone surfaces to assess the extent of digging adaptations in the forelimb of *Thrinaxodon*. Specifically, by incorporating a structural analysis of internal properties (e.g., cross-sectional geometry) combined with mechanical modelling of limb bone diaphyses through FEA, the present study will contribute to more accurate reconstructions of habitual limb postures and use during the habitual locomotion of these extinct taxa.

Aims

1. Determine the mechanical response (strain and stress distribution) experienced by the humerus in the forelimb of *Thrinaxodon* for the following postural configurations: parasagittal, semi-sprawling and sprawling limb postures.
2. Determine the mechanical response (strain and stress distribution) experienced by the femur in the hind limb of *Thrinaxodon* for the following postural configurations: parasagittal, semi-sprawling, and sprawling limb postures.
3. Relate the above mechanical responses occurring in individual proximal limb segment bones to overall limb morphology and purported behavioural activity patterns (e.g., fossorial vs. non-fossorial).
4. Compare *Thrinaxodon* mechanical responses in overall limb morphology to those of other cynodonts (i.e., *Cynognathus* and *Galesaurus*) and in therocephalian (i.e.,

Glanosuchus and *Tetracynodon darti*) overall limb morphology in order to identify optimized postural configurations, particularly in *Thrinaxodon*.

5. Relate configurations of selected modern analog taxa (e.g., *Didelphis* and *Tachyglossus*) to prevailing ideas about cynodont gait, and to the evolution of parasagittal limb postures/gaits in order to understand the extent to which *Thrinaxodon* limbs may be structurally optimised for a sprawling and/or semi-sprawling posture.

Hypotheses

Thrinaxodon humeral cross-sectional properties and biomechanical behaviour are optimised (most effective implementation of the posture under the measurable loading conditions) for semi-sprawled posture. Its hind limb posture is optimized for parasagittal postural loading.

Significance of the Study

This research is the first biomechanical study using FEA on the postcrania of *Thrinaxodon* and broadly-speaking, it is one of the first applications in therapsid research in general. This multidisciplinary research incorporates methodologies from Palaeontology and Mechanical Engineering. It emphasizes the application of FEA in studying the functional morphology of fossils. The project explores loading conditions of remodelled skeletal elements associated with different locomotor postures. Stress and strain that occur on humeral and femoral diaphyses, as well as the capability of limb morphology to withstand externally-induced stresses that arise by a particular postural configuration, are compared. This provides robust quantitative evidence for the type of limb posture that may have characterized these intermediate grade non-mammalian therapsids as limb structure transitioned from reptilian to mammalian in form. It also provides evidence of the extent to which gait kinematic flexibility is structurally possible in these extinct taxa. Ultimately, these insights into the functional morphology of these taxa allow interpretations of particular traits as adaptations to their palaeobiology (i.e., habitats and preferred niches).

CHAPTER 2

Materials and Methods

Materials

Humeral and femoral elements were included for *Thrinaxodon liorhinus* (specimen BP/1//1/7199 found in burrow cast BP/1//1/ 5558) (n = 4); *Cynognathus* (n=1); *Galesaurus* (n = 3); and the therocephalians, *Glanosuchus* and *Tetracynodon darti* (n=2).The humerus and femur of the extant taxon, *Tachyglossus* were analysed for comparison with the fossil taxa. Fossils representing all 11 of these individuals are housed at the Evolutionary Studies Institute, University of the Witwatersrand. Due to the challenges associated with acquiring high resolution image data from specimens from other collections, and the varying thresholds that were required for sufficient segmentation, only a limited set of fossil taxa were under investigation. Moreover, certain specimens that were suitable for the study (TM 171, BP/1/4637, BP/1/2820 and BP/1/2294) (Table 2.1) did not contain sufficient image contrast to allow for a reliable separation of bone from the surrounding sediment.

Table 2.1: Sample composition and length measurements for the species under investigation at the ESI.

Category	Taxon	*Specimen number	Behavioural Category	Skeletal elements	Length (mm)	Circumference (mm)
Cynodont	*Thrinaxodon liorhinus*	BP/1/7199	Fossorial	Humerus	35.41	17.497
				Femur	37.92	16.973
Cynodont	*Thrinaxodon liorhinus*	BP/1/1693	Fossorial	Humerus	41.85	20.451
				Femur	43.42	17.193
Cynodont	*Thrinaxodon liorhinus*	BP/1/1730	Fossorial	Humerus	41.73	17.298
				Femur	45.33	17.385
Cynodont	*Cynognathus*	BP/1/1675	Non-fossorial	Humerus	101.12	50.242
				Femur	193.38	72.211
Cynodont	*Galesaurus*	BP/1/4506	Fossorial	Humerus	56.57	29.022
				Femur	62.85	22.918
Therocephalia	*Tetracynodon darti*	BP/1/4335	Non-fossorial	Humerus	57.62	17.813
				Femur	69.52	18.055
Therocephalia	*Glanosuchus macrops*	BP/1/6228	Non-fossorial	Humerus	119.52	35.21
				Femur	121.86	48.426
Monotreme	*Tachyglossus*	Echidna	Fossorial	Humerus	44.13	38.166
				Femur	47.61	28.688

Methods

Biomechanically relevant features of limb bones include their size, shape, loading conditions and material properties (Erickson *et al*. 2002). Fossilized limb bones of the specimens under investigation (except *Thrinaxodon* BP/1/7199) were scanned using the Nikon Metrology XT H 225 LC microCT scanner located in the Evolutionary Studies Institute (ESI) at the University of the Witwatersrand (www.wits.ac.za/microct) (see Table 2.1 for specimen-specific scan parameters). One *Thrinaxodon liorhinus* specimen (BP/1/ 7199) was scanned at the European Synchrotron Radiation Facility (ESRF proposal EC-847, France, Grenoble) on ID 17 beamline using a monochromatic beam 96 keV, isotropic voxels of 45.5 microns, and 4000 projections (Fernandez *et al*. 2013; Iqbal *et al*. In prep). This particular specimen was synchrotron scanned in order to improve the quality and contrast by reducing the noise ratio without decreasing spatial resolution (Fernandez *et al*. 2013).

Table 2.2: Scan parameters that were used to microCT scan species under investigation at the ESI.

Category	Taxon	*Specimen number	Tube voltage (kV)	Tube current (µA)	Projections	Isotropic voxel size (micron)
Cynodont	*Thrinaxodon liorhinus*	BP/1/7199	96		4000	45.5
Cynodont	*Thrinaxodon liorhinus*	BP/1/1693	130	175	2000	77
Cynodont	*Thrinaxodon liorhinus*	BP/1/1730	140	155	2000	38
Cynodont	*Thrinaxodon liorhinus*	TM 171**	140	150	1000	499
Cynodont	*Cynognathus*	BP/1/1675	135	135	2000	109.8
Cynodont	*Galesaurus*	BP/1/4637**	145	130	3142	49.9
Cynodont	*Galesaurus*	BP/1/2820**	130	175	2000	76
Cynodont	*Galesaurus*	BP/1/4506	140	155	2000	59
Therocephalia	*Tetracynodon darti*	BP/1/4335	140	145	2000	63.2
Therocephalia	*Ictidosuchops intermedius*	BP/1/2294**	135	135	2000	79
Therocephalia	*Glanosuchus macrops*	BP/1/6228	135	135	2000	114.2
Monotreme	*Tachyglossus*	Echidna	70	120	2000	52.1

* ESI (BPI): Evolutionary Studies Institute at the University of the Witwatersrand (South Africa); DNMNH (TM): Ditsong National Museum of Natural History (South Africa); APES: Animal, Plant and Environmental Sciences

** Specimens that were scanned, but not analysed due to insufficient contrast between the embedded bone and surrounding matrix.

In order to create sufficient individual renderings, acquired image data (i.e., TIFF stacks) were imported into VG Studio Max 3.0 (Volume Graphics, Heidelberg, Germany), and/or Avizo 9.0 (VSG, Merignac, France). Elements that remained *in situ* and/or in contact with other elements were digitally

extracted or separated using VG Studio Max 3.0. This process involved segmentation using the region growing tool to highlight voxel data of interest. Once these regions of interest (ROIs) were extracted, the resulting digital elements were smoothed out. These ROI's were then exported as TIFF stacks and imported into Avizo 9.0 to create either an .stl or .ply (surface) file that were used to obtain images of the midshaft (50%) cross-section.

Cross-sectional properties

Cross-sectional properties are calculated to determine mechanical characteristics of bone in a given section (Marchi and Tarli 2004). They are known to exhibit allometric relationships with body size (Lieberman *et al*. 2004). The scale for cross-sectional images were obtained using ImageJ v1.50i and analysed using the plugin; BoneJ v1.4.2 was used to calculate properties (Doube *et al*. 2010) from each image at 50% diaphyseal length (Table 3.1; Appendix A1-A2). The mid-point (i.e., 50%) of diaphyseal length is where the largest bending loads theoretically exist in a beam that is loaded from either end (Lieberman *et al*. 2004). The following standard cross-sectional properties were acquired from each cross-section (Figure 2.1): Cortical Area (CA), second moments of area about anteroposterior (AP: I_x) and mediolateral (ML: I_y) axes, principal moments of area (I_{max}, I_{min}) (Carlson 2014; Iqbal 2015; Iqbal *et al.* in prep), and section moduli (Z_x, Z_y, Z_{min}, Z_{max}). Note that CA is cortical thickness of the diaphysis, which differs from the circumference measurement of the diaphyseal external dimension (Figure 2.1). The AP and ML axes on each cross-sectional image were oriented with established anatomical position of the humerus and femur being determined beforehand, thus allowing for meaningful comparisons of the I_y and I_x properties across individuals. The polar moment of area (J), was calculated as the sum of I_{max} and I_{min}. Cross-sectional properties (I_y, I_x, I_{max}, I_{min} and J) were size-standardised by natural logging the variable divided by the length of the humerus (for humeri) and by the length of the femur (for femora) to the fourth power (Eq. 1):

$$\left[\ln\left(\frac{\text{variable}}{\text{length}^4}\right)\right] \qquad \text{Eq. 1(Table 3.1)}$$

Diameters of the cross-section (i.e., AP and ML) were calculated using the orientation option in ImageJ.

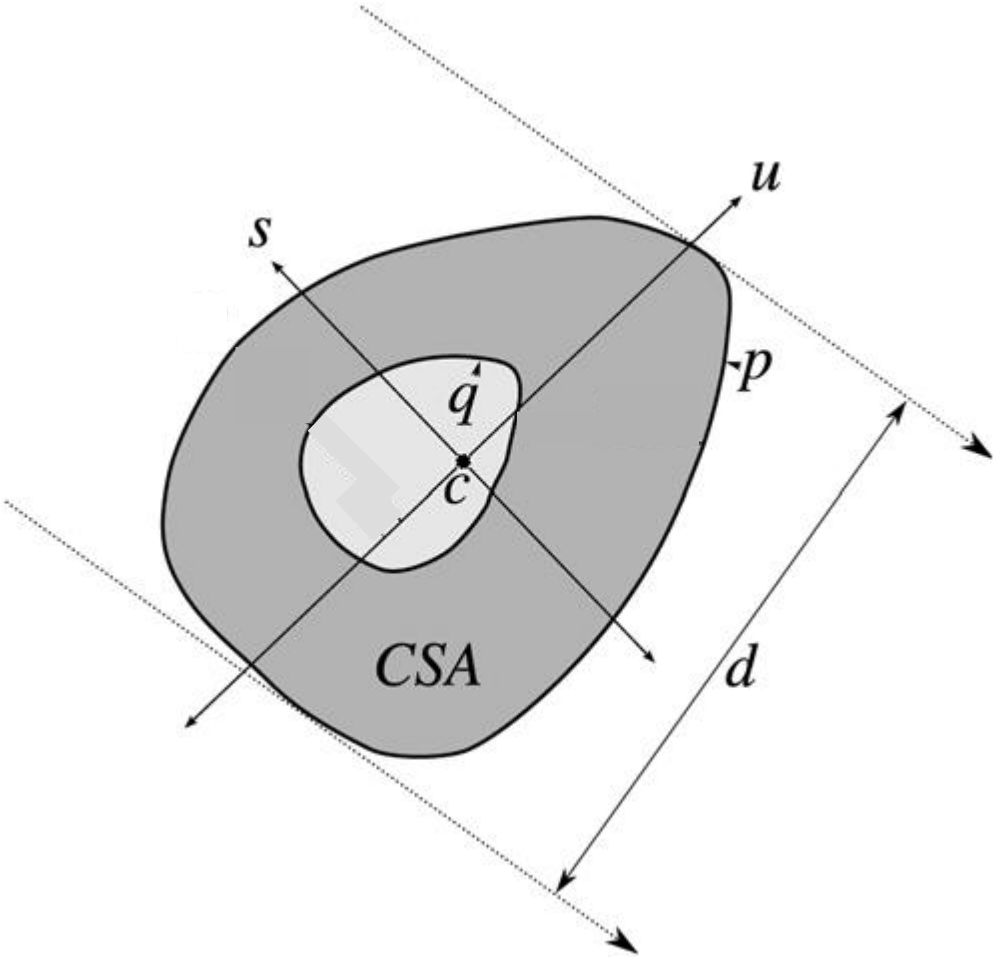


Figure 2.1: Cross sectional measurements: c – centroid, u and s – major and minor principal axes, p and q – outer and inner perimeters, CSA – cross sectional area, and d – diameter (Figure adapted from Doube *et al*. 2009).

Body Mass

One of the essential biological properties that are associated with the physiological and ecological aspect of an individual is Body Mass (BM). These relationships may aid in understanding the palaeobiology of fossil species that is inferred by estimating BM. As BM increases in an evolving

lineage, anatomical and physiological dimensions change (Biewener 1983). A different rate of change in a parameter compared to the rate of change in BM is called allometry. A higher rate of change in the parameter is defined as positive allometry (Schmidt-Nielsen 1975; Casinos *et al*. 1993). Conversely, a lower rate of change in the parameter is defined as negative allometry (Casinos *et al*. 1993; Dial *et al.* 2008). If the rate of change is the same in parameter and BM, it is defined as isometry. The average BM of a fossil species was calculated using the phylogenetic correlation scaling equation derived by Campione and Evans (2012).

$$\text{Log BM} = 2.754 - \log C_{h+f} - 1.097 \qquad \text{Eq. 2 (Table 2.2)}$$

Where C_{h+f} is the total humeral and femoral circumference and the circumference measurement refers to only the external dimension of the diaphysis. By log transforming BM, this will reduce the effect of outliers and simplify the numerical data (Campione and Evans 2012).

Finite Element Analyses

Pre-Process: Model Creation

Prior to cleaning the models, the medullary cavity and cortical bone of a humerus or femur must be separated. Modelling trabecular bone becomes difficult when assigning material properties to each individual region of the internal structure (Martin 1991). Thus, the internal structure of bone is modelled to be included as part of the external structure (cortical area) such that only the morphology of the cortical bone is analysed (Martin 1991). In other words, due to computational limitations in modelling precise structure of trabecular bone, and the focus of the study being diaphyseal properties, proximal and distal articular ends of these limb bone elements were modelled as solids (i.e., trabecular bone regions were treated as solids). This is accomplished by filling in the gaps in trabecular bone to produce a complete solid bone (Tamvada 2014). After generating bone renderings in Avizo, they were cleaned in MeshMixer (Autodesk research, Inc., United States of America) and imported into Geomagic Studio 14.0 (CAD

software, 3D Systems, Inc. Geomagic Solutions, USA). The cleaning process created .sat files where each skeletal surface was meshed with fewer triangles, and all surface holes were patched and spurious triangles were deleted. Further mesh adjustments included aligning displaced nodes, and reducing triangles in order to reduce the node count while still retaining the accurate3D morphology of the bone.

Once suitable models were produced, they were imported into ANSYS Inc. 18.0 (FEA software, ANSYS, Canonsburg, PA) to assess the deformation, stress and strain response. Constraints (e.g., joint movements and limb kinematics) and external forces (e.g., gravitational forces and local stresses placed on the object at muscle attachment sites) were estimated for the FEA modelling by assuming comparability of *Canis familiaris* (Greyhound, Williams *et al*. 2008), *Didelphis virginiana* (Virginia opossum, Gosnell 2010), *Scalopus aquaticus* (Mole, Rose *et al*. 2013) and *Ambystoma tigrinum* (Tiger salamander, Kawano *et al*. 2016) as living analogues. The suitability of these extant analogues was largely because of their featured roles in extensive research in parasagittal, semi-sprawled and sprawling gaits, respectively. There is a significant amount of experimental data that exist for bone loading conditions on the posture and gait of these extant species (Peters *et al*. 1984; Ross 2005; Jiang 2007; Spiers *et al.* 2007; Rayfield 2007; Kupczik 2008; Rhee *et al.* 2009; Zysset *et al.* 2013). There have been additional FEA studies compiled with alligators (*Alligator mississippiensis*) and lizards (*Iguana iguana*) (Blob and Biewener 1999; Ross 2005; Padian *et al*. 2010), although these are not homologous to the specimens under investigation.

Pre-Process: Mechanical Properties

These properties determine mechanical usage of the remodelled bone during activity (Martin 1991). Due to the change in bone composition, fossil material properties are defined as inorganic materials. Histological research on extinct species has shown relatively similar material properties that can be observed in extant species, which established relatively similar characteristics (Reilly and Burnstein 1975; Chinsamy 1997; Christiansen and Paul 2001; Erickson *et al*. 2002; Olesiak *et al*. 2007;

Rayfield 2007; Young *et al*. 2012). This relationship is based on the study by Witmer (1995) who stated that there must be phylogenetic characteristics that can be inferred from extant taxa to extinct taxa in addition to having a correlation with the osteological structure (Erickson *et al*. 2002). Therefore, extant species are used as a proxy for material properties when investigating fossil taxa in order to apply FEA to the biomechanical features of extinct species.

Material properties of bovine bones have been shown to resemble those of certain sauropod dinosaurs (Reilly and Burnstein 1975; Reid 1996; Moreno *et al*. 2006; Young *et al*. 2012). These properties include modelling the fossil as: isotropic, density = 1.895 kg/m^3, Young's modulus (elastic - E) = 10 000 MPa, Poisson's ratio (v) = 0.4 (Moreno *et al*. 2006). Research based on directly testing the material properties of bone (Reilly and Burstein 1975) rendered it isotropic in the transverse plane. Isotropic material properties are assumed in a simplification of bone models since bone composition is nonhomogeneous, i.e., trabecular bone is anisotropic while cortical bone is transversely isotropic (Bankoff 2012). However, this simplification in the modelling of bone enables its application (Strait *et al*. 2005; Vignoli and Kenedi 2016; Sheng *et al*. 2017), thus, allowing for a general and broad interpretation of the results obtained. These mechanical properties are determined for the standing phase of locomotion.

Pre-Process: Mesh Generation

Models exported from Geomagic Studio initially consisted of 400 000 triangles, which acted as a framework for mesh generation in ANSYS. This framework was subjected to an adaptive, patch conforming method of tetrahedrons that was comprised of a number of elements and nodes (Table 2.2).

Table 2.3: Species body mass and bone mesh of the humeri and femora.

Species	Species Number	Body Mass (g)	Elements (Humeri)	Nodes (Humeri)	Elements (Femora)	Nodes (Femora)
Thrinaxodon liorhinus	BP/1/1693	1748	264418	406217	191 603	297 352
Thrinaxodon liorhinus	BP/1/1730	1395	459013	708123	344 184	532 407
Thrinaxodon liorhinus	BP/1/7199	1371	200316	308594	482 703	748 254
Cynognathus	BP/1/1675	45006	167 408	251 567	115 378	180 005
Galesaurus planiceps	BP/1/4506	4241	382882	589081	606 283	930 704
Glanosuchus macrops	BP/1/6228	15750	664432	1022506	790 617	1 214 543
Tetracynodon darti	BP/1/4335	1530	388965	599261	387 594	598 562
Tachyglossus sp.	Echidna	8500	223028	342585	893 282	1 367 298

Pre-Process: Constraints

External applied forces used in models were calculated according to estimated body mass (Eq. 2). Fixed supports were applied (Appendix A3-A4), as a distribution over an area of 3 mm, to the condyle attachments (joints) on the proximal and distal ends of each bone to stabilise the geometry in virtual space (Figure 2.2). The humeri and femora head were fixed in virtual space at an angle of 20˚ relative to the body for the parasagittal gait, whereas for the semi-sprawled gait the angle was increased to 45˚ and for the sprawled gait the angle was at 60˚ (Blob 2001). All three angles were with respect to the vertical and

anteroposterior sagittal plane. These fixed supports imitate the actual biological joint system of the glenohumeral joint of the humerus and the femoral/acetabular joint of the femur. Compression support was performed on the geometry to account for the ground reaction force (GRF).

Pre-Process: Boundary Conditions

Loading data (Williams *et al*. 2008, 2008; Gosnell 2010; Rose *et al*. 2013; Kawano *et al*. 2016) consisted of muscle contractile forces applied at precise muscle origins (output of force) and insertions (input of force) (Figure 2.2; Appendix A3-A4) on humeri and femora (Table 2.3). The muscles presumed to generate loading conditions included: abductors, adductors, extensors, flexors, protractors and retractors, which allowed for an extensive array of force conditions induced on the bone. These loading data (i.e., muscle force magnitude - Williams *et al*. 2008, 2008; Gosnell 2010; Rose *et al*. 2013; Kawano *et al*. 2016) were obtained from direct observations of the extant taxa behaviour and their structural peculiarities were inferred to the extinct taxa under investigation (Oliveira and Schultz 2015). These inferences were based on the anatomy of the humerus and femur as well as the muscle attachments to the bone. Each muscle force was distributed over an area of 3 mm^2 at the specific origin/insertion point of the muscles.

Table 2.4: Muscle forces used in boundary conditions for finite element models of the humerus and femur

Muscle	Origins (Force out of the Bone)	Insertions (Force into the Bone)	Abr.	*Parasagittal Fmax (N) 0,3MPa/20	**Semi-sprawled Fmax (N) 0,3MPa	***Sprawled Fmax (N) 0,3MPa
Humeri Muscles						
m. Latissimus dorsi	Vertebrae	Teres Tuberosity	LD	23,100	11,070	1,203
m. Pectoralis	Sternum	Crest of humerus distal to deltoid tuberosity	PE	69,909	46,140	3,032
m. Subscapularis	Scapula	Medial Tubercle	SS	70,821	18,480	0,928
m. Anconeus	Distal condyle	Olecranon	AN	11,246	22,200	3,008
m. Flexor carpi radialis	Medial Epicondyle		FCR	10,942	7,620	0,945
m. Flexor carpi ulnaris	Medial Epicondyle		FCU	57,143	23,970	0,471
Femora Muscles						
mm. Gluteal muscle	Illial shaft	Greater Trochanter (Lateral)	GM	174,468	15,540	0,673
m. Semimembranous	Pelvic head	Medial condyle	SM	24,012	38,160	1,112
mm. Adductor muscles		Medial shaft	AD	78,116	11,010	0,666
m. Vastus Lateralis	Lateral proximal diaphysis		VL	30,699	3,570	2,207
m. Vastus Medialis	Medial proximal diaphysis		VM	78,419	30,150	0,479
m.Vastus Intermedius	Proximal diaphysis		VI	25,532	9,630	1,846

*Parasagittal force reference: Williams *et al*. 2008; ** Semi-sprawled force reference: Rose *et al*. 2013 and Gosnell 2011; *** Sprawled force reference: Kawano *et al*. 2016

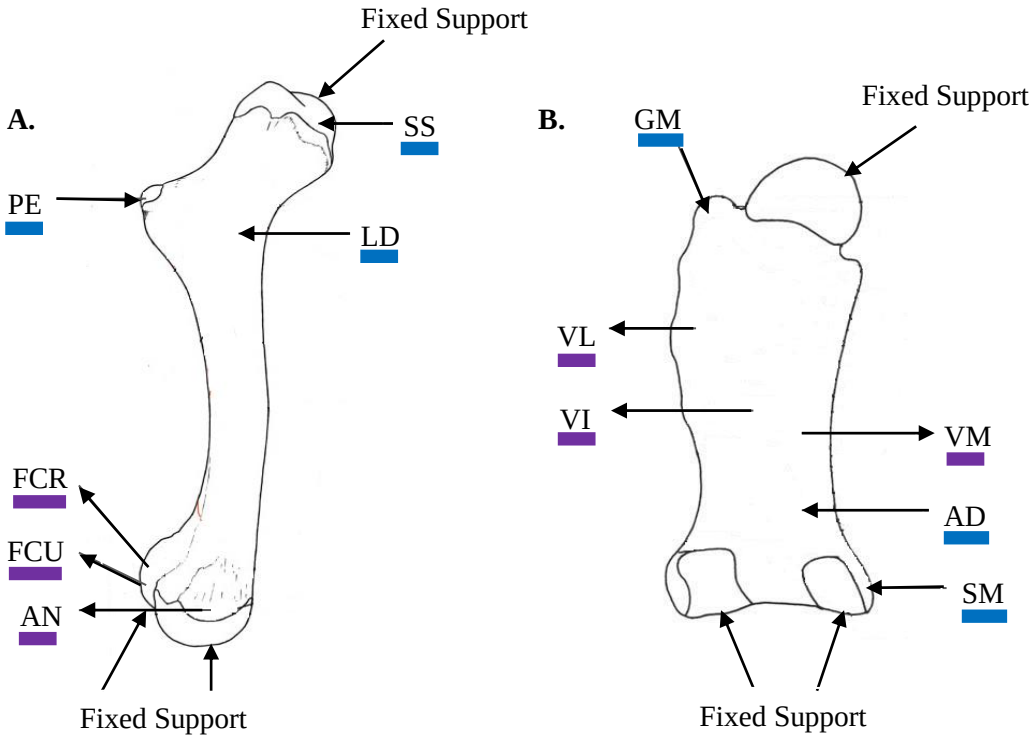


Figure 2.2: Regions of applied muscle forces of the A – humerus of *Tachyglossus* and B –Femur of *Tachyglossus*. AD: *mm. Adductor muscles*, AN: *m. Anconeus*, FCR: *m. Flexor carpi radialis*, FCU: *m. Flexor carpi ulnaris*, GM: *mm. Gluteal muscles*, LD: *m. Latissimus dorsi*, PE: *m. Pectoralis*, SM: *m. Semimembranous*, SS: *m. Subscapularis*, VI: *m. Vastus intermedius*, VL: *m. Vastus lateralis*, VM: *m. Vastus medialis*. ▬ – Origin of forces, input of muscle forces. ▬ – Insertion of forces, input of muscle forces.

FE Solver: Model Solution

Model solving involved the interpretation of total deformation (mm), directional deformation (mm), equivalent (von Mises) elastic strain (mm/mm) and equivalent (von Mises) stress (MPa) distributions in limb bone diaphyses. The ANSYS solver calculates the directional deformation experienced by the bone that supports an applied force. The total deformation is the vector sum of the directional deformation components. The von Mises stress determines the fracture location in multi-directions of the bone and von Mises strain is a good indicator of bone remodelling (Fortuny *et al*. 2015).

Post-Process: Hypothesis Confirmation

The ANSYS post-processer provides a visual means of comparing von Mises stress magnitudes and distributions in each model. Due to the difference in the angle of muscle forces for each posture (i.e., the joint reaction force), the colour scale setting was set according to the maximum and minimum analysis for each model. This will help understand limb configuration (i.e., posture) for which observed and quantified diaphyseal morphology is optimally adapted.

The post-process was conducted in order to compare maximum stresses and strains calculated by FEM in ANSYS relative to the values calculated by cross-sections and *in-vivo* studies by Blob and Biewener (1999) and Gosnell (2010). Since cross-sectional properties reflect stress and displacement, which in turn reflects bending and torsional loads, the cross-sectional methodology was applied (O' Neill and Ruff 2004; Lieberman *et al*. 2004; Ruff and Larson 2014; Iqbal 2015; Iqbal *et al*. in prep). Due to the solution being dependent on the mesh, a mesh-dependency was conducted (Russell *et al*. 2002). This allows for the geometry to have an acceptable mesh structure while still maintaining high computational accuracy in a sufficient amount of time. Mesh structures are compared from a coarse to a finer mesh iteration until an adequate mesh geometry is obtained (Russell *et al*. 2002).

Statistical Analysis

The statistical analyses were obtained on Microsoft Excel 2007 using the plugin, XLSTAT 2018 (Paris, France). A Kruskal-Wallis test was conducted on the fossil taxa to determine whether there were any significant difference between the three postures that were under investigation. The Kruskal-Wallis test was used when samples differed from a normal distribution. In the cases where the computed p-value was lower than the significant level ($p < 0.05$), resulting in rejection, and the null hypothesis (H0) would be rejected, one or more species is different from another for a given gait. To identify which of the gaits contributed to the H0 rejection, a multiple pair-wise comparisons using Dunn's procedure was used. A

post-hoc Bonferroni correction was performed to statistically assess the differences among the species for each gait. For all statistical testing in the study, statistical significance was achieved when $p < 0.05$.

Note: all resultant images where generated as the anatomically anterior view.

CHAPTER 3

Results

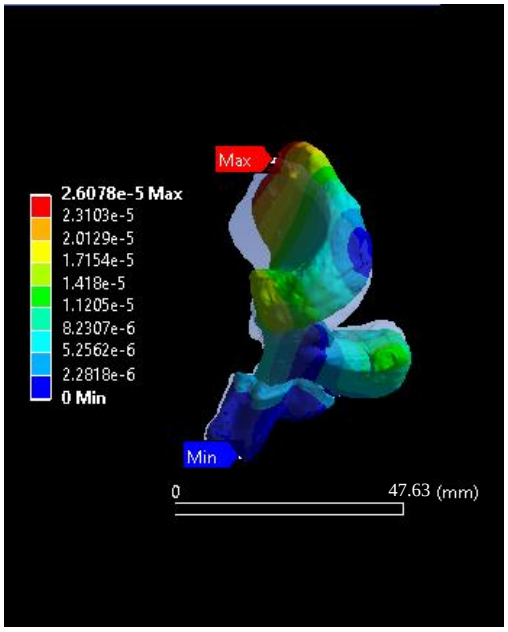
FEA Results – Humerus

Most strain deformation of the element occurred at the same location that exhibited the peak stress during the modelling conditions. In evaluating strain deformation of the elements (Figure 3.1), the humerus underwent torsion with the peak stress concentrated mainly on the proximal end, or on the deltopectoral crest (Figure 3.1A).

FEA Results – Femur

Femora underwent bending with the standard peak stress located at the midpoint of the diaphysis during the modelling conditions (Figure 3.1B). *Cynognathus* (BP/1/1675), *Tetracynodon darti* (BP/1/4335), *Galesaurus* (BP/1/4506), *Thrinaxodon* (BP/1/7199) and *Tachyglossus* femora bent in the posterior to anterior direction. The AP orientated bending stress on the femur represented compressing the posterior surface (posteriorly concave) and tensing the anterior surface. In contrast, *Thrinaxodon* (BP/1/1693 and BP/1/1730) and *Glanosuchus* (BP/1/6228) femora bent in the opposite direction – anterior to posterior direction. This resulted in an opposite pattern of strains on the anterior surface (compressive – anteriorly concave) and the posterior surface (tensile).

A:



B:

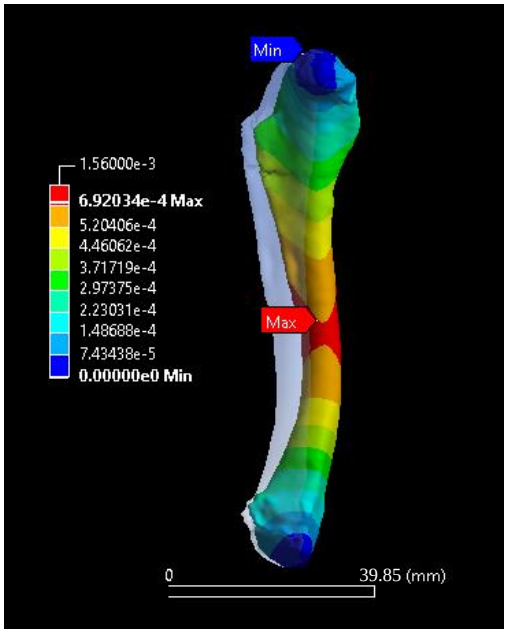


Figure 3.1: Strain deformation of A: Humerus and B: Femur of the species under investigation for all three gait postures (i.e., 20˚, 45˚ and60˚ angles). The units for the calculated deformation range were mm with the red level being the maximum - Max and the blue level being the minimum - Min . The bar at the bottom of each image represents the scale of the bone for evaluating its dimensions illustrated.

FEA Results – Humerus

Parasagittal Gait

Thrinaxodon liorhinus

The three *Thrinaxodon* humeri (BP/1/7199, BP/1/1730 and BP/1/1693) had a peak Directional Deformation (DD) on the deltopectoral crest. *Thrinaxodon* (BP/1/7199) had a min. DD on the lesser tuberosity whereas, *Thrinaxodon* (BP/1/1730 and BP/1/1693) min. DD were found on the distal ends of the humeri (Figure 3.2: 1A, 1B, 1C). The humeral peak Total Deformation (TD) for *Thrinaxodon* (BP/1/7199, BP/1/1730 and BP/1/1693) were observed on the deltopectoral crest and the min. TD was on

the distal end (Figure 3.2: 2A, 2B, 2C). The peak Equivalent Elastic Strain (EES) for *Thrinaxodon* (BP/1/7199, BP/1/1730 and BP/1/1693) were concentrated on the proximal end of the humeri (Figure 3.2: 3A, 3B, 3C). *Thrinaxodon* (BP/1/7199, BP/1/1730 and BP/1/1693) peak Equivalent Stress (ES) were also on the proximal ends, however, the peak stress was also located on the distal ends of the humerus with the min. stress seen on the deltopectoral crest (Figure 3.2: 4A, 4B, 4C; 3.17).

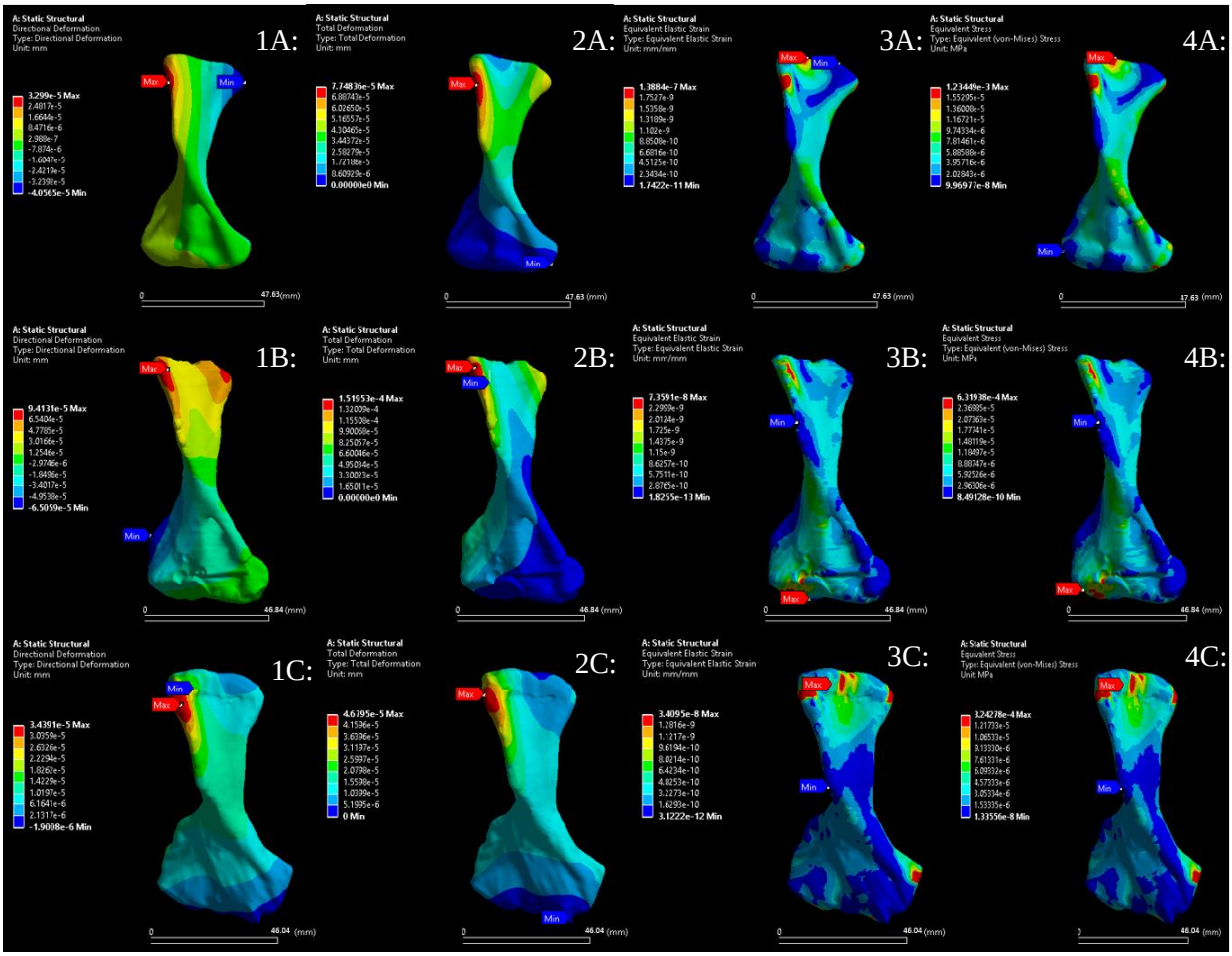


Figure 3.2: Parasagittal modelled humeri of *Thrinaxodon* (A – BP/1/7199), *Thrinaxodon* (B – BP/1/1730), *Thrinaxodon*(C – BP/1/1693): DD (1A, 1B, 1C), TD (2A, 2B, 2C), EES (3A, 3B, 3C), ES (4A, 4B, 4C).The units for the calculated DD and TD range were mm, strain range was mm/mm, and stress range was MPa with the red level being the maximum - Max and the blue level being the minimum - Min . The bar at the bottom of each image represents the scale of the bone for evaluating its dimensions illustrated.

Cynognathus

The min. DD for *Cynognathus* (BP/1/1675) was located on the deltopectoral crest, conversely, the peak DD was found on the distolateral side of the humerus (ectepicondyle) (Figure 3.3: 1). The humeral peak TD was observed on the deltopectoral crest and the min. TD was on the distal end (Figure 3.3: 2). The peak EES was concentrated at the proximal end of the humeri (Figure 3.3: 3). *Cynognathus* (BP/1/1675) min. ES was distributed on almost the entire humeri except for the peak stress on the distolateral surface (Figure 3.3: 4; 3.17).

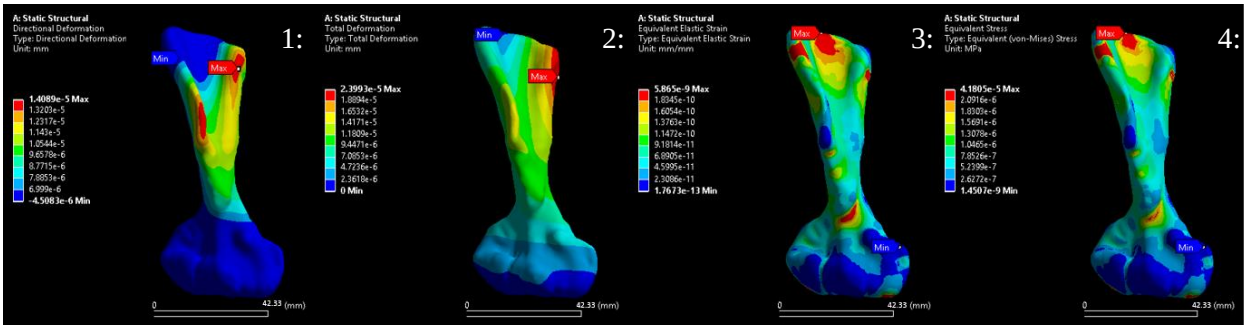


Figure 3.3: Parasagittal modelled humerus of *Cynognathus*: DD (1), TD (2), EES (3), ES (4).The units for the calculated DD and TD range were mm, strain range was mm/mm, and stress range was MPa with the red level being the maximum - Max and the blue level being the minimum - Min. The bar at the bottom of each image represents the scale of the bone for evaluating its dimensions illustrated.

Galesaurus

Galesaurus (BP/1/4506) peak DD was found on the deltopectoral crest and min. DD was found on the proximomedial side of the humerus (Figure 3.4: 1).The humeral peak TD of *Galesaurus* (BP/1/4506) was found on the proximomedial side (Figure 3.4: 2). *Galesaurus* (BP/1/4506) was the only humerus to have an EES located from the proximal end extending towards the middle of the diaphysis (Figure 3.4: 3). The humeral peak stress was observed at the proximal end and the min. ES was on the distal end (Figure 3.4: 4; 3.17).

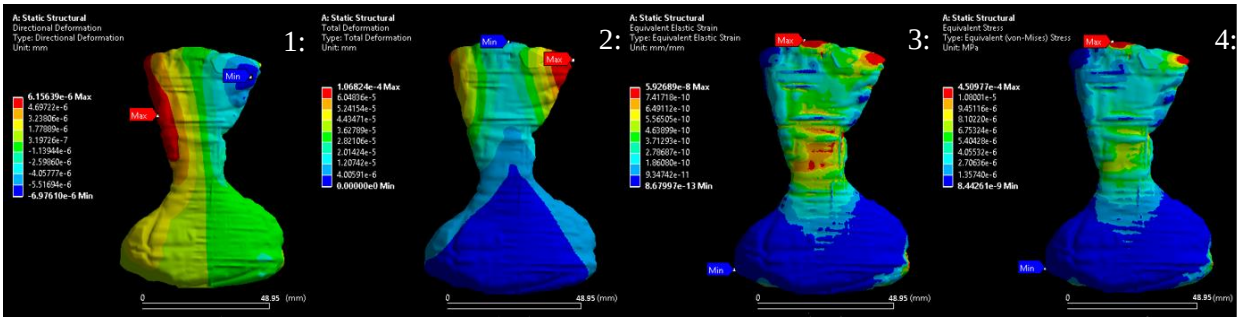


Figure 3.4: Parasagittal modelled humerus of *Galesaurus*: DD (1), TD (2), EES (3), ES (4).The units for the calculated DD and TD range were mm, strain range was mm/mm, and stress range was MPa with the red level being the maximum - Max and the blue level being the minimum - Min . The bar at the bottom of each image represents the scale of the bone for evaluating its dimensions illustrated.

Therocephalia

The peak DD for *Glanosuchus* (BP/1/6228) was found on the distal end of the humerus and the minimum DD was on the deltopectoral crest (Figure 3.5: 1A). However, for *Tetracynodon darti* (BP/1/4335), the peak DD was found on the deltopectoral crest and the min. DD was on the lesser tuberosity (Figure 3.5: 1B). The humeral peak TD for Therocephalia (BP/1/6228 and BP/1/4335) were observed on the deltopectoral crest and the min. TD was on the distal end (Figure 3.5: 2A, 2B). Therocephalia (BP/1/6228 and BP/1/4335) peak strain was concentrated on the proximal end of the humeri (Figure 3.5: 3A, 3B). The peak stress for Therocephalia (BP/1/6228 and BP/1/4335) were situated at the proximal end and the min. stress was distributed down the diaphysis to the distal end of the humerus (Figure 3.5: 4A, 4B; 3.17).

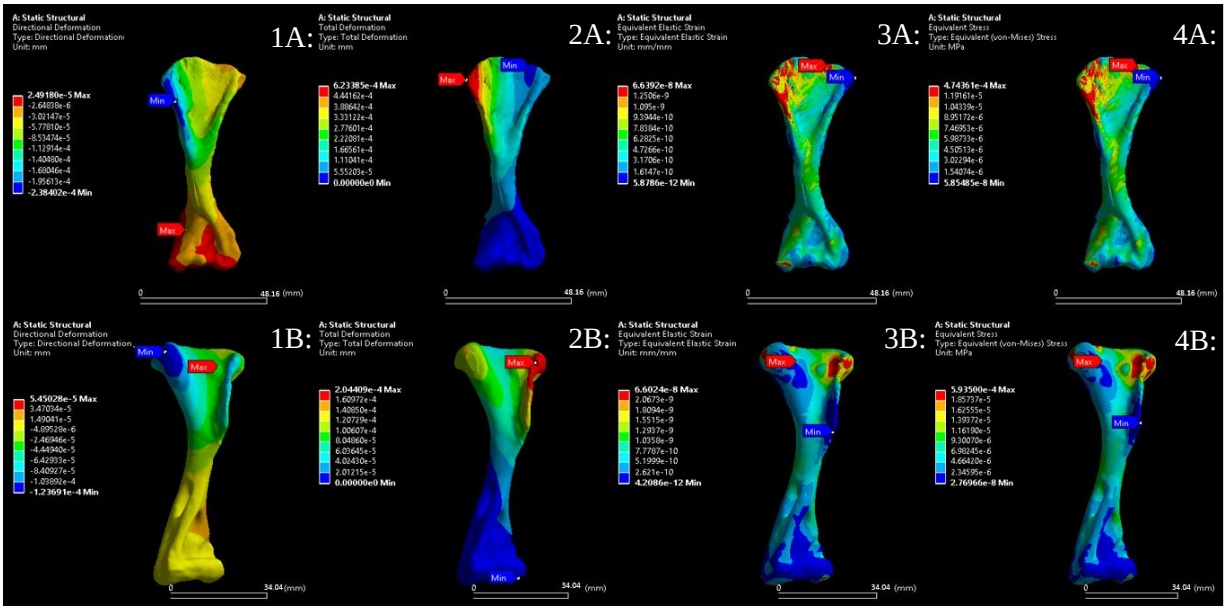


Figure 3.5: Parasagittal modelled humeri of Therocephalia (*Glanosuchus* A – BP/1/6228 and *Tetracynodon darti* B – BP/1/4335): DD (1A and 1B), TD (2A and 2B), EES (3A and 3B), ES (4A and 4B).The units for the calculated DD and TD range were mm, strain range was mm/mm, and stress range was MPa with the red level being the maximum - Max and the blue level being the minimum - Min . The bar at the bottom of each image represents the scale of the bone for evaluating its dimensions illustrated.

Tachyglossus

The min. DD was observed on the humerus deltopectoral crest of *Tachyglossus* and the peak DD was found on the lesser tuberosity and distolateral side (Figure 3.6: 1). The peak TD was found on the distolateral side of the humerus, the min. TD was the same as the other species (Figure 3.6: 2). *Tachyglossus* has a peak EES at the distal end of the humerus with the min. EES covers a majority of the species bone structure (Figure 3.6: 3). Min. stress was distributed on almost the entire humeri except for the peak stress on the distolateral surface (Figure 3.6: 4; 3.17).

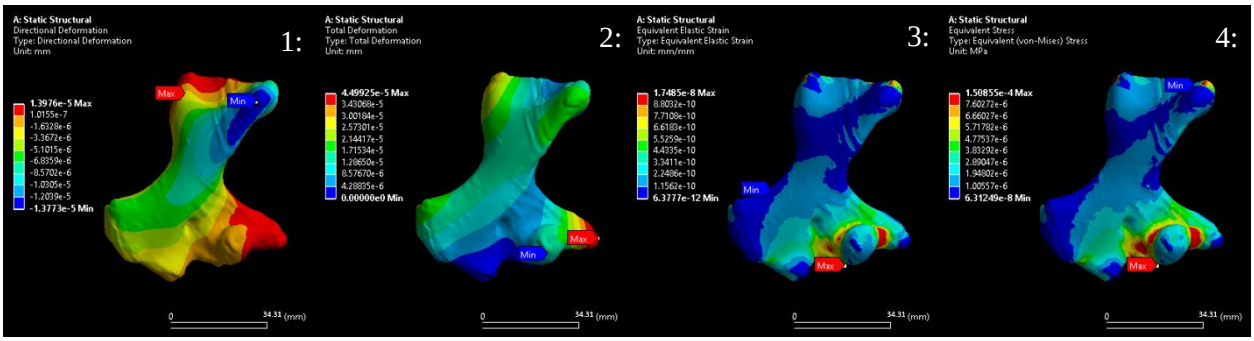


Figure 3.6: Parasagittal modelled humerus of *Tachyglossus*: DD (1), TD (2), EES (3), ES (4).The units for the calculated DD and TD range were mm, strain range was mm/mm, and stress range was MPa with the red level being the maximum - Max and the blue level being the minimum - Min. The bar at the bottom of each image represents the scale of the bone for evaluating its dimensions illustrated.

FEA Comparative Taxa Results

The maximum directional deformation of the humerus was highest for *Cynognathus* (BP/1/1675) and lowest for *Glanosuchus* (BP/1/6228) and *Tachyglossus* (Appendix A1). There was variation within the same species for the directional deformation (Appendix A1). *Thrinaxodon* (BP1693, BP/1/7199) and *Glanosuchus* (BP/1/6228) overlapped for the maximum DD (Appendix A1). For TD, *Glanosuchus* (BP/1/6228) had the highest and *Thrinaxodon* (BP/1/1693) and *Tachyglossus* had the lowest TD (Appendix A1). There was variation for the humeri within the same species of Therocephalia (Appendix A1). The highest EES was found for *Cynognathus* (BP/1/1675) and the lowest EES was found to be the *Tachyglossus* (Appendix A1). There was overlap for the humeri EES of *Thrinaxodon* (BP/1/1730) and *Glanosuchus* (BP/1/6228) (Appendix A1). The highest ES was attained for *Cynognathus* (BP/1/1675) and *Tachyglossus* had the lowest (Appendix A1). There was overlap between the humeri of *Thrinaxodon* (BP/1/1730) and *Tetracynodon darti* (BP/1/4335) (Appendix A1).

Semi-Sprawled Gait

Thrinaxodon liorhinus

The location of the peak and min. DD for the semi-sprawled gait was similar to the parasagittal gait (i.e., on the deltopectoral crest) except for *Thrinaxodon* (BP/1/1693) where the peak DD was found on the distal lateral side of the humerus and the min. DD was observed on the deltopectoral crest (Figure 3.7: 1C). The peak and min. TD for the species humeri were found on the same location as observed for the parasagittal gait (i.e., on the deltopectoral crest), except for *Thrinaxodon* (BP/1/1693), whose peak TD was situated on the lateral distal end (Figure 3.7: 2C). The location of the peak and min. EES for the semi-sprawled humerus was observed on the proximal end, except for *Thrinaxodon* (BP/1/1730), which the peak EES was situated at the distal lateral side (Figure 3.7: 3B). The distribution of the humeral peak and min. stress was situated on the proximal and distal ends of the humerus (Figure 3.7: 4A, 4B, 4C). The locations for the peak and min. stress and strain were at the same locations for the parasagittal gait with differences in the magnitude (Figure 3.2, 3.17).

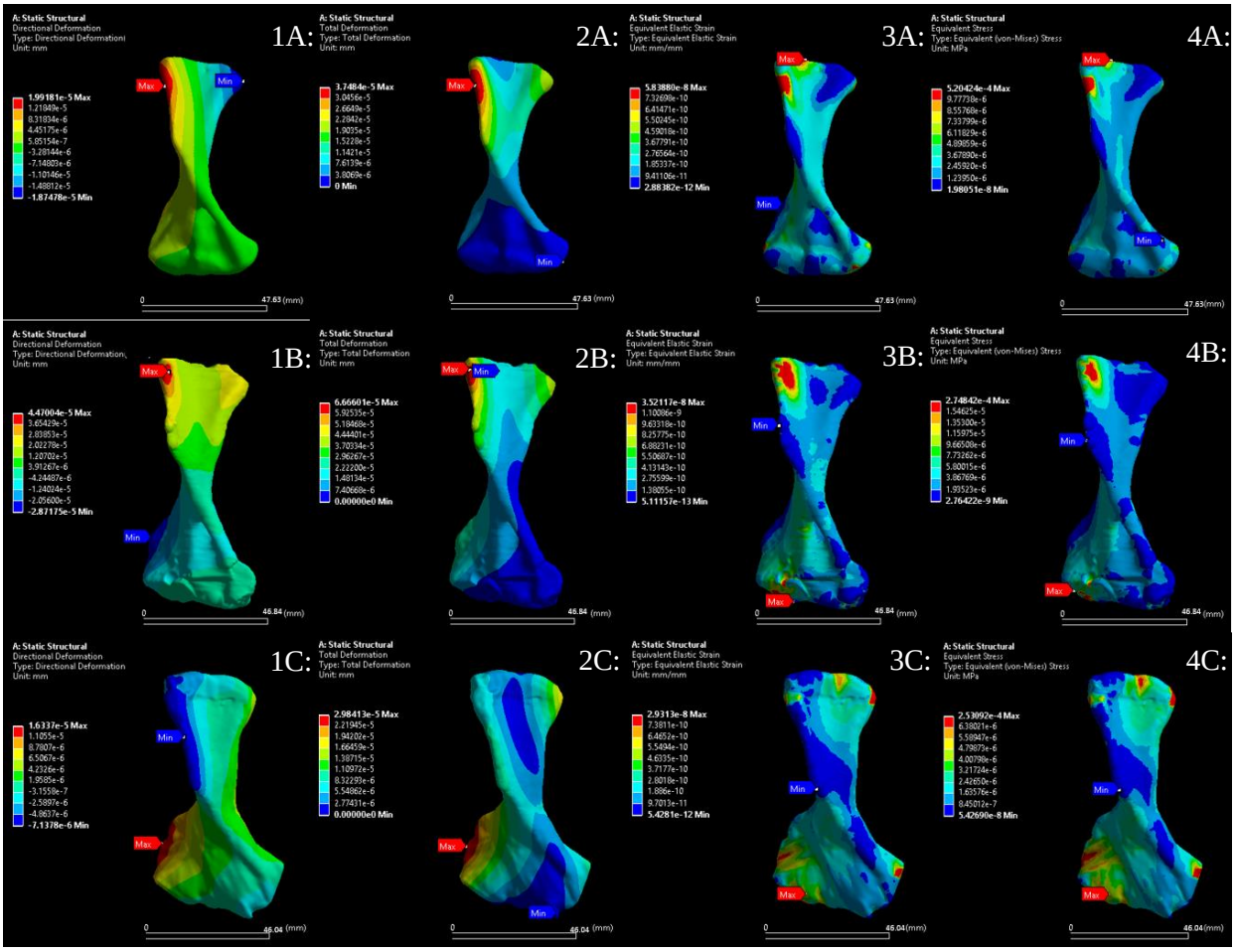


Figure 3.7: Semi-sprawled modelled humeri of *Thrinaxodon* (A – BP/1/7199), *Thrinaxodon* (B –BP/1/1730), *Thrinaxodon* (C – BP/1/1693): DD (1A, 1B, 1C), TD (2A, 2B, 2C), EES (3A, 3B, 3C), ES (4A, 4B, 4C).The units for the calculated DD and TD range were mm, strain range was mm/mm, and stress range was MPa with the red level being the maximum - Max and the blue level being the minimum - Min. The bar at the bottom of each image represents the scale of the bone for evaluating its dimensions illustrated.

Cynognathus

The peak DD for *Cynognathus* was situated at the distal end of the humerus and the min. DD was on the deltopectoral crest (Figure 3.8: 1). In comparison, the peak TD was on the deltopectoral crest and the min. TD was located at the distal end (Figure 3.8: 2). The distribution of EES and ES was similar

except for the location of the peak stress and strain (Figure 3.8: 3, 4). The peak EES was located at the proximal end of the humerus while that peak ES was at the distal end (Figure 3.8: 3, 4). The locations for the peak and min. stress and strain were at the same locations for the parasagittal gait with differences in the magnitude (Figure 3.3; 3.17).

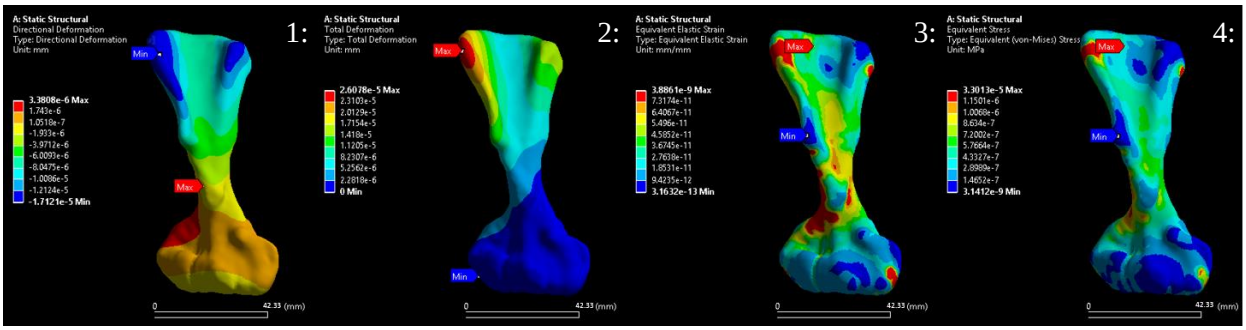


Figure 3.8: Semi-sprawled modelled humerus of *Cynognathus*: DD (1), TD (2), EES (3), ES (4).The units for the calculated DD and TD range were mm, strain range was mm/mm, and stress range was MPa with the red level being the maximum - Max and the blue level being the minimum - Min. The bar at the bottom of each image represents the scale of the bone for evaluating its dimensions illustrated.

Galesaurus

The location of the peak DD and TD were on the deltopectoral crest, however, the min. DD was on the proximal lateral side of the humerus and the min. TD was found on the distal end (Figure 3.9: 1, 2). The min. and peak distribution was the same for both EES and ES (Figure 3.9: 3, 4). Even though, the max. EES and ES were situated on the head of the humeri, the diaphysis also experiences an excessive amount of strain and stress (Figure 3.9: 3, 4). The locations for the peak and min. stress and strain were at the same locations for the parasagittal gait with differences in the magnitude (Figure 3.4; 3.17).

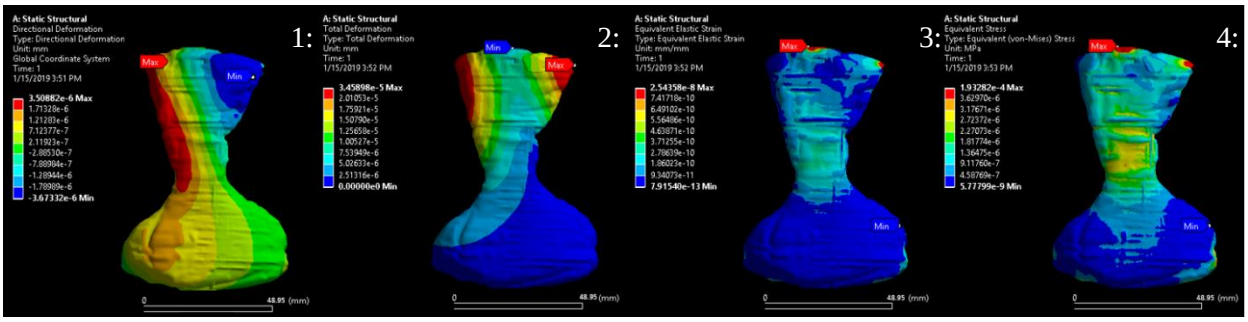


Figure 3.9: Semi-sprawled modelled humerus of *Galesaurus*: DD (1), TD (2), EES (3), ES (4).The units for the calculated DD and TD range were mm, strain range was mm/mm, and stress range was MPa with the red level being the maximum - Max and the blue level being the minimum - Min. The bar at the bottom of each image represents the scale of the bone for evaluating its dimensions illustrated.

Therocephalia

The location of the peak DD for *Glanosuchus* (BP/1/6228) was found on the distal end (Figure 3.10: 1A). The min. DD for *Glanosuchus* (BP/1/6228) was observed on the deltopectoral crest, which is the proximal lateral side of the humerus, on the contrary, *Tetracynodon darti* (BP/1/4335) min. DD was on the lesser tuberosity, which is the proximal medial side of the humerus (Figure 3.10: 1A, 1B). Glanosuchus (BP/1/6228) peak and min. TD were situated at the proximal end of the humerus (Figure 3.10: 1B). *Tetracynodon darti* (BP/1/4335) peak TD was observed on the deltopectoral crest and the min. TD was on the distal end (Figure 3.10: 2B). For both EES and ES, the peak and min. distribution was the same across the humerus for Glanosuchus (BP/1/6228) (Figure 3.10: 3A, 4A). As seen in *Tetracynodon darti* (BP/1/4335), the peak and min. EES and ES distribution was the same across the humerus (Figure 3.10: 3B, 4B). The locations for the peak and min. stress and strain were at the same locations for the parasagittal gait with differences in the magnitude (Figure 3.5; 3.17).

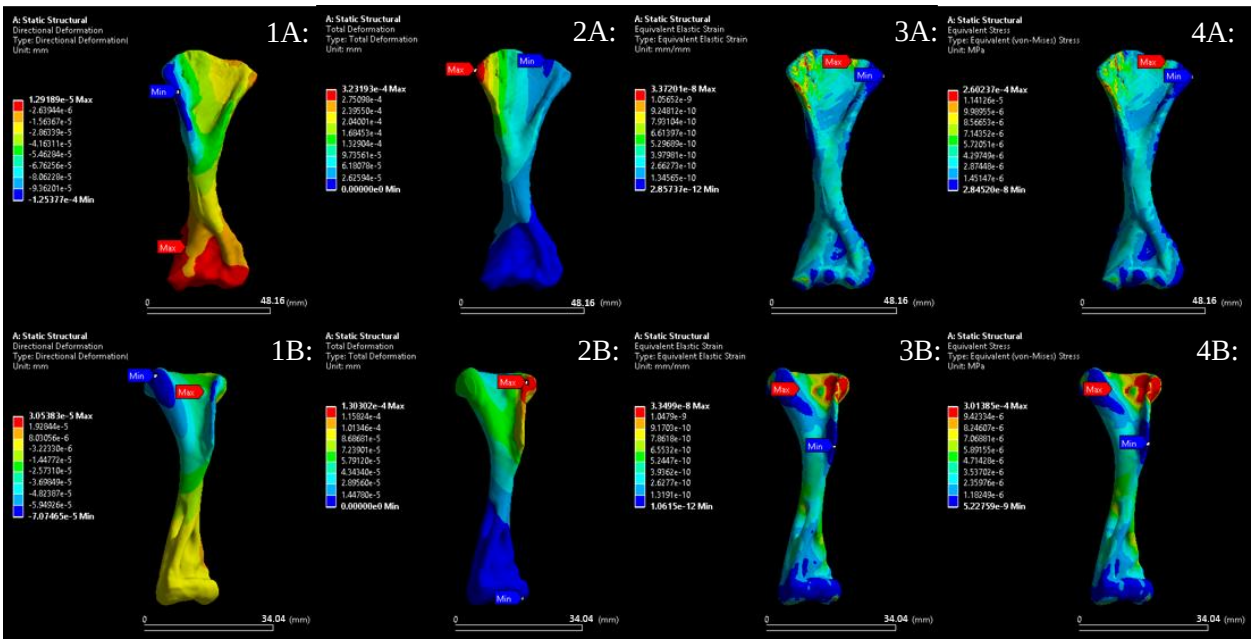


Figure 3.10: Semi-sprawled modelled humeri of Therocephalia (*Glanosuchus* A – BP/1/6228 and *Tetracynodon darti* B – BP/1/4335): DD (1A and 1B), TD (2A and 2B), EES (3A and 3B), ES (4A and 4B). The units for the calculated DD and TD range were mm, strain range was mm/mm, and stress range was MPa with the red level being the maximum - Max and the blue level being the minimum - Min. The bar at the bottom of each image represents the scale of the bone for evaluating its dimensions illustrated.

Tachyglossus

The location of the peak DD was found on the lesser tuberosity and the min. DD was observed on the deltopectoral crest (Figure 3.11: 1). *Tachyglossus* peak TD was found on the distal lateral side (Figure 3.11: 2). For both EES and ES, the peak and min. distribution was the same across the humerus (Figure 3.11: 3, 4). The locations for the peak and min. stress and strain were at the same locations for the parasagittal gait with differences in the magnitude (Figure 3.6; 3.17).

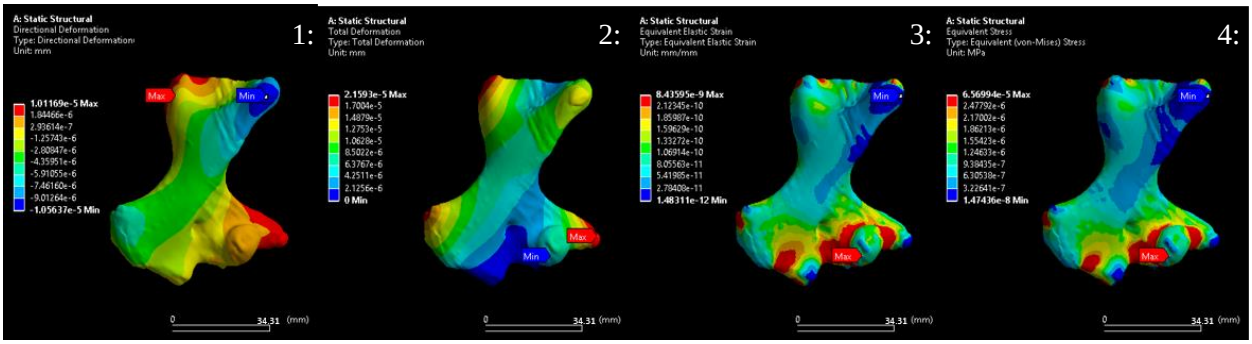


Figure 3.11: Semi-sprawled modelled humerus of *Tachyglossus*: DD (1), TD (2), EES (3), ES (4).The units for the calculated DD and TD range were mm, strain range was mm/mm, and stress range was MPa with the red level being the maximum - Max and the blue level being the minimum - Min. The bar at the bottom of each image represents the scale of the bone for evaluating its dimensions illustrated.

FEA Comparative Taxa Results

The max. DD was obtained for *Cynognathus* (BP/1/1675) and the lowest for *Tachyglossus* (Appendix B2). There was overlap between *Thrinaxodon* (BP/1/1730) and *Galesaurus* (BP/1/4506) humeri (Appendix B2). Specimens of *Thrinaxodon* (BP/1/1693 and BP/1/7199) display similarities in their humeri DD (Appendix B2). *Glanosuchus* (BP/1/6228) had the highest TD and *Tachyglossus* had the lowest TD (Appendix B2). There was overlap within species, *Thrinaxodon* (BP/1/1693 and BP/1/7199) (Appendix B2). Minor similarities were observed in the TD of the humeri between *Galesaurus* (BP/1/4506) and Therocephalia (BP/1/4335) (Appendix B2). The highest EES for the humerus was found for *Cynognathus* (BP/1/1675) and the lowest was *Tachyglossus* (Appendix B2). There was overlap among *Thrinaxodon* (BP/1/1693 and BP/1/1730), Therocephalia (BP/1/4335 and BP/1/6228) and *Galesaurus* (BP/1/4506) (Appendix B2). *Cynognathus* (BP/1/1675) illustrate the highest humerus ES and *Tachyglossus* had the lowest (Appendix B2). There was overlap in the humerus ES between *Thrinaxodon* (BP/1/1693 and BP/1/1730) and Therocephalia (BP/1/4335 and BP/1/6228) (Appendix B2).

Sprawled Gait

Thrinaxodon liorhinus

The location of the peak and min. DD for the sprawled gait was similar to the parasagittal gait, i.e., on the deltopectoral crest, except for *Thrinaxodon* (BP/1/1693) where the peak DD was on the distal lateral side of the humerus and the min. DD was observed on the deltopectoral crest as seen in the semi-sprawled gait (Figure 3.12: 1C). The peak and min. TD for the species humeri was on the same location as observed for the parasagittal gait, however, for *Thrinaxodon* (BP/1/1693), as in the semi-sprawled gait, the peak TD was situated on the lateral distal end (Figure 3.12: 2C). The location of the peak and min. EES for the sprawled humerus was the same as for the semi-sprawled gait, where *Thrinaxodon* (BP/1/1730) peak EES was situated at the distal lateral side (Figure 3.12: 3B). The locations of the humeral peak and min. stress for the sprawled gait was the same as observed in the parasagittal and semi-sprawled gait (Figure 3.2 and Figure 3.7, respectively), with differences in the magnitude (Figure 3.2; 3.7; 3.17).

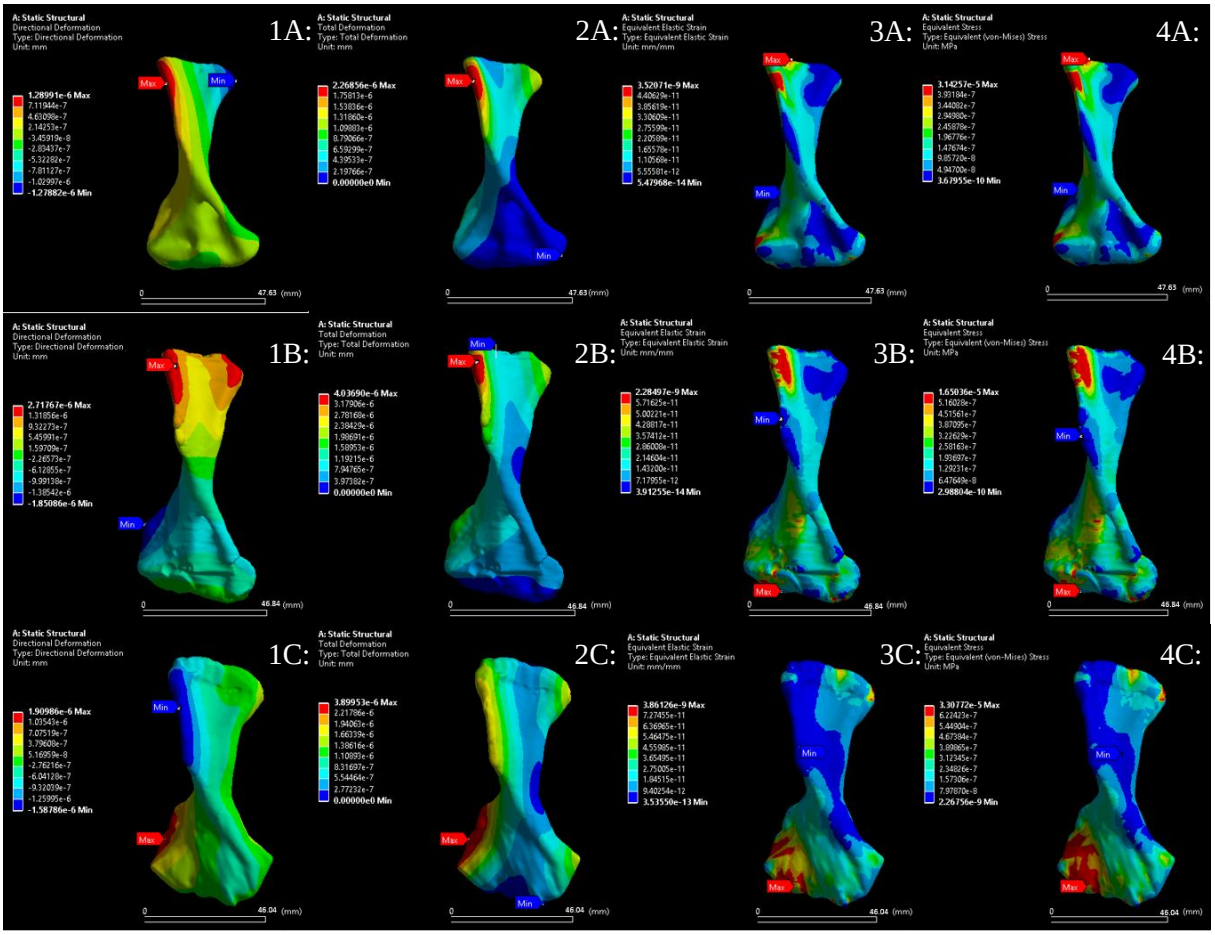


Figure 3.12: Sprawled modelled humeri of *Thrinaxodon* (A – BP/1/7199), *Thrinaxodon* (B – BP/1/1730), *Thrinaxodon* (C – BP/1/1693): DD (1A, 1B, 1C), TD (2A, 2B, 2C), EES (3A, 3B, 3C), ES (4A, 4B, 4C).The units for the calculated DD and TD range were mm, strain range was mm/mm, and stress range was MPa with the red level being the maximum - Max and the blue level being the minimum - Min . The bar at the bottom of each image represents the scale of the bone for evaluating its dimensions illustrated.

Cynognathus

The peak DD for *Cynognathus* was situated at the distal lateral end of the humerus and the min. DD was on the deltopectoral crest (Figure 3.13: 1). In contrast, the peak TD was on the deltopectoral crest and the min. TD was located at the distal end (Figure 3.13: 2). The distribution of EES and ES was

similar except for the location of the peak stress and strain (Figure 3.13: 3, 4). The peak EES was located at the proximal end of the humerus while that peak ES was at the distal end (Figure 3.13: 3, 4). The locations for the peak and min. stress and strain were at the same locations for the parasagittal gait with differences in the magnitude (Figure 3.3; 3.8; 3.17).

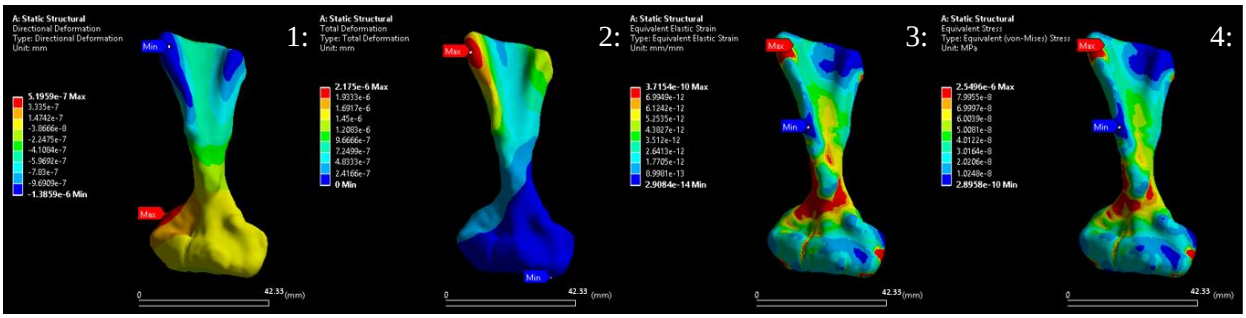


Figure 3.13: Sprawled modelled humerus of *Cynognathus*: DD (1), TD (2), EES (3), ES (4).The units for the calculated DD and TD range were mm, strain range was mm/mm, and stress range was MPa with the red level being the maximum - Max and the blue level being the minimum - Min. The bar at the bottom of each image represents the scale of the bone for evaluating its dimensions illustrated.

Galesaurus

The location of the peak DD and TD were found on the deltopectoral crest, however, the min. DD was on the proximal lateral side of the humerus and the min. TD was on the distal end (Figure 3.14: 1, 2). The min. and peak distribution was the same for both EES and ES (Figure 3.14: 3, 4). Although, the max. EES and ES were situated on the head of the humeri, the diaphysis also experiences an excessive amount of strain and stress (Figure 3.14: 3, 4). These distribution patterns were similar to those observed for the semi-sprawled gait (Figure 3.9). The locations for the peak and min. stress and strain were at the same locations for the parasagittal gait with differences in the magnitude (Figure 3.4; 3.9; 3.17).

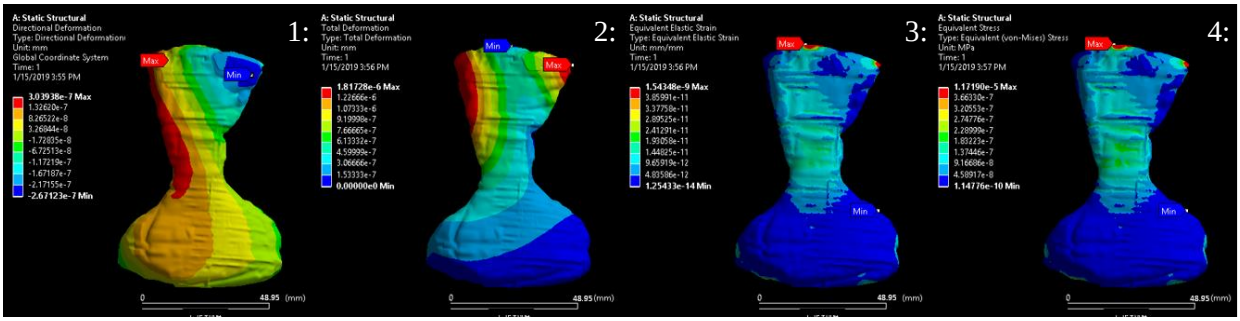


Figure 3.14: Sprawled modelled humerus of *Galesaurus*: DD (1), TD (2), EES (3), ES (4).The units for the calculated DD and TD range were mm, strain range was mm/mm, and stress range was MPa with the red level being the maximum - Max and the blue level being the minimum - Min. The bar at the bottom of each image represents the scale of the bone for evaluating its dimensions illustrated.

Therocephalia

The location of the peak DD for *Glanosuchus* (BP/1/6228) was found on the distal end (Figure 3.15: 1A). The min. DD for *Glanosuchus* (BP/1/6228) was on the deltopectoral crest which is the proximal lateral side of the humerus, on the contrary, Therocephalia (BP/1/4335) min. DD was on the lesser tuberosity which is the proximal medial side of the humerus (Figure 3.15: 1A, 1B). *Glanosuchus* (BP/1/6228) peak and min. TD were situated at the proximal end of the humerus (Figure 3.15: 2A). Therocephalia (BP/1/4335) peak TD was observed on the deltopectoral crest and the min. TD was on the distal end (Figure 3.15: 2B). The peak and min. EES for *Glanosuchus* (BP/1/6228) was situated on the proximal end of the humerus (Figure 3.15: 3A). Whereas, only the min. ES was situated on the proximal end. For both EES and ES, the peak and min. distribution was the same across the humerus for Therocephalia (BP/1/4335) (Figure 3.15: 4B). The locations for the peak and min. stress and strain were at the same locations for the parasagittal gait with differences in the magnitude (Figure 3.5; 3.10; 3.17).

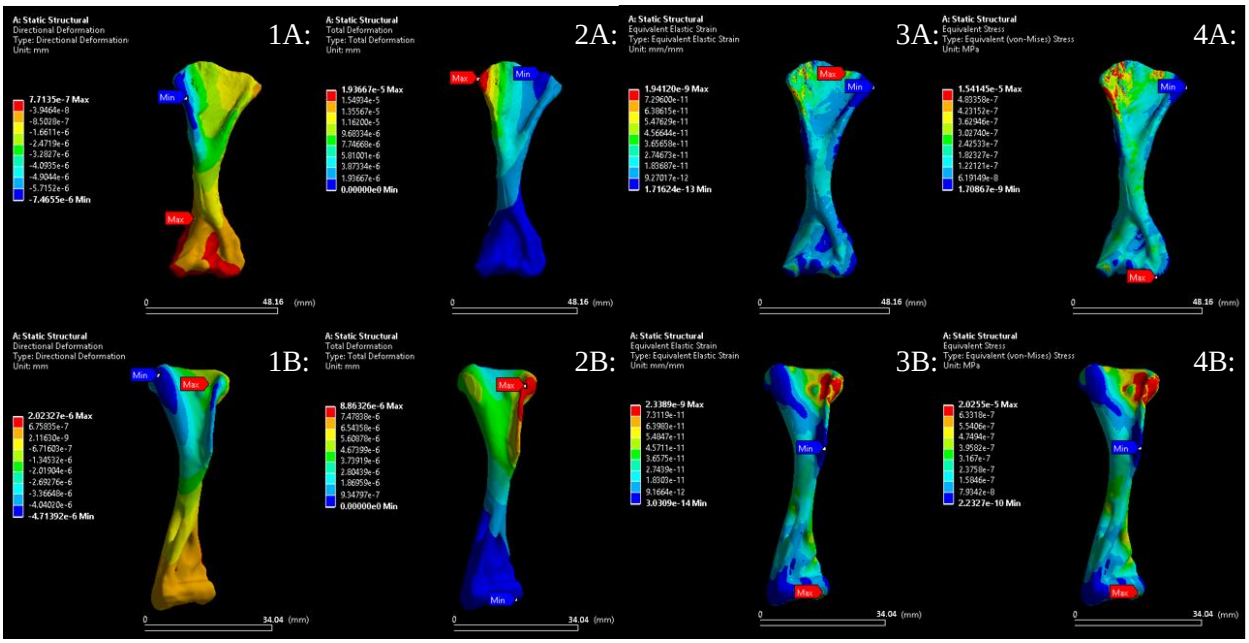


Figure 3.15: Sprawled modelled humeri of Therocephalia (*Glanosuchus* A – BP/1/6228 and *Tetracynodon darti* B – BP/1/4335): DD (1A and 1B), TD (2A and 2B), EES (3A and 3B), ES (4A and 4B).The units for the calculated DD and TD range were mm, strain range was mm/mm, and stress range was MPa with the red level being the maximum - Max and the blue level being the minimum - Min . The bar at the bottom of each image represents the scale of the bone for evaluating its dimensions illustrated.

Tachyglossus

The location of the peak DD was found on the lesser tuberosity and the distal lateral end, while the min. DD was on the deltopectoral crest (Figure 3.16: 1). *Tachyglossus* peak TD was found on the distal medial side (Figure 3.16: 2). For both EES and ES, the peak and min. distribution was the same across the humerus (Figure 3.16: 3, 4). The locations for the peak and min. stress and strain were at the same locations for the parasagittal gait with differences in the magnitude (Figure 3.6; 3.11; 3.17).

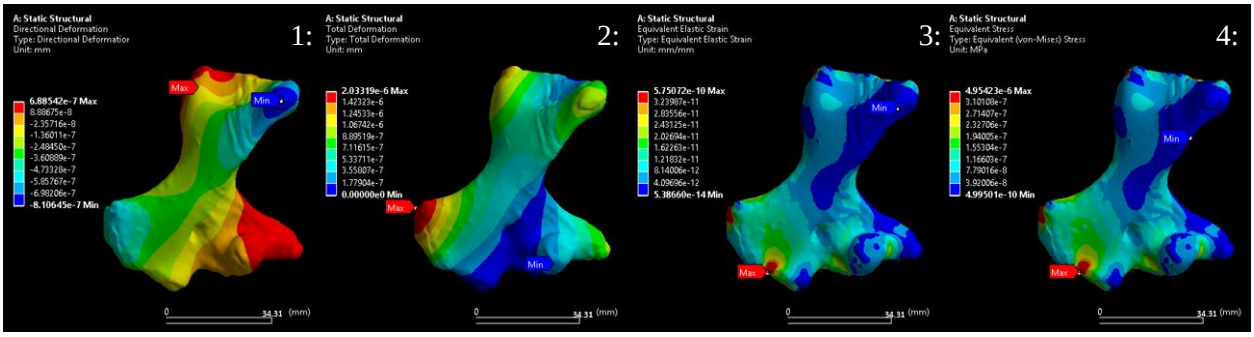


Figure 3.16: Sprawled modelled humerus of *Tachyglossus*: DD (1), TD (2), EES (3), ES (4).The units for the calculated DD and TD range were mm, strain range was mm/mm, and stress range was MPa with the red level being the maximum - Max and the blue level being the minimum - Min. The bar at the bottom of each image represents the scale of the bone for evaluating its dimensions illustrated.

FEA Comparative Taxa Results

Cynognathus (BP/1/1675) was found to have the highest DD for the humerus (Appendix B3). The lowest humerus DD was found in *Glanosuchus* (BP/1/6228). There was overlap between *Glanosuchus* (BP/1/6228) and *Tachyglossus* (Appendix B3). *Thrinaxodon* (BP/1/1693) overlapped with Therocephalia (BP/1/4335) for humeral DD (Appendix B3). *Glanosuchus* (BP/1/6228) was found to have the highest TD and *Tachyglossus* was found to have the lowest TD (Appendix B3). There was overlap within the same species for humeral TD (*Thrinaxodon* BP/1/1693, BP/1/1730 and BP/1/7199) (Appendix B3). *Cynognathus* (BP/1/1675) was observed to have the highest humeral EES and *Tachyglossus* was observed to have the lowest humeral EES (Appendix B3). There were three distinct overlapping pairs for the humeral EES, first between *Thrinaxodon* (BP/1/1693 and BP/1/7199), the second overlap was among *Thrinaxodon* (BP/1/1730), Therocephalia (BP/1/4335 and BP/1/6228) and *Galesaurus* (BP/1/4506) and the third overlap was within the same species (Therocephalia BP/1/4335 and BP/1/6228) (Appendix B3). *Cynognathus* (BP/1/1675) had the highest ES and *Tachyglossus* had the lowest (Appendix B3). There was

overlap in the humeral ES between *Thrinaxodon* (BP/1/1693 and BP/1/7199) (Appendix B3). *Thrinaxodon* (BP/1/1730) overlapped with *Glanosuchus* (BP/1/6228) in humeral ES (Appendix B3).

Comparison of the humeral FEA results for the different gaits analysed for each taxa

ANOVA

The overall grouping of the fossil taxa exhibited statistically significant differences for EES and ES between the parasagittal, semi-sprawled and sprawled gait models ($p < 0.001$) (Appendix D). With a Bonferroni corrected significant p-value (0.0167), one or more species within the semi-sprawled vs. sprawled and parasagittal vs. sprawled gait comparisons differed. When the comparative extant species (*Tachyglossus*) was included in the ANOVA test, the significant difference among the different gait models remained ($p < 0.001$) (Appendix D).

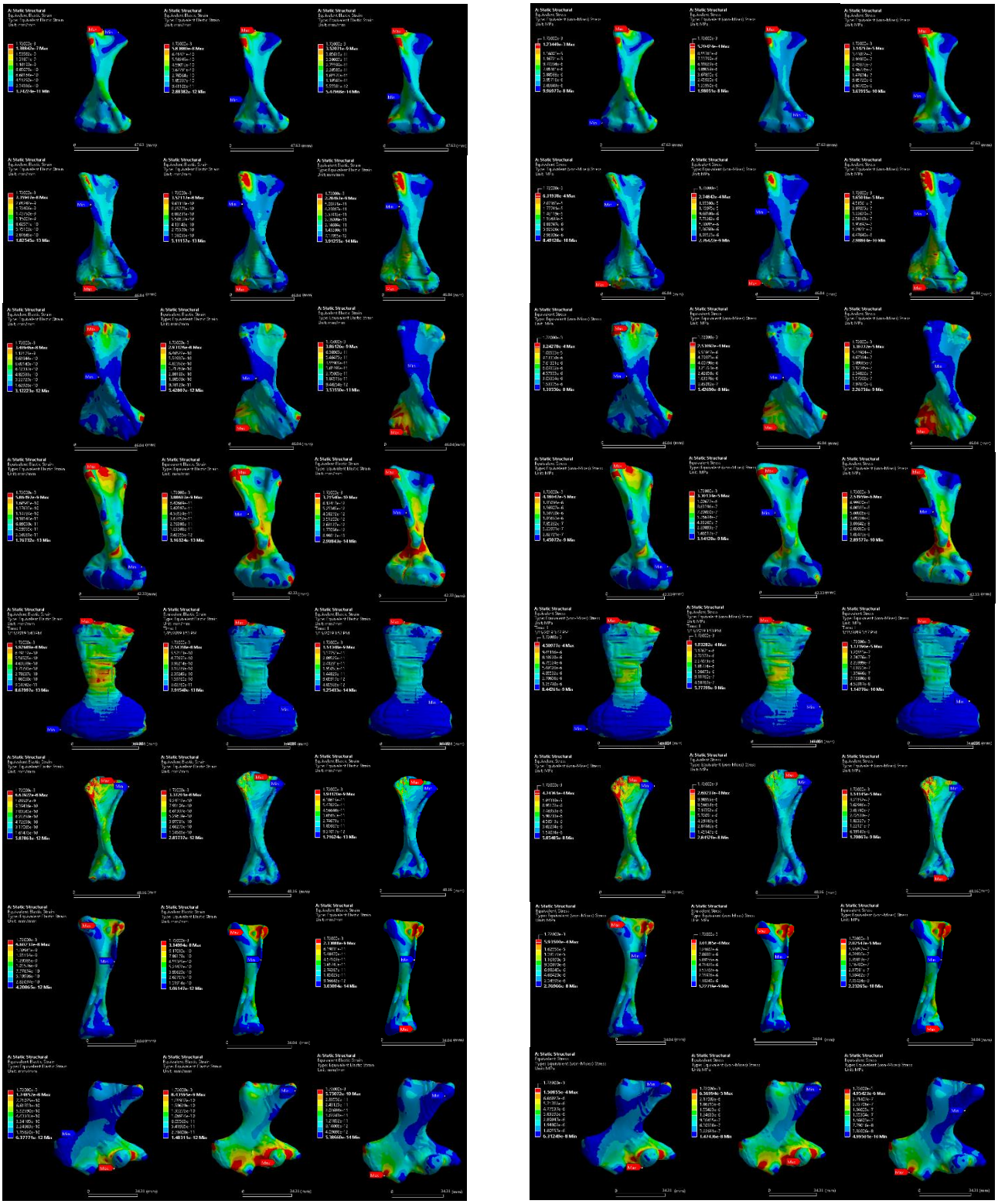


Figure 3.17:EES and ES for comparative gaits by species; from left to right: Humeri - parasagittal, semi sprawled, sprawled gaits scaled to the maximum magnitude of 1.72e-3: *Thrinaxodon* (BP/1/7199 – D1, 2, 3; BP/1/1730 – D4, 5, 6;BP/1/1693 – D7, 8, 9), *Cynognathus* (BP/1/1675 – D10, 11, 12), *Galesaurus* (BP/1/4506 – D13, 14, 15), Therocephalia (BP/1/6228 – D16, 17, 18; BP/1/4335 – D19, 20, 21) and *Tachyglossus* (D22, 23, 24).

FEA Results – Femur

Parasagittal Gait

Thrinaxodon liorhinus

Peak and min. DD for the femur was found to differ within the three *Thrinaxodon* specimens (Figure 3.18). *Thrinaxodon* (BP/1/7199) was observed to experience a similar min. DD as *Cynognathus* (BP/1/1675), but peak DD of the former was found on the lesser trochanter (Figure 3.18: 1A and Figure 3.18: 1). Peak DD for *Thrinaxodon* (BP/1/1730), on the other hand, was found on the lateral side of the femur and min. DD was located on the proximal medial side (Figure 3.18: 1B). The min. DD for *Thrinaxodon* (BP/1/1693) was observed to be on the proximal end of the femur, while peak DD originated closer to the distal end of the diaphysis (Figure 3.18: 1C). Femoral min. TD for the three *Thrinaxodon* specimens were on the extreme proximal and distal ends (Figure 3.18). *Thrinaxodon* (BP/1/1730 and BP/1/1693) peak TD was located on the midpoint of the femur diaphysis (Figure 3.18: 2B, 2C). While, *Thrinaxodon* (BP/1/7199) peak TD was on the greater trochanter of the femur (Figure 3.18: 2A).The min. EES for *Thrinaxodon* (BP/1/7199, BP/1/1730 and BP/1/1693) was located on the proximal end (Figure 3.18). The peak EES for *Thrinaxodon* (BP/1/7199) was on the distal end (Figure 3.18: 3A). However, the peak EES for *Thrinaxodon* (BP/1/1730 and BP/1/1693) were distributed from the diaphysis to the distal ends (Figure 3.18: 3B, 3C). The peak ES for (BP/1/7199) was on the lesser trochanter while *Thrinaxodon* (BP/1/1730 and BP/1/1693) distributions were the same as they were for the EES (Figure 3.18: 4A, 4B, 4C; 3.33).

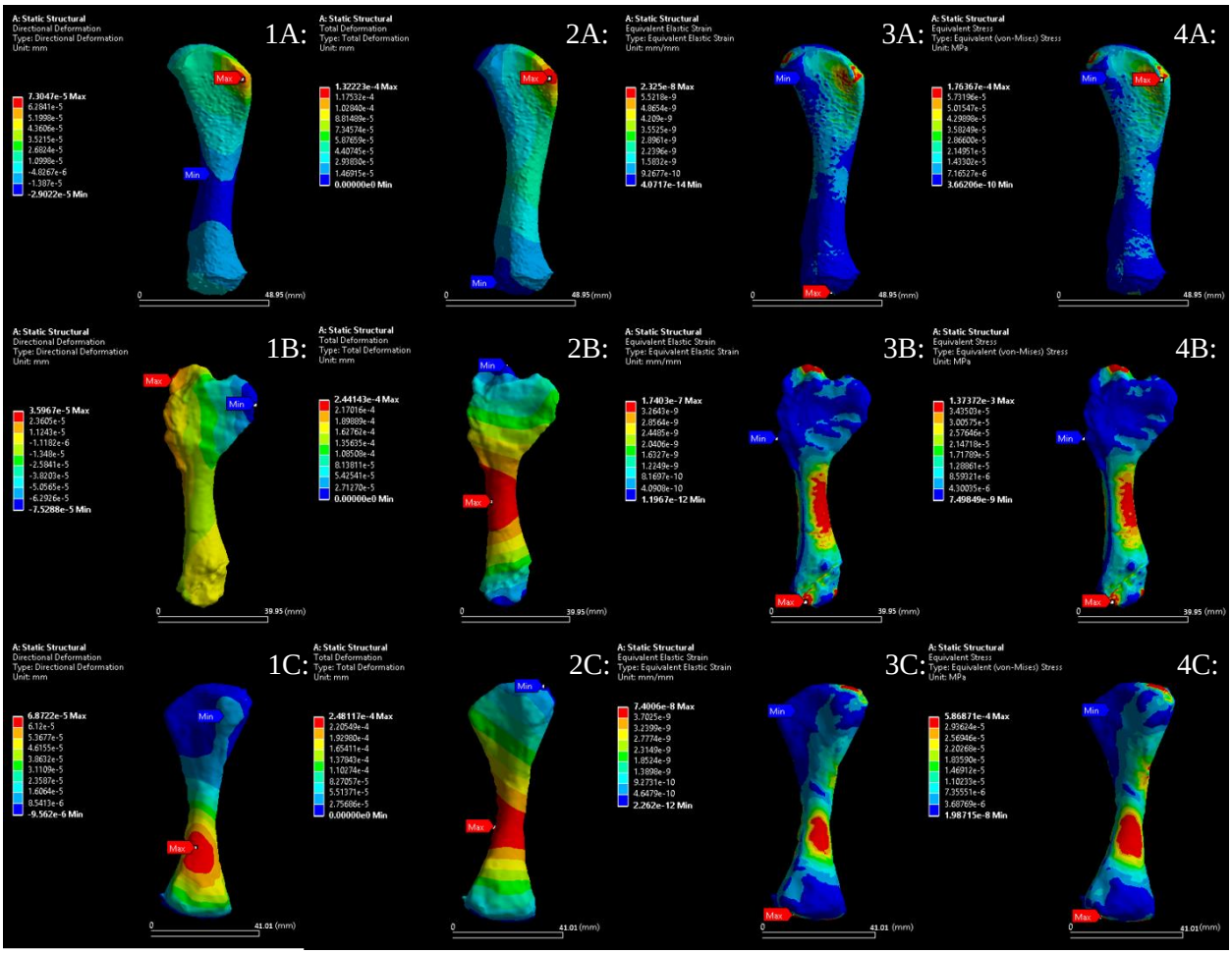


Figure 3.18: Parasagittal modelled femora of *Thrinaxodon* (A – BP/1/7199), *Thrinaxodon* (B –BP/1/1730), *Thrinaxodon* (C – BP/1/1693): DD (1A, 1B, 1C), TD (2A, 2B, 2C), EES (3A, 3B, 3C), ES (4A, 4B, 4C).The units for the calculated DD and TD range were mm, strain range was mm/mm, and stress range was MPa with the red level being the maximum - Max and the blue level being the minimum - Min. The bar at the bottom of each image represents the scale of the bone illustrated.

Cynognathus

Peak DD for *Cynognathus* (BP/1/1675) was found on the head of the femur and the min. DD was found on the diaphysis (Figure 3.19: 1). Femoral min. TD was found on the extreme proximal and distal ends, while peak TD was found on the midpoint of the femur diaphysis (Figure 3.19: 2). While their

distributions were the same, the magnitudes of EES and ES differed for the femur (Figure 3.19: 3, 4; 3.33).

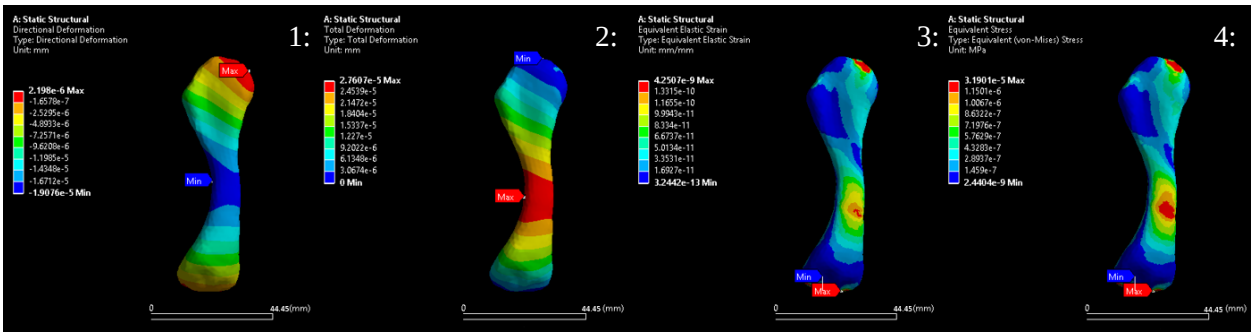


Figure 3.19: Parasagittal modelled femur of *Cynognathus*: DD (1), TD (2), EES (3), ES (4).The units for the calculated DD and TD range were mm, strain range was mm/mm, and stress range was MPa with the red level being the maximum - Max and the blue level being the minimum - Min. The bar at the bottom of each image represents the scale of the bone illustrated.

Galesaurus

The peak DD of *Galesaurus* (BP/1/4506) was observed on the distal medial side and the min. DD was on the proximal medial side (Figure 3.20: 1). The peak TD was found on the midpoint of the femur diaphysis and the min. TD was on the proximal and distal ends (Figure 3.20: 2). For EES, the peak and min. values were situated at the distal end (Figure 3.20: 3). The min. ES was observed on the distal end, while the peak ES was at the midpoint of the femoral diaphysis (Figure 3.20: 4; 3.33).

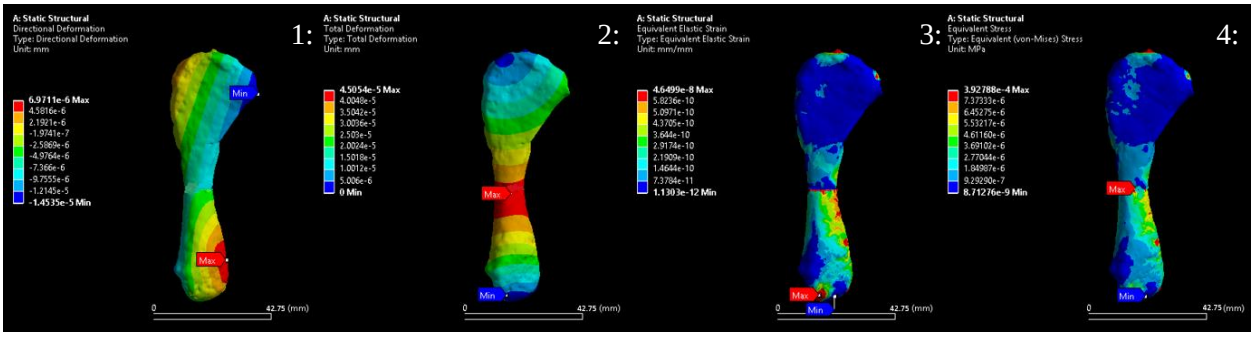


Figure 3.20: Parasagittal modelled femur of *Galesaurus*: DD (1), TD (2), EES (3), ES (4).The units for the calculated DD and TD range were mm, strain range was mm/mm, and stress range was MPa with the red level being the maximum - Max and the blue level being the minimum - Min. The bar at the bottom of each image represents the scale of the bone illustrated.

Therocephalia

Glanosuchus (BP/1/6228) exhibited a peak DD at the lateral side of the diaphysis and the min. DD was exhibited at the extreme proximal and distal end of the femur (Figure 3.21: 1A). In contrast, Therocephalia (BP/1/4335) peak DD was exhibited on the proximal end underneath the head of the femur (Figure 3.21: 1B). The min. TD for both Therocephalia taxa were exhibited on the extreme proximal and distal ends. Therocephalia (BP/1/6228 and BP/1/4335) peak TD were exhibited on the midpoint of the femur diaphysis (Figure 3.21: 2A, 2B). Peak EES was exhibited on the proximal end for both Therocephalia taxa, while min. EES was exhibited on the head of the femur for *Glanosuchus* (BP/1/6228) (Figure 3.21) and on the lesser trochanter for Therocephalia (BP/1/4335) (Figure 3.21: 3B). Peak ES for Therocephalia (BP/1/6228 and BP/1/4335) was located at the extreme proximal end of the femur (Figure 3.21: 4A, 4B; 3.33).

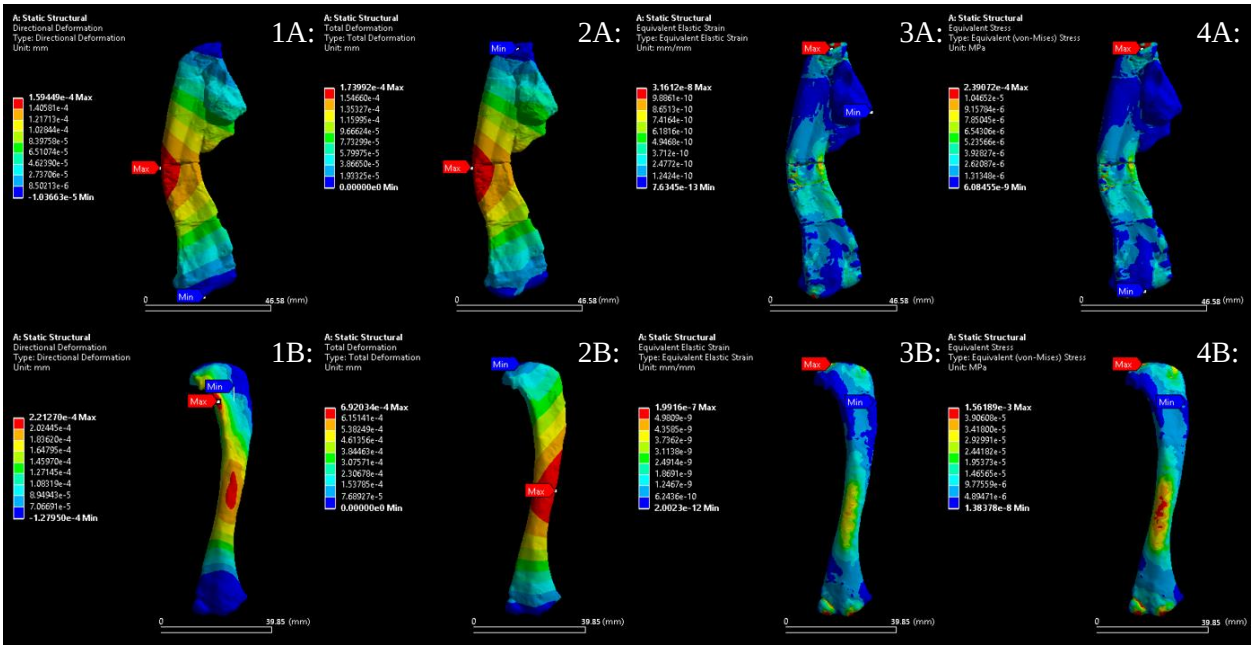


Figure 3.21: Parasagittal modelled femora of Therocephalia (*Glanosuchus* A – BP/1/6228 and *Tetracynodon darti* B – BP/1/4335): DD (1A and 1B), TD (2A and 2B), EES (3A and 3B), ES (4A and 4B).The units for the calculated DD and TD range were mm, strain range was mm/mm, and stress range was MPa with the red level being the maximum - Max and the blue level being the minimum - Min . The bar at the bottom of each image represents the scale of the bone illustrated.

Tachyglossus

For the *Tachyglossus* femur, peak DD was observed on the greater trochanter and min. DD was observed to cover most of the diaphysis (Figure 3.22: 1). Peak TD was observed on the greater trochanter of the femur and the min. TD was observed on the extreme proximal and distal ends (Figure 3.22: 2). Peak EES and ES of *Tachyglossus* were positioned on the greater trochanter of the femur, while min. EES and ES were positioned on the distal end (Figure 3.22: 3, 4; 3.33).

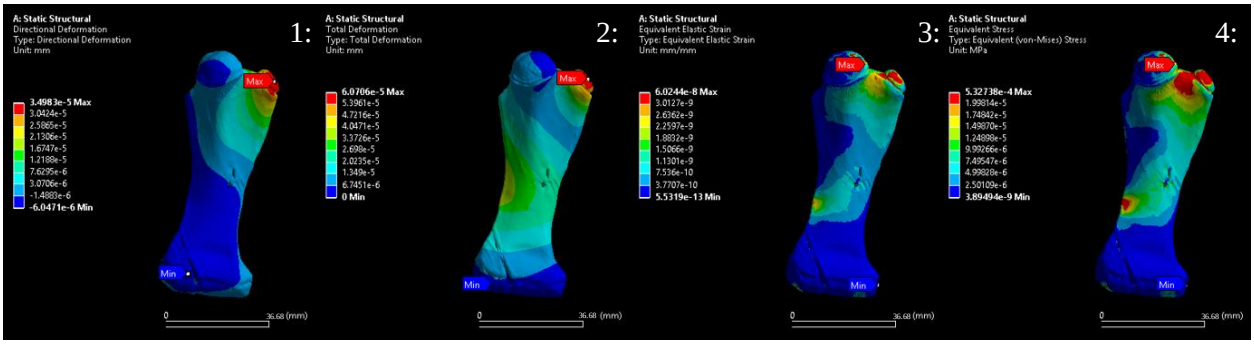


Figure 3.22: Parasagittal modelled femur of *Tachyglossus*: DD (1), TD (2), EES (3), ES (4). The units for the calculated DD and TD range were mm, strain range was mm/mm, and stress range was MPa with the red level being the maximum - Max and the blue level being the minimum - Min. The bar at the bottom of each image represents the scale of the bone illustrated.

FEA Comparative Taxa Results

The max. DD was highest for Therocephalia (BP/1/4335) and lowest for *Cynognathus* (BP/1/1675) and *Galesaurus* (BP/1/4506) (Appendix C1). There was similarity within *Thrinaxodon* for BP/1/1693 and BP/1/7199 (Appendix B1). *Thrinaxodon* (BP/1/1730) overlapped with the *Tachyglossus* femur (Appendix C1). Therocephalia (BP/1/ 4335) exhibited the highest TD (Appendix C1), while *Cynognathus* (BP/1/1675) exhibited the lowest TD, including minor overlap with *Tachyglossus* (Appendix C1). Two *Thrinaxodon* specimens were comparable for femoral TD (*Thrinaxodon* BP/1/1693 and BP/1/7130) (Appendix C1). The highest EES for the femur was exhibited by Therocephalia (BP/1/4335) and the lowest EES was exhibited by *Cynognathus* (BP/1/1675) (Appendix C1). There appears to be similarity between *Thrinaxodon* (BP/1/1693 and BP/1/7199), *Galesaurus* (BP/1/4506) and *Glanosuchus* (BP/1/6228) (Appendix C1). The highest ES was attained for Therocephalia (BP/1/4335), while *Cynognathus* (BP/1/1675) attained the lowest ES (Appendix C1). There was overlap between the femora of *Thrinaxodon* (BP/1/1693) and *Tachyglossus* at point 1 (Appendix C1). *Glanosuchus* (BP/1/6228) and *Thrinaxodon* (BP/1/7199) shared similar maximum ES of the femur (Appendix C1).

Semi-Sprawled Gait

Thrinaxodon liorhinus

Thrinaxodon (BP/1/7199, BP/1/1730 and BP/1/1693) femora exhibited the same DD locations (Figure 3.23: 1A, 1B, 1C) as were observed in the parasagittal gait models (Figure 3.18), i.e., on the lesser trochanter. For all *Thrinaxodon*, peak TD was located on the femoral diaphysis, although the *Thrinaxodon* (BP/1/7199) peak TD was located on the greater trochanter and descended to the midpoint of the diaphysis (Figure 3.23: 2A). For both EES and ES, the peak and min. distributions were the same across the femur of *Thrinaxodon* (BP/1/7199) (Figure 3.23: 3A). The distribution patterns for *Thrinaxodon* (BP/1/1730) were also the same for the EES and ES (Figure 3.23: 3B, 4B). Both EES and ES exhibited the same peak and min. locations for *Thrinaxodon* (BP/1/1693) (Figure 3.23: 4C). Locations for the peak and min. stress and strain occurred at the same locations as those for the parasagittal gait models, but differences in magnitudes were observed (Figure 3.18; 3.33).

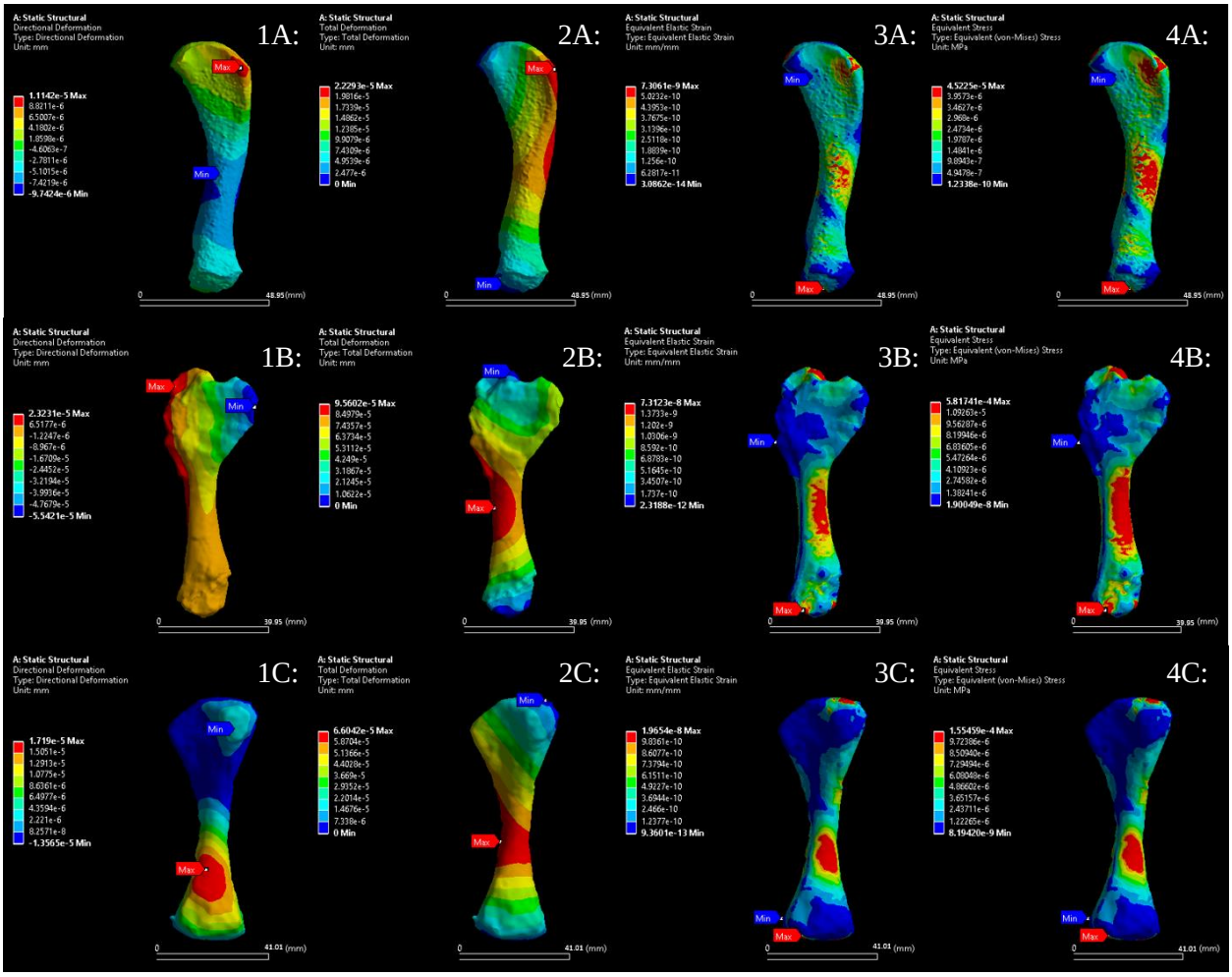


Figure 3.23: Semi-sprawled modelled femora of *Thrinaxodon* (A – BP/1/7199), *Thrinaxodon* (B –BP/1/1730), *Thrinaxodon* (C – BP/1/1693): DD (1A, 1B, 1C), TD (2A, 2B, 2C), EES (3A, 3B, 3C), ES (4A, 4B, 4C). The units for the calculated DD and TD range were mm, strain range was mm/mm, and stress range was MPa with the red level being the maximum - Max and the blue level being the minimum - Min. The bar at the bottom of each image represents the scale of the bone illustrated.

Cynognathus

The min. DD of *Cynognathus* (BP/1/1675) was found on the same location as was found in the parasagittal gait models, i.e., on the femoral diaphysis, although peak DD was found on the lesser

trochanter of the femur (Figure 3.24: 1). The min. TD was situated on the head of the femur, while the peak TD was situated on the diaphysis (Figure 3.24: 2). Locations of the EES and ES peak and min. distributions were the same, but different magnitudes were observed (Figure 3.24: 3, 4). Locations for the peak and min. stress and strain were observed at the same locations as were observed for the parasagittal gait models, but with differences in observed magnitudes (Figure 3.19; 3.33).

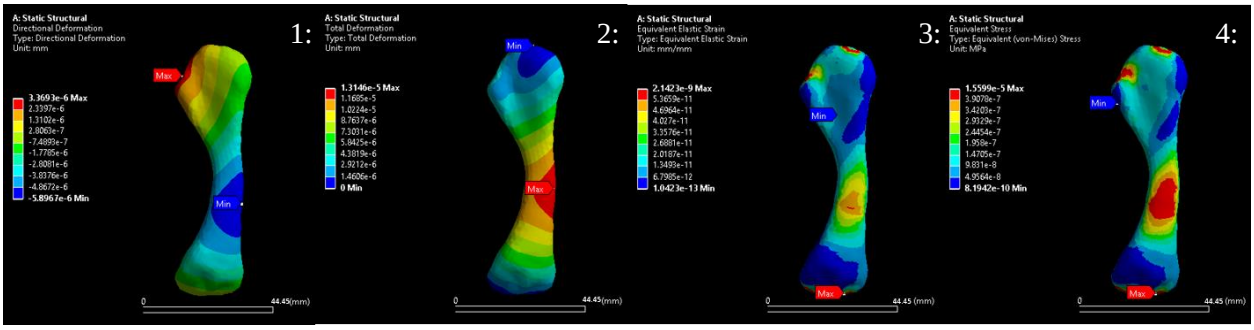


Figure 3.24: Semi-sprawled modelled femur of *Cynognathus*: DD (1), TD (2), EES (3), ES (4). The units for the calculated DD and TD range were mm, strain range was mm/mm, and stress range was MPa with the red level being the maximum - Max and the blue level being the minimum - Min. The bar at the bottom of each image represents the scale of the bone illustrated.

Galesaurus

Galesaurus (BP/1/4506) peak DD was located on the distal medial side and the min. DD was located on the lateral side of the femur (Figure 3.25: 1). Peak TD was situated at the midpoint of the diaphysis and the min. TD was situated on the distal end (Figure 3.25: 2). Locations of the peak and min. EES and ES were the same, but different magnitudes were observed (Figure 3.25: 3, 4). Locations for the peak and min. stress and strain occurred at the same locations as were observed for the parasagittal gait models, but with differences in observed magnitudes (Figure 3.20; 3.33).

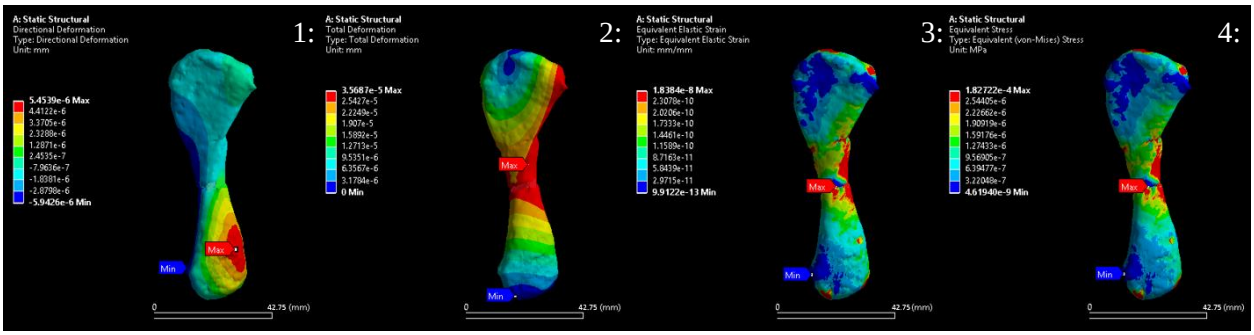


Figure 3.25: Semi-sprawled modelled femur of *Galesaurus*: DD (1), TD (2), EES (3), ES (4). The units for the calculated DD and TD range were mm, strain range was mm/mm, and stress range was MPa with the red level being the maximum - Max and the blue level being the minimum - Min. The bar at the bottom of each image represents the scale of the bone illustrated.

Therocephalia

Locations of the DD and TD for the femur of *Glanosuchus* (BP/1/6228) were observed to be the same (Figure 3.26: 1A). Therocephalia (BP/1/4335) min. DD had the same location as was observed in the parasagittal gait model, however, the peak DD was observed on the diaphysis of the femur (Figure 3.26: 1B). The peak TD for Therocephalia (BP/1/4335) occurred at the midpoint of the diaphysis (Figure 3.26: 2B). The locations were the same for peak and min. EES and ES for *Glanosuchus* (BP/1/6228) (Figure 3.26: 3A, 4A). For Therocephalia (BP/1/4335), the peak and min. EES and ES were on the proximal end of the femur (Figure 3.26: 3B, 4B). Locations for peak and min. stress and strain occurred at the same locations as for the parasagittal gait model, but with differences in observed magnitude (Figure 3.21; 3.33).

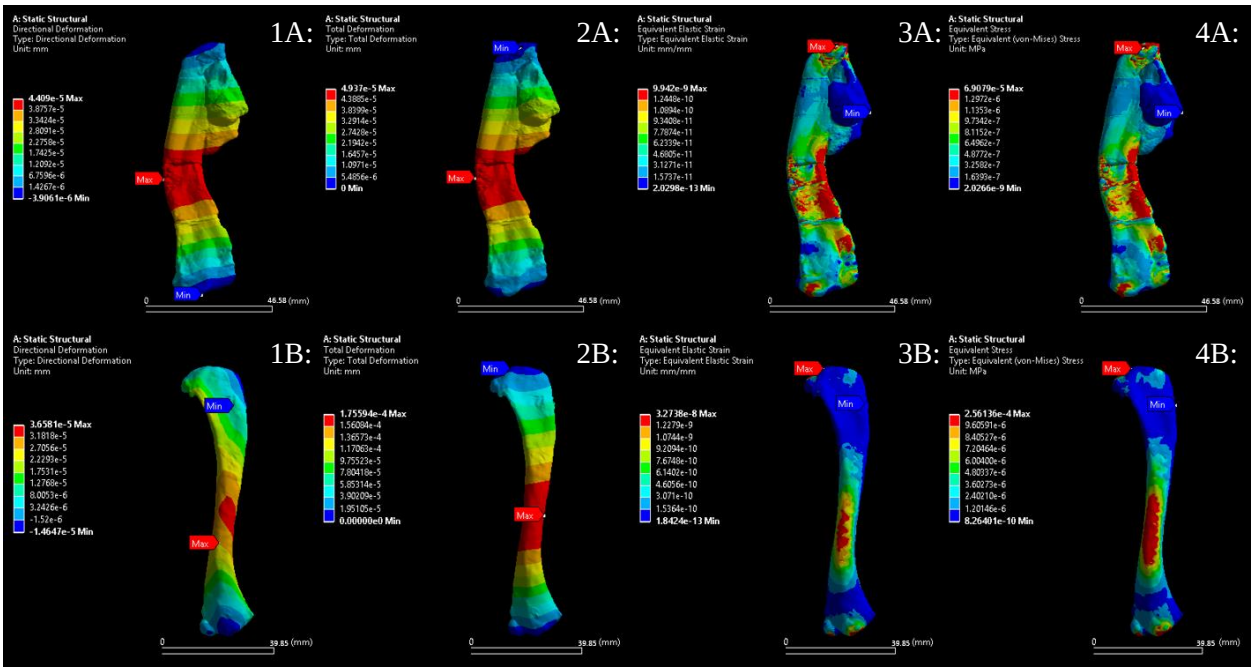


Figure 3.26: Semi-sprawled modelled femora of Therocephalia (*Glanosuchus* A – BP/1/6228 and *Tetracynodon darti* B – BP/1/4335): DD (1A and 1B), TD (2A and 2B), EES (3A and 3B), ES (4A and 4B). The units for the calculated DD and TD range were mm, strain range was mm/mm, and stress range was MPa with the red level being the maximum - Max and the blue level being the minimum - Min. The bar at the bottom of each image represents the scale of the bone illustrated.

Tachyglossus

Peak DD for the *Tachyglossus* femur was located on the greater trochanter, which is in contrast to the location in the parasagittal gait model; the min. DD was reduced to an area closer to the distal end of the diaphysis in the semi-sprawled model (Figure 3.27: 1). Peak TD was observed on the diaphysis of the femur (Figure 3.27: 2). Locations of the EES and ES were the same, but different magnitudes were observed (Figure 3.27: 3, 4). Locations for the peak and min. stress and strain occurred at the same locations as those for the parasagittal gait model, but with differences in observed magnitudes (Figure 3.22; 3.33).

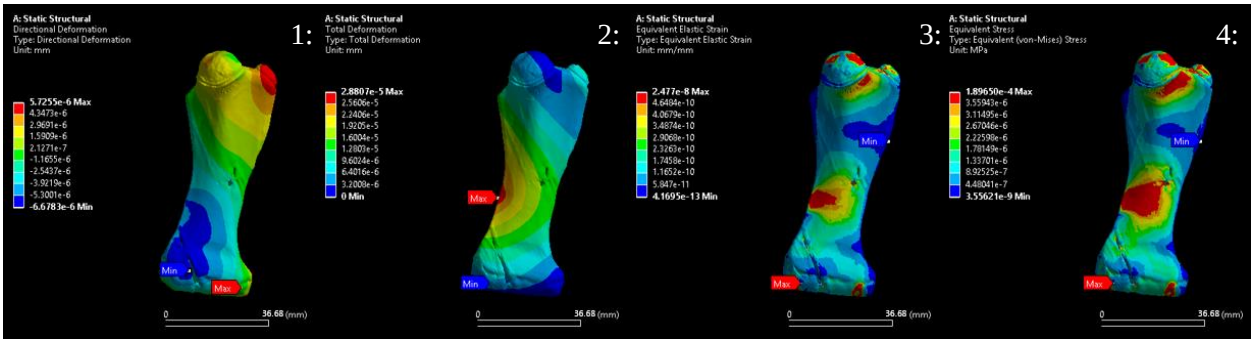


Figure 3.27: Semi-sprawled modelled femur of *Tachyglossus*: DD (1), TD (2), EES (3), ES (4). The units for the calculated DD and TD range were mm, strain range was mm/mm, and stress range was MPa with the red level being the maximum - Max and the blue level being the minimum - Min. The bar at the bottom of each image represents the scale of the bone illustrated.

FEA Comparative Taxa Results

The highest DD was exhibited by *Glanosuchus* (BP/1/6228) and the lowest was exhibited by *Cynognathus* (BP/1/1675) (Appendix C2). There was overlap between femora of *Galesaurus* (BP/1/4506) and *Tachyglossus* (Appendix C2). The highest TD was exhibited by Therocephalia (BP/1/4335) and the lowest was exhibited by *Cynognathus* (BP/1/1675) (Appendix C2). There was overlap for TD between *Thrinaxodon* (BP/1/7199) and *Tachyglossus* (Appendix C2). The highest EES for the femur was obtained for *Thrinaxodon* (BP/1/1730), while the lowest EES was obtained for *Cynognathus* (BP/1/1675) (Appendix C2). There was overlap in femoral EES between *Thrinaxodon* (BP/1/1693) and *Galesaurus* (BP/1/4506), and also between *Glanosuchus* (BP/1/6228) and *Thrinaxodon* (BP/1/7199) (Appendix C2). *Thrinaxodon* (BP/1/1730) was found to have the highest femoral ES and *Cynognathus* (BP/1/1675) was found to have the lowest femoral ES (Appendix C2).

Sprawled Gait

Thrinaxodon liorhinus

The lowest min. DD observed in the femur of *Thrinaxodon* (BP/1/7199) (Figure 3.28: 1A). *Thrinaxodon* (BP/1/1730) exhibited the same locations of properties as were observed in the semi-sprawled gait (Figure 3.28: 1B). The min. DD exhibited a reduced area on the femur in contrast to the min. DD that were observed in the semi-sprawled gait models (Figure 3.23). The min. TD for the femora were situated on the extreme proximal and distal ends, as were seen in the parasagittal and semi-sprawled gait models (Figure 3.18, Figure 3.23 and Figure 3.28). *Thrinaxodon* (BP/1/7199, BP/1/1730 and BP/1/1693) peak TD were located on the lateral side of the diaphysis (Figure 3.28: 2A, 2B, 2C). Locations of the EES (Figure 3.28: 3A, 3B, 3C) and ES (Figure 3.28: 4A, 4B, 4C) had similar distributions along the femora of *Thrinaxodon* (BP/1/7199, BP/1/1730 and BP/1/1693). However, magnitudes of the EES and ES differed for each of the specimens. Locations for the peak and min. stress and strain occurred at the same locations as were observed for the parasagittal gait models, but with differences in observed magnitudes (Figure 3.18; 3.23; 3.33).

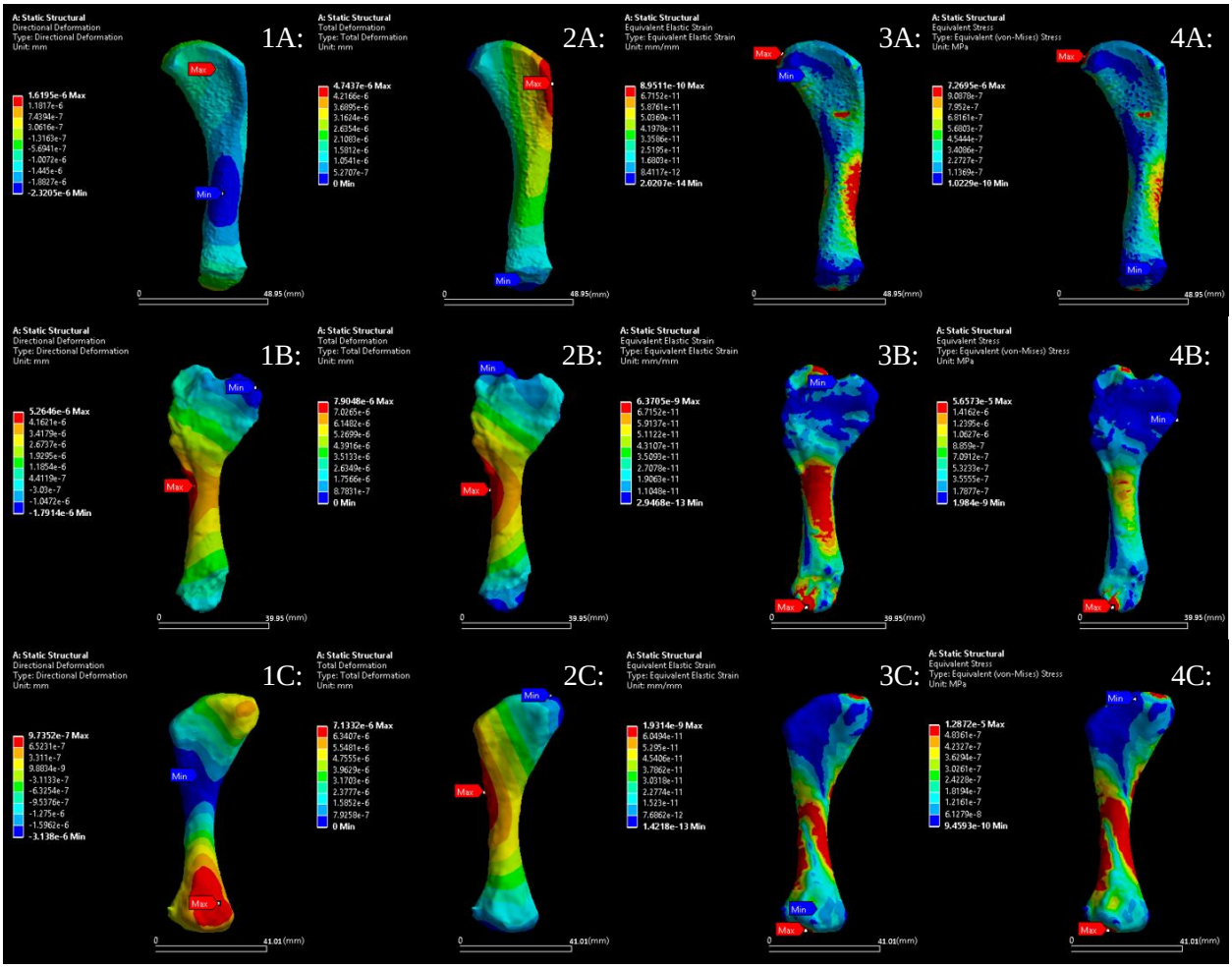


Figure 3.28: Sprawled modelled femora of *Thrinaxodon* (A – BP/1/7199), *Thrinaxodon* (B – BP/1/1730), *Thrinaxodon* (C – BP/1/1693): DD (1A, 1B, 1C), TD (2A, 2B, 2C), EES (3A, 3B, 3C), ES (4A, 4B, 4C). The units for the calculated DD and TD range were mm, strain range was mm/mm, and stress range was MPa with the red level being the maximum - Max and the blue level being the minimum - Min . The bar at the bottom of each image represents the scale of the bone illustrated.

Cynognathus

The peak DD was situated on the proximal end of *Cynognathus* (BP/1/1675) femur (Figure 3.29: 1). The min. TD was situated on the extreme proximal and distal ends, as was seen in the parasagittal

(Figure 3.19) and semi-sprawled gait models (Figure 3.24). The peak TD was observed on the midpoint of the femoral diaphysis (Figure 3.29: 2). Locations of the EES and ES were the same as those for the peak and min (Figure 3.29: 3, 4). Locations for the peak and min. stress and strain occurred at the same locations as those observed for the parasagittal gait model, but with differences in observed magnitudes (Figure 3.19; 3.34; 3.33).

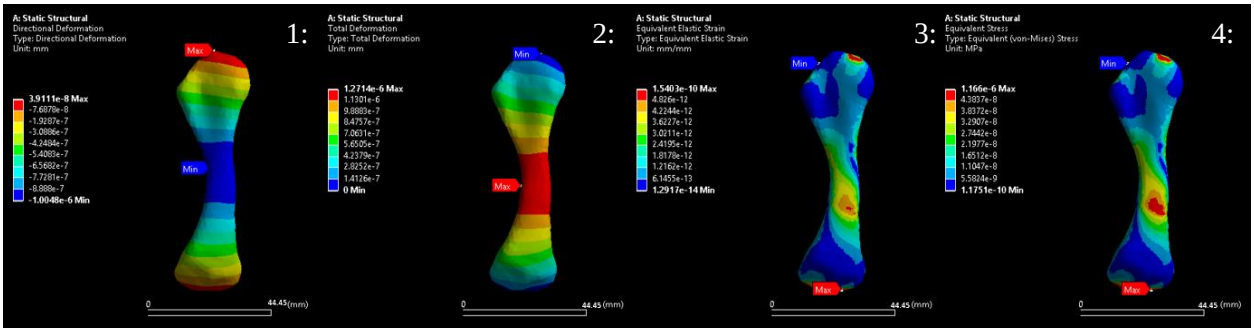


Figure 3.29: Sprawled modelled femur of *Cynognathus*: DD (1), TD (2), EES (3), ES (4). The units for the calculated DD and TD range were mm, strain range was mm/mm, and stress range was MPa with the red level being the maximum - Max and the blue level being the minimum - Min. The bar at the bottom of each image represents the scale of the bone illustrated.

Galesaurus

Galesaurus (BP/1/4506) min. DD was observed on the lateral side of the femur, while peak DD was observed on the lesser trochanter (Figure 3.30: 1). The min. TD for the femur was situated on the extreme proximal and distal ends, as was seen in the parasagittal (Figure 3.20) and semi-sprawled gait models (Figure 3.25). The peak TD was observed on the midpoint of the femoral diaphysis (Figure 3.30: 2). Locations of the EES and ES occurred in the same locations as for the peak and min (Figure 3.30: 3, 4). Locations for the peak and min. stress and strain occurred at the same locations as those for the parasagittal gait model, but with differences in observed magnitudes (Figure 3.20; 3.25; 3.33).

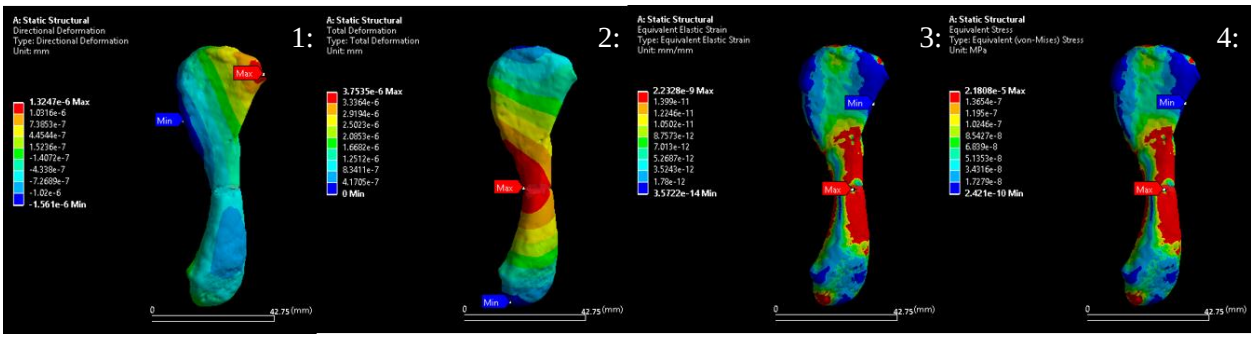


Figure 3.30: Sprawled modelled femur of *Galesaurus*: DD (1), TD (2), EES (3), ES (4). The units for the calculated DD and TD range were mm, strain range was mm/mm, and stress range was MPa with the red level being the maximum - Max and the blue level being the minimum - Min. The bar at the bottom of each image represents the scale of the bone illustrated.

Therocephalia

Locations of the peak and min. DD for the *Glanosuchus* (BP/1/6228) femur were the same as those observed in the parasagittal and semi-sprawled gait models (Figure 3.31: 1A). The peak and min. DD for Therocephalia (BP/1/4335) occurred at the same locations as were observed in the semi-sprawled gait model, although the position of peak stress increased in magnitude (Figure 3.31: 1B). The min. TD for the femur was situated on the extreme proximal and distal ends, as was seen in the parasagittal and semi-sprawled gait models. The peak TD was situated on the midpoint of the femur diaphysis for Therocephalia (BP/1/6228 and BP/1/4335) (Figure 3.31: 2A, 2B). Locations of the peak and min. EES and ES were the same as those for *Glanosuchus* (BP/1/6228) (Figure 3.31: 3A, 4A). Locations of the peak and min. EES and ES were the same as those for Therocephalia (BP/1/4335), however, their magnitudes differed (Figure 3.31: 3B, 4B). Locations for the peak and min. stress and strain occurred at the same locations as those for the parasagittal gait model, but with differences in observed magnitudes (Figure 3.21; 3.26; 3.33).

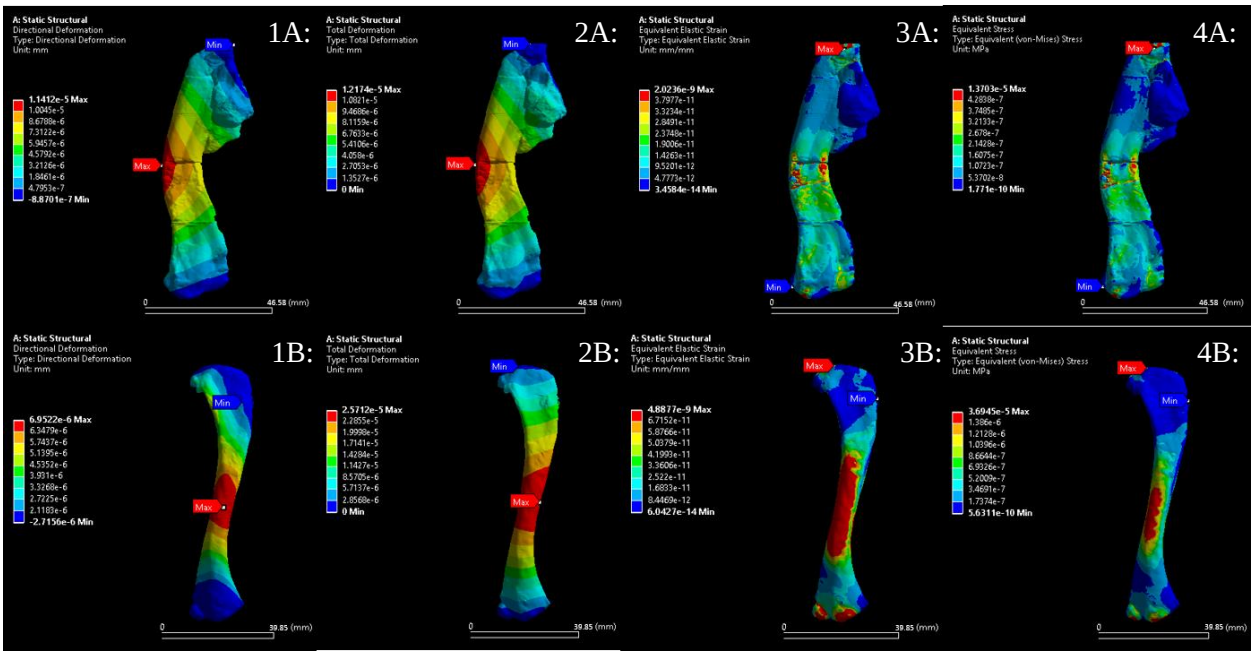


Figure 3.31: Sprawled modelled femora of Therocephalia (*Glanosuchus* A – BP/1/6228 and *Tetracynodon darti* B – BP/1/4335): DD (1A and 1B), TD (2A and 2B), EES (3A and 3B), ES (4A and 4B). The units for the calculated DD and TD range were mm, strain range was mm/mm, and stress range was MPa with the red level being the maximum - Max and the blue level being the minimum - Min . The bar at the bottom of each image represents the scale of the bone illustrated.

Tachyglossus

The location of the min. DD (Figure 3.32: 1) of *Tachyglossus* resembled the same location, i.e., on the diaphysis, as was seen in the parasagittal gait model (Figure 22). The min. TD (Figure 3.32: 2) for the femur was situated on the extreme proximal and distal ends, as was seen in the parasagittal (Figure 3.22) and semi-sprawled gait models (Figure 3.27). *Tachyglossus* peak TD was located on the lateral side of the diaphysis (Figure 3.32: 2). Locations of the peak and min. EES (Figure 3.32: 3) and ES (Figure 3.32: 4) were the same. Locations for the peak and min. stress and strain occurred at the same locations as those for the parasagittal gait model, but with differences in observed magnitude (Figure 3.22; 3.27; 3.33).

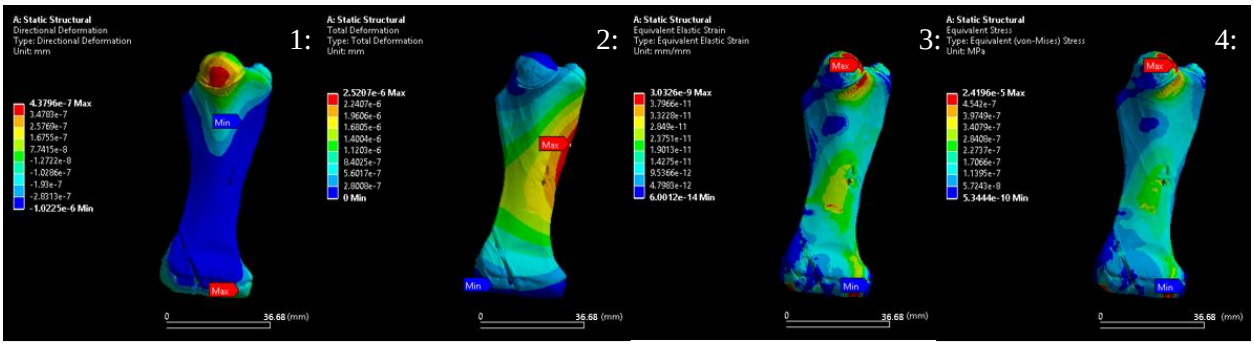


Figure 3.32: Sprawled modelled femur of *Tachyglossus*: DD (1), TD (2), EES (3), ES (4). The units for the calculated DD and TD range were mm, strain range was mm/mm, and stress range was MPa with the red level being the maximum - Max and the blue level being the minimum - Min. The bar at the bottom of each image represents the scale of the bone illustrated.

FEA Comparative Taxa Results

Glanosuchus (BP/1/6228) was found to have the highest femoral DD (Appendix C3). There was comparability among the femoral DD for *Cynognathus* (BP/1/1675), *Thrinaxodon* (BP/1/1693 and BP/1/7199), *Galesaurus* (BP/1/4506) and *Tachyglossus* (Appendix C3). Therocephalia (BP/1/4335) was observed to have the highest TD, while *Cynognathus* (BP/1/1675) was observed to have the lowest TD (Appendix C3). There was overlap for femoral TD between *Thrinaxodon* specimens (BP/1/1693 and BP/1/1730). *Galesaurus* (BP/1/4506) femoral TD was found to overlap with that of *Thrinaxodon* (BP/1/7199) (Appendix C3). *Thrinaxodon* (BP/1/1730) was found to have the highest femur EES, while *Cynognathus* (BP/1/675) was found to have the lowest (Appendix C3). *Thrinaxodon* (BP/1/1693), *Galesaurus* (BP/1/4506), *Glanosuchus* (BP/1/6228) and *Tachyglossus* overlapped in femoral EES (Appendix C3). *Thrinaxodon* (BP/1/1730) had the highest ES, while *Cynognathus* (BP/1/1675) had the lowest (Appendix C3).

Comparison of the femoral FEA Results for the different gaits analysed for each taxa

ANOVA

The overall group of fossil taxa exhibited statistically significant differences for EES and ES between the parasagittal, semi-sprawled and sprawled gait models ($p < 0.001$) (Appendix D). Even after a Bonferroni correction of the p-value ($p = 0.0167$), it was clear that one or more species modelled with parasagittal vs. sprawled gait differed. When the comparative extant species (*Tachyglossus*) was included in the ANOVA, the significant difference in properties among the different gait models remained the same ($p < 0.001$) (Appendix D).

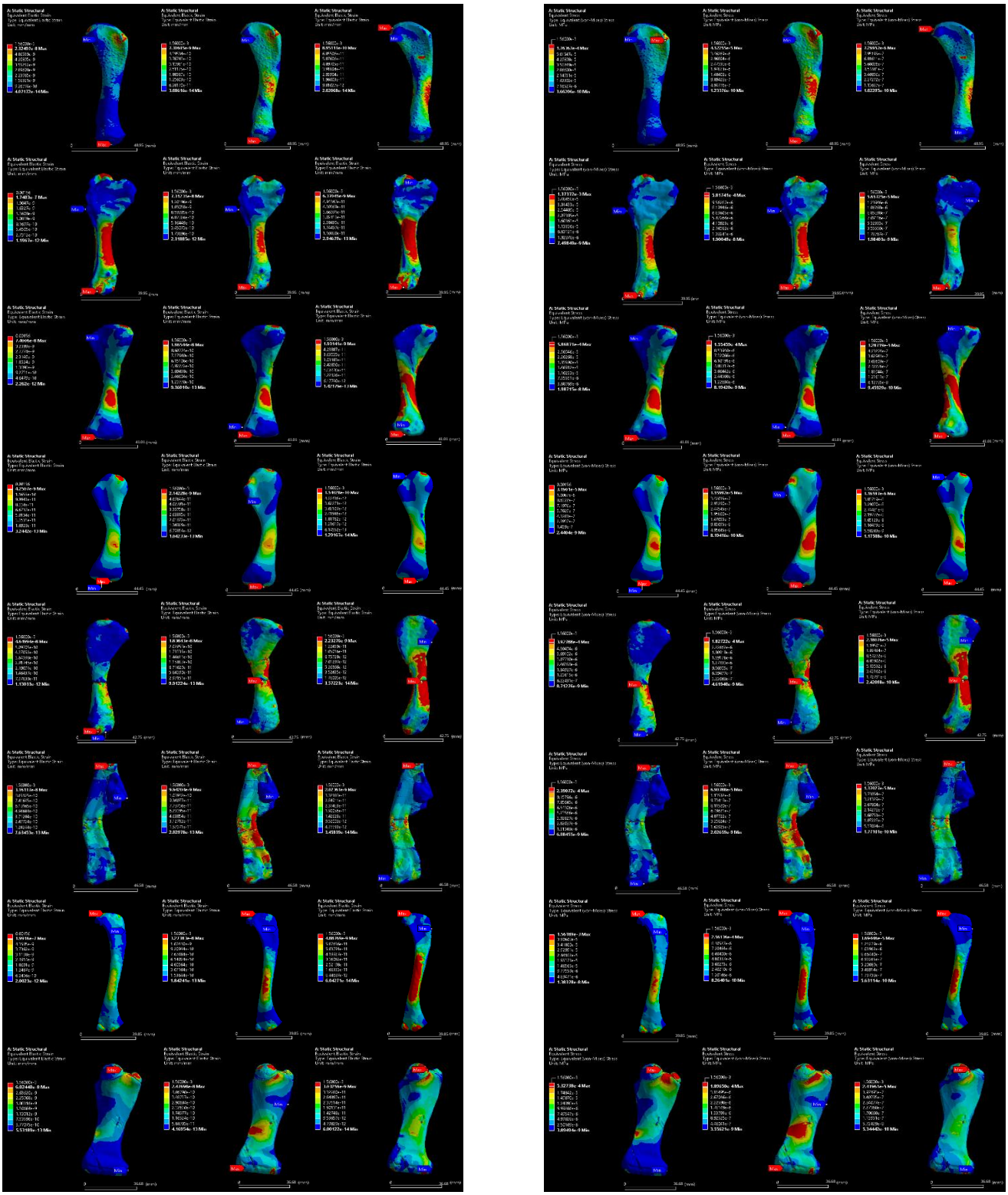


Figure 3.33: EES and ES comparative gaits models for each species; from left to right: Femora – parasagittal, semi-sprawled, sprawled gaits scaled to the maximum magnitude of 1.56e-3: *Thrinaxodon* (BP/1/7199 – D1, 2, 3; BP/1/1730 – D4, 5, 6; BP/1/1693 – D7, 8, 9), *Cynognathus* (BP/1/1675 – D10, 11, 12), *Galesaurus* (BP/1/4506 – D13, 14, 15), Therocephalia (BP/1/6228 – D16, 17, 18; BP/1/4335 – D19, 20, 21) and *Tachyglossus* (D22, 23, 24).

Summary of overall humeri and femora EES and ES

The *Cynognathus* (BP/1/1675) humerus exhibited the highest parasagittal strain and stress (Figure 3.34), however, its femur exhibited the lowest parasagittal strain and stress (Figure 3.34). *Thrinaxodon* (BP/1/1693) exhibited a humerus that experienced the same strain and stress for the parasagittal and semi-sprawled gait models (Figure 3.34). The *Tachyglossus* humerus underwent similar magnitudes of strain for all three gait conditions that were considered (Figure 3.34). *Tetracynodon darti* (BP/1/4335) had the highest parasagittal strain and stress for femora (Figure 3.34). *Thrinaxodon* (BP/1/1730) had the highest strain and stress among the semi-sprawled femoral models (Figure 3.34). The semi-sprawled and sprawled femoral models exhibited a strain and stress for *Glanosuchus* (BP/1/6228) that were similar to each other (Figure 3.34). This pattern was also observed in the *Thrinaxodon* (BP/1/7199) femur (Figure 3.34). Parasagittal gait models generally exhibited stress and strain for the taxa that proved to be higher than those exhibited for the semi-sprawled and sprawled gait models (Figure 3.34).

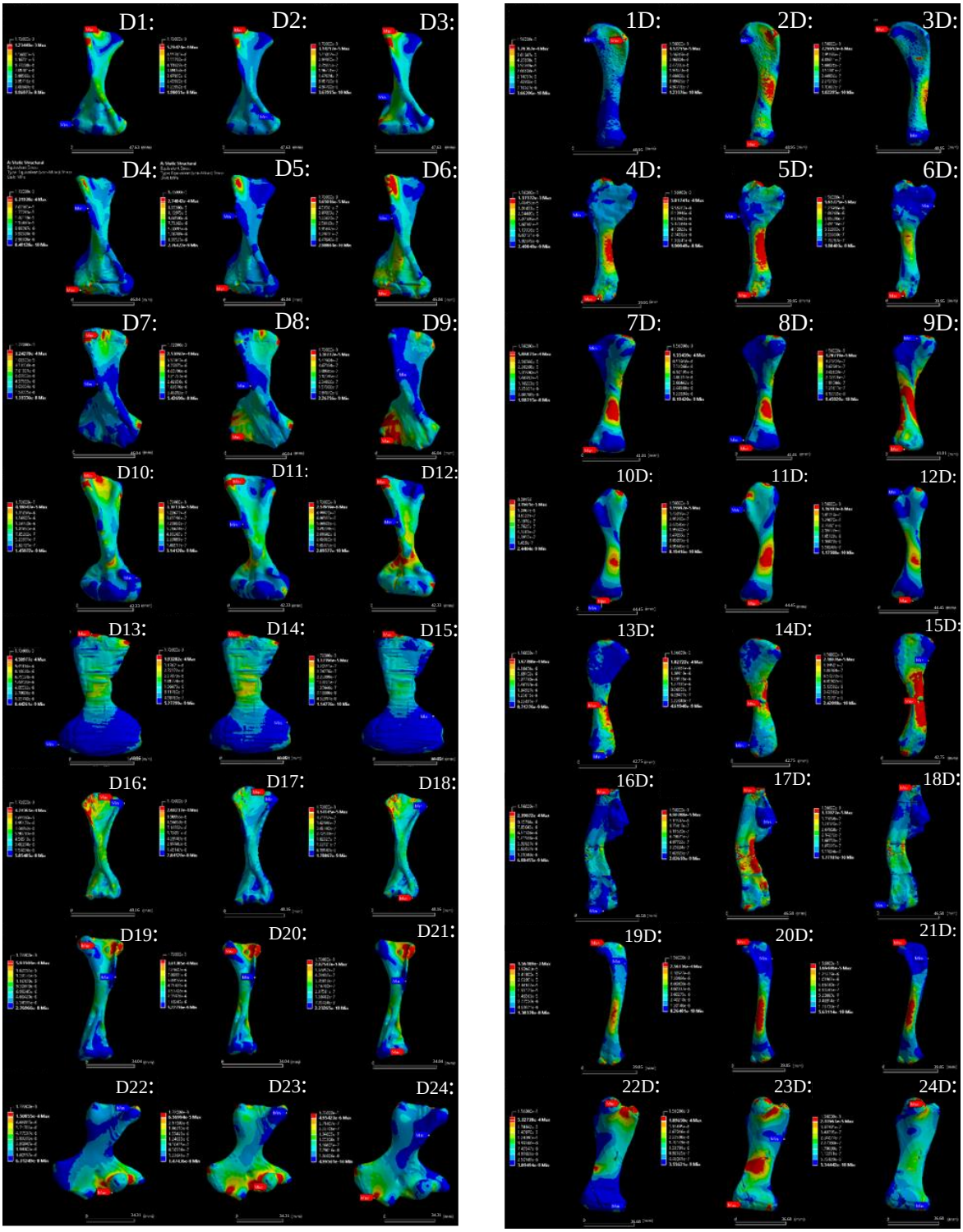


Figure 3.34: Limb differentiation EES and ES comparative gaits models for each species; from left to right: Humeri - parasagittal, semi sprawled, sprawled gaits scaled to the maximum magnitude of 1.72e-3.Femora – parasagittal, semi sprawled, sprawled gaits scaled to the maximum magnitude of 1.56e-3: *Thrinaxodon* (BP/1/7199 – D1, 2, 3; BP/1/1730 – D4, 5, 6;BP/1/1693 – D7, 8, 9), *Cynognathus* (BP/1/1675 – D10, 11, 12), *Galesaurus*(BP/1/4506 – D13, 14, 15),Therocephalia (BP/1/6228 – D16, 17, 18; BP/1/4335 – D19, 20, 21) and *Tachyglossus* (D22, 23, 24).

Cross-sectional Properties

Note: all cross-sectional properties (i.e., I_x, I_y, I_{max}, and I_{min}) were size-standardized by taking the natural log of the variable divided by length to the fourth power.

Humerus

Anteroposterior (AP) bending rigidity [sI_x]

The three *Thrinaxodon* humeri varied in AP bending rigidity between 10.72 and 11.32 (Table 3.1). *Cynognathus* AP bending rigidity lies within the *Thrinaxodon* bending rigidity range (Figure 3.35). Therocephalia species were found to exhibit the highest bending rigidity in the AP direction among all the humeri (Figure 3.35). The *Tachyglossus* humerus exhibited the lowest AP bending rigidity (7.86) when compared to those of other species (Figure 3.35 and Table 3.1).

Mediolateral (ML) bending rigidity [sI_y]

The three *Thrinaxodon* humeri varied in ML bending rigidity between 10.48 and 11.51, which was overall similar to the observed range of AP bending rigidity values (Table 3.1). The *Galesaurus* forelimb exhibited higher ML bending rigidity than AP bending rigidity (Figure 3.35). The highest ML humeral bending rigidity that was observed occurred in the Therocephalia species (Figure 3.35). The *Tachyglossus* humerus exhibited the lowest ML bending rigidity (8.41), which was slightly higher than its AP bending rigidity (Figure 3.35).

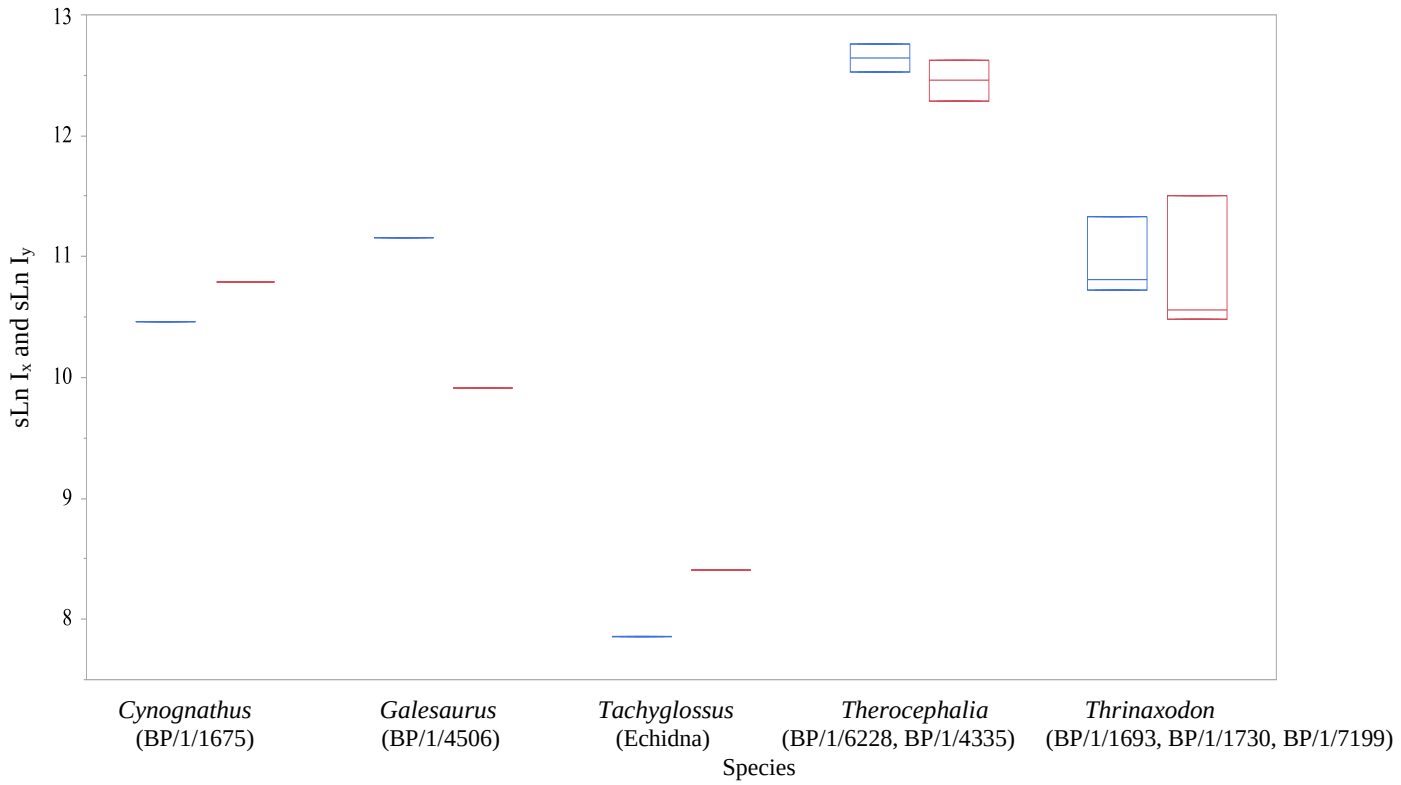


Figure 3.35: Box plot of the size-standardized anteroposterior (AP) bending rigidity [(sLn I_x)] and mediolateral (ML) bending rigidity [(sLn I_y)] for the humeri at 50% region of interest. □ - I_x and □ - I_y

Rigidity index (I_y/ I_x) and shape ratio (I_{max}/I_{min})

The rigidity index for *Thrinaxodon* humeri varied between 0.97 and 1.02, which further exemplified their equivalent rigidities in these two anatomical planes (Table 3.1). *Tachyglossus* had the highest humeral rigidity index of 1.07, while *Galesaurus* had the lowest humeral rigidity index of 0.89 (Figure 3.36). This demonstrates their greater discrepancies in rigidities in the two anatomical planes compared to humeri of other taxa. The humeral shape ratios for the taxa under investigation ranged between 0.87 and 0.98 (Figure 3.36).

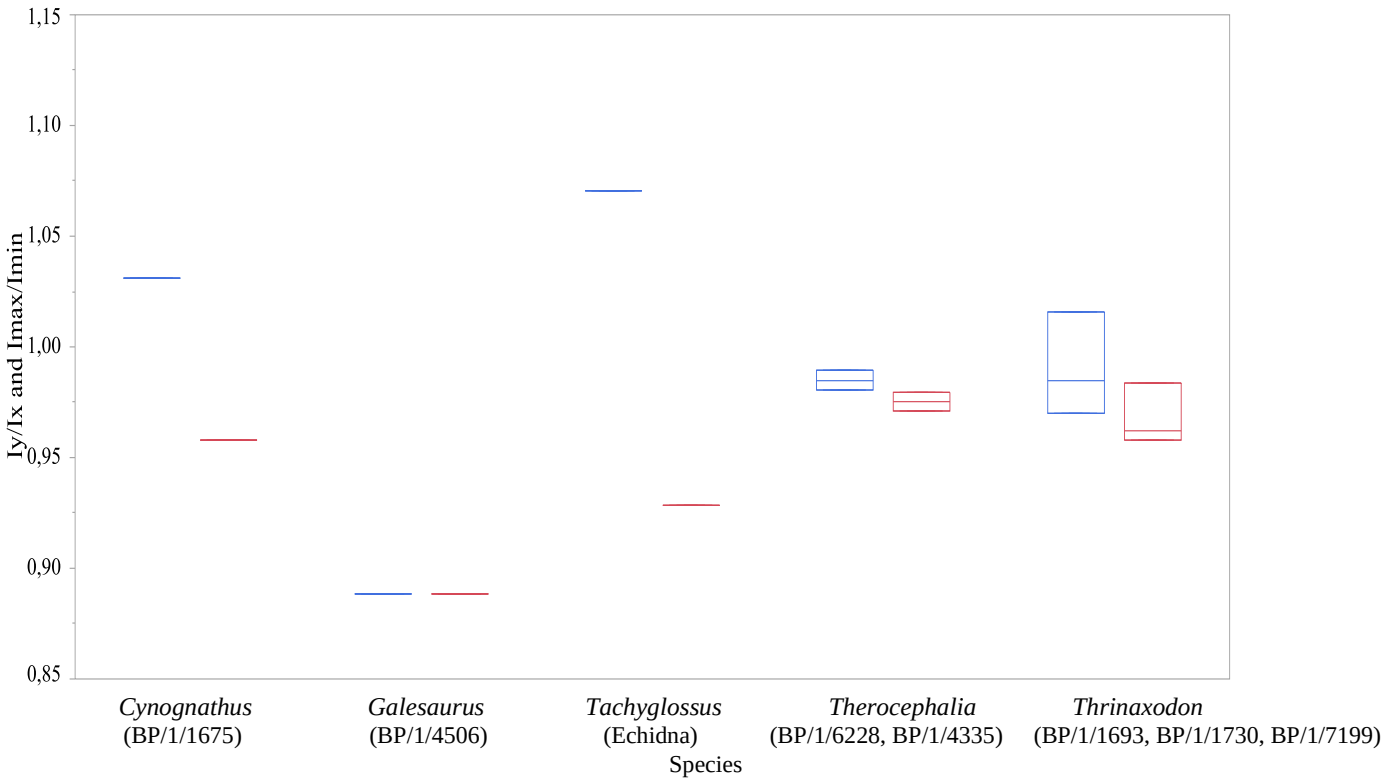


Figure 3.36: Box plot of the humeral ratios of second moments of area (I_y/I_x) and principal moments of area (I_{max}/I_{min}) at the 50% region of interest. ☐ - I_y/I_x and ☐ - I_{max}/I_{min}

Polar moment of area, torsional rigidity (sLn J) and Average bending rigidity (J/2)

Two *Thrinaxodon* humeri (BP/1/1693 and BP/1/7199) exhibited similar torsional rigidity: 9.94. Therocephalia species had the highest humeral torsional rigidity at just over 11.15 (Figure 3.37). The lowest humeral torsional rigidity was observed in *Tachyglossus* 7.4 (Figure 3.37).

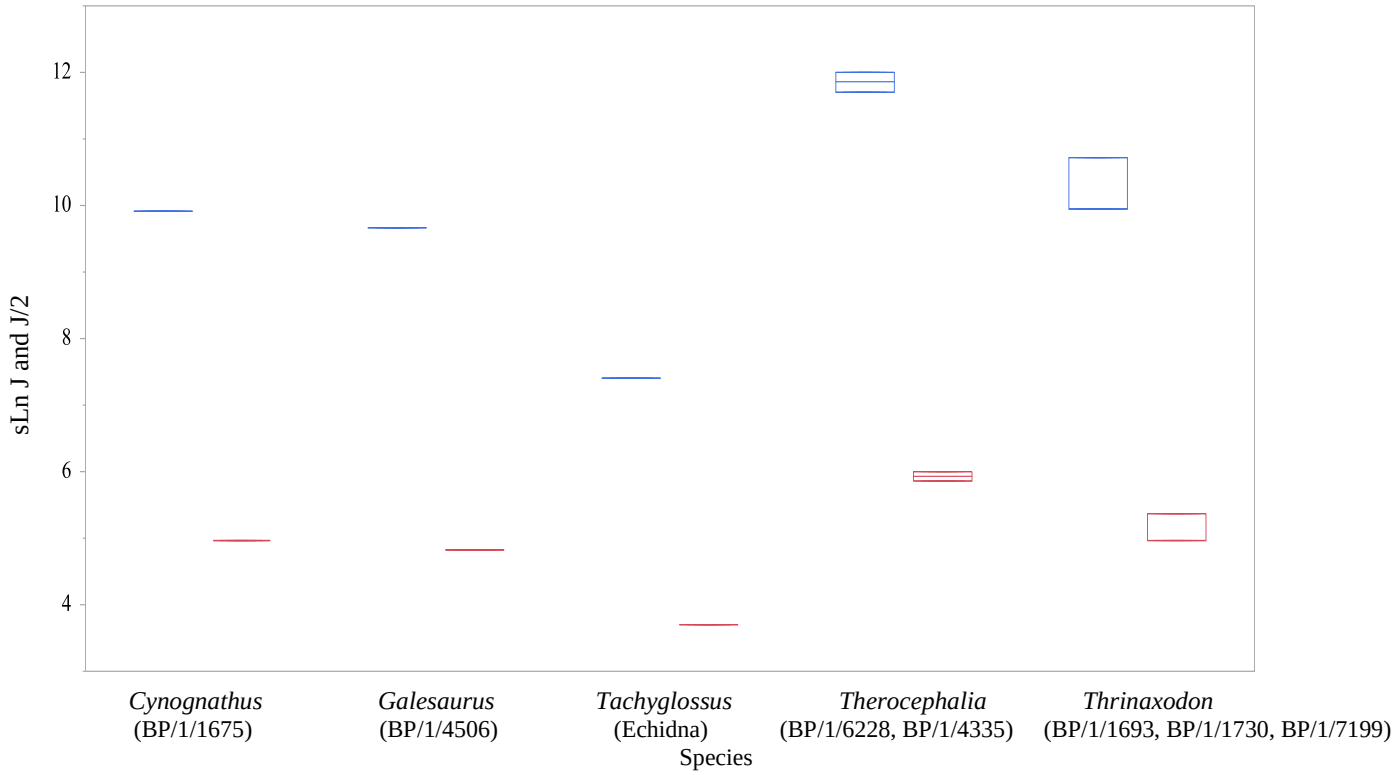


Figure 3.37: Box plot of the size-standardized humeral polar moment of area, torsional rigidity (sLn J) and average bending rigidity (J/2) at the 50% region of interest. □ - sLnJ and □ - J/2

Table 3.1: Size-standardized cross-sectional properties of humeri at the 50% region of interest.

Species	sl_x	sl_y	sI_{max}	sI_{min}	I_y/I_x	I_{max}/I_{min}	sLn J	J/2
Cynognathus BPI1675	10,465	10,789	10,412	10,867	1,030	0,958	9,921	4,960
Thrinaxodon BPI1693	10,810	10,484	10,448	10,862	0,969	0,961	9,941	4,970
Thrinaxodon BPI1730	11,328	11,508	11,326	11,511	1,015	0,983	10,721	5,360
Therocephalia BPI4335	12,528	12,285	12,232	12,599	0,980	0,970	11,706	5,853
Galesaurus BPI4506	11,155	9,912	9,911	11,158	0,888	0,888	9,659	4,829
Therocephalia BPI6228	12,761	12,624	12,568	12,829	0,989	0,979	11,997	5,998
Thrinaxodon BPI7199	10,723	10,558	10,433	10,893	0,984	0,957	9,944	4,972
Tachyglossus Echidna	7,855	8,408	7,837	8,440	1,070	0,928	7,400	3,700

*I_x, I_y, I_{max}, I_{min} and J were size-standardized by taking the natural log of the variable divided by length to the fourth power.

Femur

Anteroposterior (AP) bending rigidity [sI_x]

The three *Thrinaxodon* femora varied between 11.07 and 11.79 (Table 3.2). *Cynognathus* and *Galesaurus* femora exhibited similar AP bending rigidities (Figure 3.38). The Therocephalia femora exhibited the highest bending rigidity in the AP direction (Figure 3.38). The *Tachyglossus* femur exhibited the lowest AP bending rigidity (10.64) (Figure 3.38).

Mediolateral (ML) bending rigidity [sI_y]

Thrinaxodon femoral ML bending rigidities ranged between 10.79 and 11.46, which was overall similar to the observed range of AP bending rigidity values (Table 3.2). The *Galesaurus* femora also exhibited similar AP and ML bending rigidities (Figure 3.38). The highest femoral ML bending rigidity was observed in Therocephalia (Figure 3.38). The *Tachyglossus* femur exhibited the lowest ML bending rigidity (9.57), which was slightly lower than its AP bending rigidity (Figure 3.38).

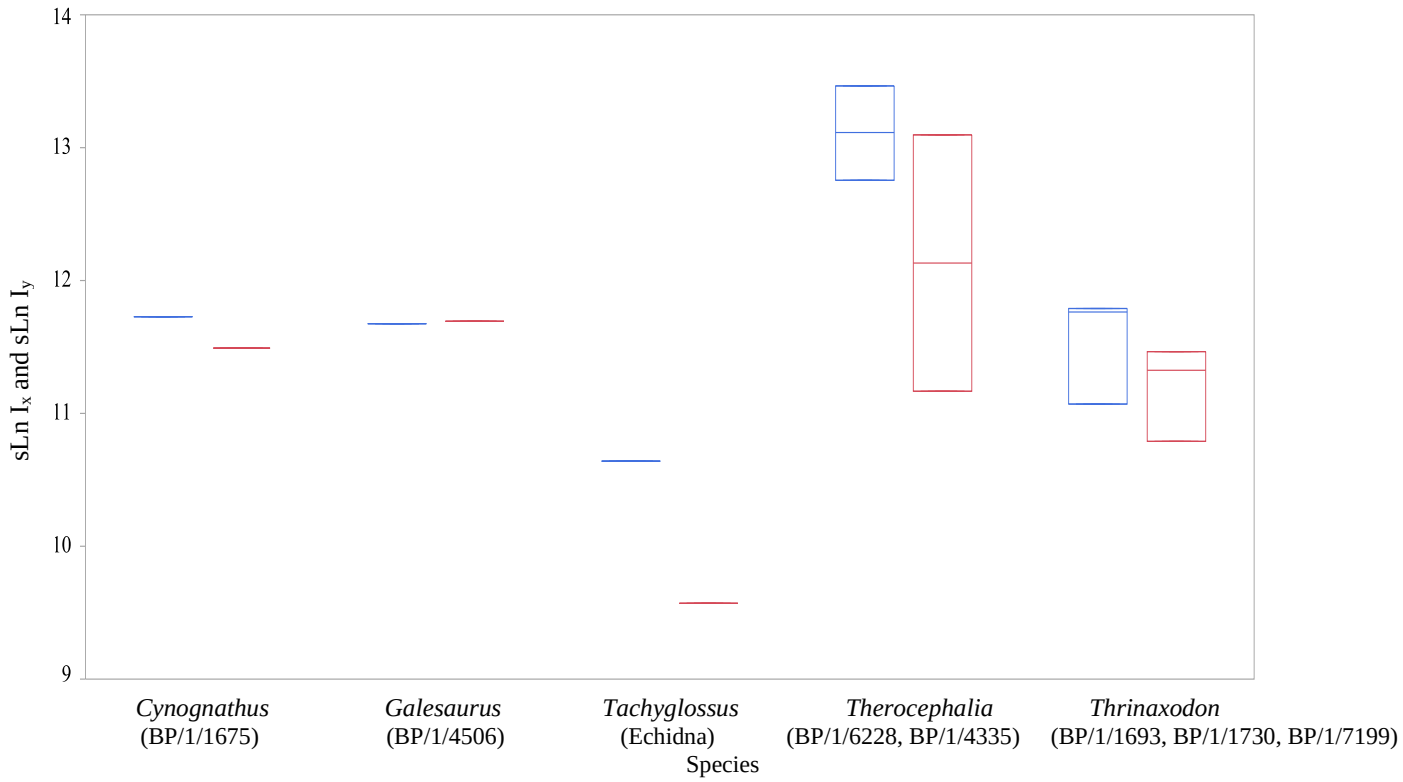


Figure 3.38: Box plot of size-standardized femoral anteroposterior (AP) bending rigidity [(sLn I_x)] and mediolateral (ML) bending rigidity [(sLn I_y)] at the 50% region of interest. ☐ - I_x and ☐ - I_y

Rigidity index (I_y/ I_x) and shape ratio (I_{max}/I_{min})

The rigidity index for *Thrinaxodon* femora varied between 0.96 and 0.98, which further exemplified their equivalent rigidities in these two anatomical planes (Table 3.2). *Galesaurus* exhibited the highest index of 1.00, while *Glanosuchus* (BP/1/6228) exhibited the lowest rigidity index at 0.88 (Figure 3.39). Femoral shape ratios for the taxa under investigation ranged between 0.87 and 0.98 (Figure 3.39).

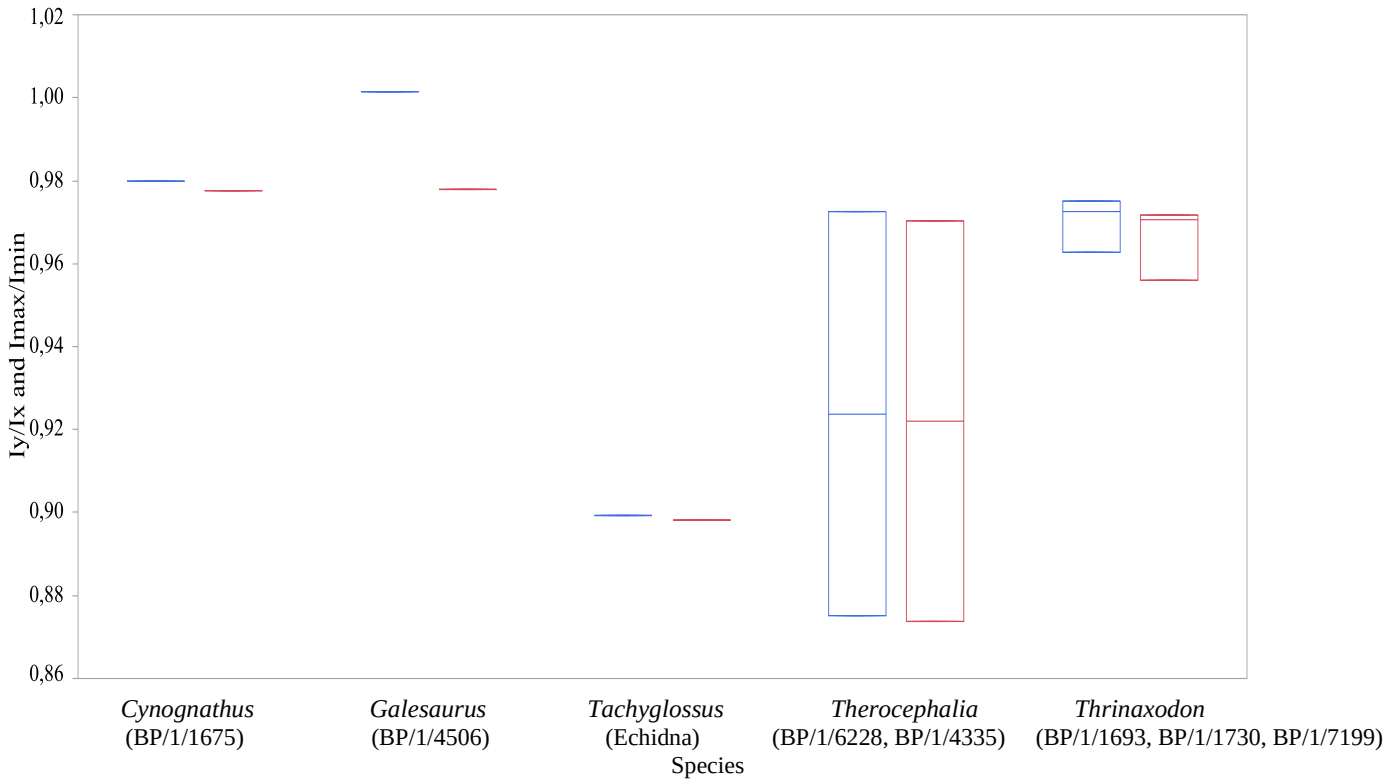


Figure 3.39: Box plot of femoral ratios of second moments of area (I_y/I_x) and principal moments of area (I_{max}/I_{min}) at the 50% region of interest. ☐ - I_y/I_x and ☐ - I_{max}/I_{min}

Polar moment of area, torsional rigidity (sLn J) and Average bending rigidity (J/2)

The *Thrinaxodon* femora exhibited torsional rigidity that varied between 10.23 and 10.92 (Table 3.2). The Therocephalia species (*Tetracynodon darti* (BP/1/4335)) exhibited the highest femoral torsional rigidity at 12.57 (Figure 3.40). The lowest femoral torsional rigidity (9.27) was observed in *Tachyglossus* (Figure 3.40).

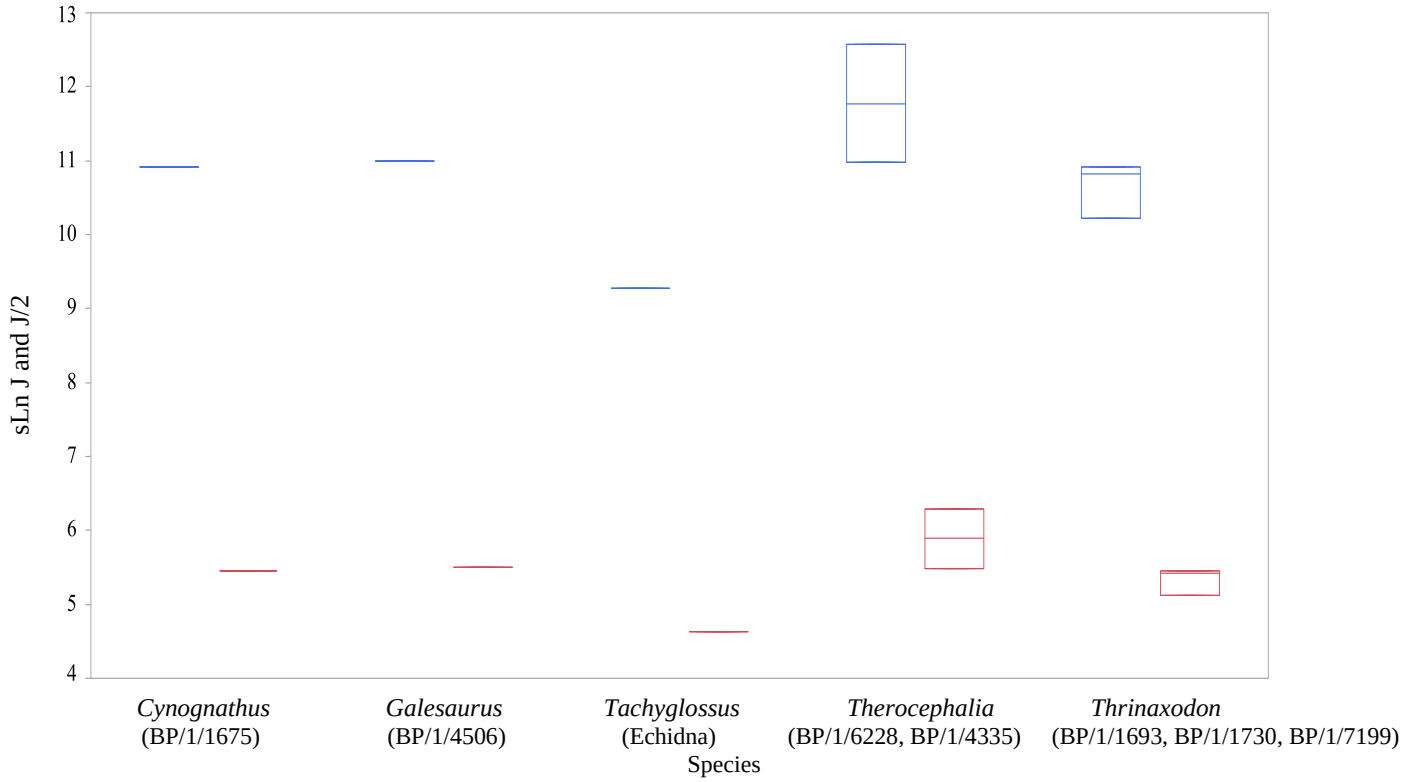


Figure 3.40: Box plot of femoral size-standardized polar moment of area, torsional rigidity (sLn J) and average bending rigidity (J/2) at the 50% region of interest. - sLnJ and - J/2.

Table 3.2: Size-standardized cross-sectional properties of femora at the 50% region of interest.

Species	I_x	I_y	I_{max}	I_{min}	I_y/I_x	I_{max}/I_{min}	sLn J	J/2
Cynognathus BPI1675	11,726	11,491	11,478	11,743	0,980	0,977	10,909	5,454
Thrinaxodon BPI1693	11,763	11,324	11,293	11,813	0,963	0,956	10,827	5,413
Thrinaxodon BPI1730	11,786	11,461	11,452	11,800	0,972	0,970	10,918	5,459
Therocephalia BPI4335	13,466	13,096	13,084	13,484	0,973	0,970	12,571	6,285
Galesaurus BPI4506	11,678	11,696	11,566	11,826	1,001	0,978	10,994	5,497
Therocephalia BPI6228	12,757	11,163	11,160	12,774	0,875	0,874	10,978	5,489
Thrinaxodon BPI7199	11,069	10,793	10,777	11,091	0,975	0,972	10,228	5,114
Tachyglossus Echidna	10,639	9,567	9,564	10,647	0,899	0,898	9,273	4,636

*I_x, I_y, I_{max}, I_{min} and J were size-standardized by taking the natural log of the variable divided by length to the fourth power.

CHAPTER 4

Discussion

The primary aim of this research thesis was to examine reconstructed limb postures for different gaits in *Thrinaxodon* by the use of FEA and bone cross-sectional geometric properties. I hypothesised that non-mammaliaform cynodonts such as *Thrinaxodon liorhinus* would have been optimised for semi-sprawled limb postures. The results of this study support the hypotheses that the *Thrinaxodon* forelimb was optimised for semi-sprawled posture, while its hind limb appears to be predisposed for semi-sprawled or parasagittal postures. These research results provide broad evidence that across the therapsid lineage (Figure 1.1 – i.e., in order of latest survival: Therocephalia, *Galesaurus*, *Thrinaxodon*, and *Cynognathus*), the limbs evolved from being optimized for a sprawled to a parasagittal posture (Figure 3.17; 3.33). Furthermore, comparing Therocephalia with the modern extant *Tachyglossus* taxon (Figure 1.4), this modification across the lineage suggests there may have been selective pressures favouring energy efficiency (Biewener 1989; Riskin *et al*. 2016) while still being able to withstand temporary stresses and strains associated with behavioural flexibility (i.e., the ability to briefly adopt any of the postures regardless of what the habitual posture was) (Appendix B-C). This suggests that the underlying changes evident in the evolutionary sequence may have been driven by selection pressures for cost-effective locomotion, with additional autopomorphic features reflecting specialized behaviours superimposed on the more general structural (and postural) changes (Reilly *et al*. 2007; Riskin *et al*. 2016).

There are significant statistical differences among the three gait models observed for the species under investigation (Appendix D). There are more statistically significant results in the femoral models than in the humeral models (Appendix D). As posture changes from sprawled to parasagittal in these taxa, there would be an increase in stresses paralleling the reduction in mechanical advantage to resist the joint moments associated with the orientation of resultant GRF (Reilly *et al*. 2007; Wright 2008). The limb bones of an animal must be able to withstand the forces that are required for body support, locomotion

and external environmental forces (i.e., GRF) (Kawano *et al*. 2016). These factors affect the stress /strain of the limbs that may result in fracture of bone (Kawano *et al*. 2016).

Each limb bone was subjected to loading conditions that mimic the actual forces and constraints experienced during parasagittal, semi-sprawled and sprawled gait in order to distinguish for which stress/strain situation the limb segment was optimised. The FEA results of the taxa under investigation revealed that the limb loadings of the humeri and femora incorporated both bending and axial compression (Figure 3.1). The humeri appeared optimised to torsional stress/strains (Figure 3.1A) rather than bending forces as was observed in the femora (Figure 3.1B). Humeral torsion implies a more sprawled posture (Gambaryan and Kielan-Jaworoska 1997), where the expanded proximal and distal ends of the diaphysis are enlarged to support muscle attachments (Szalay 1994; Iqbal *et al*. In prep). As per the results, strain deformation of the humeral head was characterised by lateral torsion as opposed to medial torsion (Larson 2007), which is beneficial when positioning the forelimb in a parasagittal gait posture. Femora were optimised for longitudinal bending, where the more curved the diaphysis was the higher degree of bending was observed (Figure 3.1B).

Factors that affect the stress and strain of limb bones

Loading conditions of limb bones reflect the forces generated by muscle contractile forces (or joint reaction forces) and GRFs (Wright 2008). As a result, these muscle force contributors are observed to extend along the diaphysis of the limb bones. The locations of the EES and ES for the humeri and femora were usually the same, however, the intensity decreased from parasagittal gait to sprawled gait postures (Figure 2.2, 3.2-3.32: 3, 4). This suggests that the limbs were sufficiently optimised for semi-sprawled posture. The higher the stress or strain a bone experiences, the more it may become susceptible to fracture. During the evolutionary process, species adapt postures to compensate for the risk of fracture by attempting to reduce the strain their limb bones experience. Movement and orientation of humeri and femora differed for each gait examined. Due to the angle of the bone relative to the orientation of the GRF

resultant, and to muscle forces applied, strains extend throughout the bone at different magnitudes. The different groups of muscles that affect the loading patterns for a specific gait also contribute to the variation of stress and strain observed on the bone (Table 2.4, Figure 2.2). Differences in muscle mass and the angle at which the muscle generates a moment on the limb bone, therefore, also play a role in the overall stress and strain that the bone experiences (Remes 2008).

Peak EES of Therocephalia (BP/1/6228 and BP/1/ 4335), *Cynognathus* (BP/1/1675) and *Thrinaxodon* (BP/1/7199 and BP/1/1693) were concentrated at the proximal end of their humeri (Figures 2.2, 3.2, 3.3, 3.5: 3). The factors that contributed to the strain that the humeral head experienced were body weight and the *m. Latissimus dorsi*, *m. Subscapularis* and *m. Pectoralis* attachments (Table 2.4 and Figure 2.2, 2.2A). For the humeral ES (Figures 2.2, 3.2-3.16: 4), the *m. Latissimus dorsi* and *m. Pectoralis* would contribute to the stress experienced on the diaphysis of Therocephalia (BP/1/6228 and BP/1/4335), *Galesaurus* (BP/1/4506) and *Thrinaxodon* (BP/1/7199 and BP/1/1730).

Variation within species was most evident among specimens of *Thrinaxodon* (specifically BPI/1/1730 - Figure 3.2) and may have been size- and structurally dependent. The *m. Pectoralis* that inserts on the deltopectoral crest is positioned to adduct the forelimb (Kawano *et al*. 2016), as this contributes to the humeral mechanical advantage. As observed in the species under investigation, the *m. Pectoralis* force is concentrated on the proximal end of the humeri for both the stress and strain (Figures 2.2). The *m. Subscapularis* is positioned to aid in stabilising and adducting the forelimb, while the *m. Latissimus dorsi* is positioned to extend and retract the limb during locomotion (Meers 2003; Iqbal *et al*. In prep). The stress and strain observed in the humeral diaphysis of *Galesaurus* (BP/1/4506) is contributed to by the *m. Latissimus dorsi* contractile force (Figures 2.2, 3.4, 3.9, 3.14).

A study conducted by Gambaryan and Kielan-Jaworoska (1997) states that the difference between parasagittal and sprawled limbs is not merely the angle of the humeri or femora to the ground or the body, but the position of the antebrachium and manus/pes with respect to the sagittal plane. This

would acknowledge the fact that not only does the humeral proximal end bear the force created by body weight, but it also bears the gravitational force that passes through the diaphysis to the distal end. The humeral distal end, and the stress and strain it experiences, is more prominent in the semi-sprawled (Figure 3.7-3.11) and sprawled gait (Figure 3.12-3.16) rather than in the parasagittal gait (Figures 3.2-3.6). The distal end of the humeral diaphysis, and its stress and strain, is a factor of the *m. flexor carpi radialis* and *m. flexor carpi ulnaris*, which are flexors of the elbow and adduct the forearm (Meers 2003; Iqbal *et al*. In Prep). Also, *m. Flexor carpi radialis*, *m. Flexor carpi ulnaris* and *m. Anconeus* attach at the distal end of the humerus and would be a factor in the EES concentration of the *Galesaurus* (BP/1/4506) diaphysis (Figure 3.4, 3.9, 3.14: 3) and the distal end of *Tachyglossus* humerus (Figure 3.6, 3.11, 3.16: 3).

Strain on the femur was concentrated at the proximal and distal ends where the *mm. Gluteal Muscles* attach (Figure 2.2B). The femoral vastus muscles would be an EES factor in the diaphysis of *Tetracynodon darti* (BP/1/4335), *Galesaurus* (BP/1/4506), *Thrinaxodon* (BP/1/1730 and BP/1/1693) and *Tachyglossus* (Figures 3.18-3.32: 3). The stress of the femur is focused on the diaphysis where the *m. Vastus intermedius* attaches (Figure 2.2B). Five of the femora experienced compressive strain on the posterior surface and tensile strain on the anterior surface, whereas the other three species, including *Thrinaxodon* (BP/1/7199), experienced tensile strain on the posterior surface and compressive strain on the anterior surface (Figure 3.1). The compression bending stress and strain experienced by the femora is a product of the *mm. Gluteal Muscles* that attaches to the greater trochanter and the *m. semimembranous* muscle that attaches to the distal epicondyle (Gambaryan *et al*. 2002). The *mm. Adductor Muscles* adduct the hind limb (Gambaryan *et al*. 2002) and contributes to the femora diaphysis stress and strain regime in both the extinct and extant species examined (Figures 3.18-3.32). There is variation within the three *Thrinaxodon* (specifically BP/1730 compared to BP/1/1693 and BP/1/7199) femora. The results obtained are dependent on the morphology of the limb bone that affects the bone's ability to withstand the stress and strain it experiences, thus the clarification for opposite compressive and tensile surfaces within species. Bending stress and strain experienced by the proximal end of the femur is an indication of body

support (Figures 3.18-3.32), which increases from sprawled posture to parasagittal posture (Blob and Biewener 1999).

Overall, among all the species under investigation, parasagittal gaits demonstrated higher deformation in the humeri and femora. This suggests that the species under investigation would have been more structurally challenged to withstand the strain the limb bones endured without possibly also being susceptible to a higher rate of fracture. Therefore, the humeri and femora appear to be optimised for sprawling postures where they are able to withstand the stress and strain experienced, but, importantly, without also elevating risks of fracture. The results obtained in this research concur with a study completed by Blob and Biewener (1999), who state that the more upright the posture is in a quadruped, the more strains limb bones experience. This suggests that an increase in limb bone loads may have been a result of postural changes among the therapsid lineage. Further structural reinforcement of these limb bones may have been required to reach a new optimal state.

Gait and Limb Posture variation

The extent of humeral torsion is significant in understanding locomotion and gait (Larson 2007). Torsion of humeri occurs in species with abducted forelimbs (Gambaryan and Kielan-Jaworoska 1997; Blob and Biewener 1999, 2001), affirming that semi-sprawled and sprawled limbs would experience humeral torsion (Iqbal *et al.* in prep). Humeri of Therocephalia, one of the oldest taxa under investigation, exhibited the highest torsional rigidity (Figure 3.4), suggesting a sprawled posture in the forelimb that was able to withstand the stress and strain experienced by the limb. *Thrinaxodon*'s humeri displayed a slightly lower torsional rigidity with a range of 9.94 and 10.72during semi-sprawled forelimb posture (Figure 3.40 and Table 3.1). *Tachyglossus*, in comparison to the fossil taxa, exhibited the lowest humeral torsional rigidity (Table 3.1). The difference between parasagittal, semi-sprawled and sprawled gaits are not only correlated with the angle of attachment of muscles that originate or insert on humeri or femora, but also with the overall activity of the complete forelimb and hind limb. This activity collectively reflects

their habitual standing posture, modes of locomotion and the relationship of limb length vs. body mass (Polly 2007), all of which may contribute to variation of postures within a species. Research conducted by Reilly and Elias (1998) proved that tetrapod postural variation depends on speed, however, this was not considered in the present model since the results obtained used loading conditions applied to the bone during a standing (static) phase rather than the high walk (dynamic) phase as Reilly and Elias (1998) examined. Collectively, the results obtained in the present study together with the results from Reilly and Elias (1998) suggest that even if a species had a sprawled posture during standing (static) phase, it could still possess the dynamic ability to change their limb position more parasagittally during the walking phase. The development of posture and gait by reduction of the peak forces such as the bending and torsional stress and strain of the limb bones is size dependent (Biewener 1983, 1989,1991). The stress experienced on a sprawled limb posture increases when the bone loads are exposed to parasagittal gait biomechanics (Blob and Biewener 2001). This is evident in the results obtained (Figure 3.2-3.32) where each humerus (Appendix B) and femur (Appendix C) of the quadruped experienced a higher stress/strain when exposed to a parasagittal bone load relative to the other gaits.

Musculoskeletal anatomy for organisms practicing sprawled posture is specialised for joint stability (Grand and Barboza 2001). Due to the angle in which the humerus and femur attach to the pectoral and pelvic girdle, respectively, the location of the min. EES and ES has a larger area along the bone (Figures 3.2-3.32: 3, 4). Humeri under investigation experienced lower stresses and strains (Figures 3.2-3.16: 3, 4), as their orientation became more perpendicular to the GRF (Blob and Biewener 1999, 2001). This suggests that the humeri under investigation are optimised for a sprawling gait. The muscles and GRF forces that affect the stress and strain of limb bones factors in the postural transition from sprawled to parasagittal gaits, but these may not be the only factors, e.g., behavioural activities that expand variability even more, such as a fossorial lifestyle (Iqbal *et al*. in prep), probably also contribute to the stress and strain that a limb bone experiences.

Hypothesis Confirmation

Overall, femora had the highest anteroposterior (I_x) and mediolateral (I_y) bending rigidity (Figure 3.38), which suggests that the limb bones differ in structure and mechanical resistance to bending stress (Kawano *et al*. 2016). An increase in AP I_x and ML I_y bending correlates with more rigidity and strain that affects the bone (Carlson 2005; Iqbal *et al*. in prep). The broadness of the humeri and femora allows for large muscle attachment, which is advantageous to support the body (i.e., limb joints) from collapsing due to gravitational forces (Turnbull and Reed 1967; Warburton *et al*. 2013; Iqbal *et al*. in prep). Femora of *Cynognathus* (BP/1/1675), *Galesaurus* (BP/1/4506), *Glanosuchus* (BP/1/4335), *Thrinaxodon* (BP/1/1693 and BP/1/7199), and *Tachyglossus* display higher AP and ML femoral rigidity relative to rigidities exhibited by their humeri (Figure 3.37 and Figure 3.38). In a previous study by Lieberman *et al*. (2004), it is stated that the higher anteroposterior rigidity correlates with an elongated midshaft of the femora. Elongation of limb bones shows a relationship to parasagittal gait (Polly 2007). ML bending is a characteristic feature in sprawled posture (Butcher *et al*. 2011). This would suggest the extent of the sprawled posture in the forelimb relative to the hind limb is higher in these species. *Thrinaxodon* (BP/1/1730 and BP/1/7199) humeri and femora may have experienced similar AP and ML bending given their equivalent bending rigidities in these anatomical planes, while the *Glanosuchus* (BP/1/6228) femur had a lower ML bending rigidity in comparison to the AP bending rigidity of its humerus (Figure 3.35) and femur (Figure 3.38). Limb bones that experience higher AP bending are hypothesised to signify substantial parasagittal locomotion (Szivek *et al*. 1992; Lieberman *et al*. 2004). The species under investigation all exhibited higher AP (I_x) bending rigidity in their femora, which supports the notion that their hind limbs were optimised for parasagittal gait postures (Figure 3.38).

Research limitations

There are limitations and advantages to the FEA technique within palaeontology. In order to understand the mechanical behaviour of fossil species, material properties are needed to be assigned to the element. This becomes difficult as fossil bone changes composition during diagenesis and in turn extant bone material properties are used (Moreno *et al*. 2006; Rayfield 2007). However, these assumptions in the model become difficult when taking into consideration actual heterogeneity in bone material properties. The finite element model (FEM) is a simplified model of the actual biological system that may produce unrealistic results. The mass of each muscle was not reported, and indeed is unknowable for fossil taxa. This muscle mass would be a relevant factor in determining (and differentiating) the forces produced among the different postures. Therefore, boundary constraints are applied such that the model is as close to the real system as possible (Rayfield 2007).

FEA in palaeontology is favourable due to the technique being non-invasive. Also, the model allows for some flexibility since it may be adjusted (i.e., convergence and sensitivity tests) such that stress may be applied to multiple nodes on the element (Rayfield 2007). The morphology of the postcranial bones of fossil species is diverse, and FEA is capable of computing complex geometries and loading regimes (Rayfield 2007). Model validation could not be undertaken in the present study, but this is a crucial step in all FEA-based investigations. As a proxy for this procedure, cross-sectional geometric properties were used to aid hypothesis testing. In order to overcome the validation challenge in Palaeontology, more research needs to be conducted on extant taxa as well as to understand the phylogenetic implications that group together extinct taxa.

Future Directions

The findings of this research thesis raise further questions. First, the induced loading conditions in the research were inferred for the standing phase of locomotion, however, this would differ for walking or running, especially for a full gait cycle that would include the stance and swing phase. Due to the complexity of validation in fossil research, more studies need to be conducted on extant taxa. However, cross-sectional properties produce a reasonable amount of knowledge on the distribution of material (e.g., estimating resistance to strain) and it would be intriguing to explore properties at different percentages of diaphyseal length (i.e., cross-sections at 25% and 75%), especially if there are ridges and processes present at the 50% cross-section, e.g., elongation of the deltopectoral crest along the diaphyseal length. Secondly, the examination of other postcranial elements (i.e., lower limb including the manus and pes) that are subjected to locomotion and posture evolution could help inform structural evaluations conducted in the present study. Future studies on the postcrania of fossil taxa will integrate FEA techniques with principal component analyses (PCA) that are generated in adopting geometric morphometrics approaches (Iqbal 2015; Iqbal *et al.* In prep).

Conclusion

The biomechanics of limbs, and their bones, play an important role in the development of posture among species. The present research was conducted to test hypotheses of the reconstructed posture of *Thrinaxodon liorhinus* limbs with a broad perspective on the postural changes exhibited in therapsids by application of FEA. The goal of this research was to explore and compare loading conditions for proximal segment limb bones across different postures: parasagittal, semi-sprawling and sprawled. The obtained results suggest that bone stress increases with change in posture, which allows for broad structural stability across all three postures, but shows a clear trend in optimal postures from a structural standpoint. The morphology of the bone reflects the forces from the muscle attachments acting upon it. The disposition of loads to which limb bones are subjected to varies in terms of the orientation of articulating bones and the GRF. Ultimately, observed stresses increase for given bones as the posture of a fossil taxon progresses from a sprawled to a more parasagittal gait. Stress and strain experienced by the humerus and femur, as estimated by FEA models, can be corroborated, in part, by humeral and femoral cross-sectional properties such as the AP and ML bending rigidities. Outcomes of the loading conditions induced in *Thrinaxodon* limb bones suggest that the forelimb is sufficiently structurally optimized for a sprawled gait posture and the hind limb for a parasagittal gait posture. Stresses that occur in the humeri and femora, as well as the capability of the limb morphology to withstand externally-induced stresses that arise by a particular postural configuration, were compared to an extant species using results of *in-vivo* studies. This provided robust evidence that limb posture appears to have transitioned from a sprawled gait to a parasagittal gait. This research brings modern methods and innovative analyses into an area of research with enduring questions and issues that has yet to fully benefit from these approaches. Thus, the study is an attempt to truly provide a new source of corroborating or refuting evidence that takes advantage of new approaches that are not often applied to these types of questions until very recently (i.e., FEA).

References:

ABDALA, F. and RIBEIRO, A. M. 2010. Distribution and diversity patterns of Triassic cynodonts (Therapsida, Cynodontia) in Gondwana. *Palaeogeography, Palaeoclimatology, Palaeoecology* **286**: 202-217.

ABDALA, F., JASINOSKI, S. C. and FERNANDEZ, V. 2013. Ontogeny of the Early Triassic cynodont *Thrinaxodon liorhinus* (Therapsida): dental morphology and replacement. *Journal of Vertebrate Palaeontology* **33**: 1408-1431.

ABDEL-WAHAB, A. A., ALAM, K. and SILBERSCHMIDT, V. V. 2011. Analysis of the anisotropic viscoelastoplastic properties of cortical bone tissues. *Journal of the Mechanical Behaviour of Biomedical Materials* **4**: 807-820.

BAKKER, R. T. 1971. Dinosaur phylogeny and the origin of mammals. *Evolution* **25**: 636-658.

BANKOFF, A. D. P. 2012. Biomechanical characteristics of the Bone. Chapter 4 in GOSWAMI, T. (ed.) *Human Musculoskeletal Biomechanics*. InTech.

BEAUPRE, G. S. and CARTER, D. R. 1992. Finite element analysis in biomechanics. In BIEWENER, A. A. (ed.). *Biomechanics: Structures and Systems*. Oxford: Oxford University Press, pp. 149–73.

BENNETT, A. F. and RUBEN, J. A. 1986. The metabolic and thermoregulatory status of therapsids. In *The ecology and biology of mammal-like reptiles.* Smithsonian Institute Press. Washington. D.C. USA.

BIEWENER, A. A. 1983. Allometry of quadrupedal locomotion: the scaling of duty factor, bone curvatures and limb orientation to body size. *Journal of Experimental Biology* **105**: 147-171.

BIEWENER, A. A. 1989. Mammalian terrestrial locomotion and size. *American Institute of Biological Sciences* **39**: 776-783.

BIEWENER, A. A. and TAYLOR, R. C. 1986. Bone strain: a determinant of gait and speed? *Journal of Experimental Biology* **123**: 383-400.

BLAKE, A. 1990. Stresses in shear and torsion. *Practical Stress Analysis in Engineering Design*. 2nd ed. New York: Marcel Dekker, Inc.

BLOB, R. 2001. Evolution of hind limb posture in nonmammalian therapsids: biomechanical tests of palaeontogical hypotheses. *Paleobiology* **27**: 14-38.

BLOB, R. W. and BIEWENER, A. A. 1999. *In vivo* locomotor strain in the hind limb bones of *Alligator mississippiensis* and *Iguana iguana*: implications for the evolution of limb bone safety factor and non-sprawling limb posture. *The Journal of Experimental Biology* **202**: 1023-1046.

BLOB, R. W. and BIEWENER, A. A. 2001. Mechanics of limb bone loading during terrestrial locomotion in the Green Iguana (*Iguana iguana*) and American Alligator (*Alligator Mississippiensis*). *The Journal of Experimental Biology* **204**: 1099-1122.

BOONSTRA, L. D. 1965. The girdles and limbs of the Gorgonopsia of the *Tapinocephalus* Zone. *Annals of the South African Museum* **48**: 237-249.

BOTHA, J. and CHINSAMY, A. 2005. Growth patterns of *Thrinaxodon liorhinus*, a non-mammalian cynodont from the Lower Triassic of South Africa. *Palaeontology* **48**: 385-394.

BOTHA, J. and SMITH, R. M. H. 2006. Rapid vertebrate recuperation in the Karoo Basin of South Africa following the End-Permian extinction. *Journal of African Earth Sciences* **45**: 502-514.

BOTHA, J., LEE-THORP, J. and CHINSAMY, A. 2005. The palaeoecology of the non-mammalian cynodonts *Diademodon* and *Cynognathus* from the Karoo Basin of South Africa, using stable light isotope analysis. *Palaeogeography, Palaeoclimatology, Palaeoecology* **223**: 303– 316.

BOUZA-RODRIGUEZ, J. B. and MIRAMONTES-SEQUEIROS, L. C. 2014. Three-dimensional biomechanical analysis of the bovine humerus. *Applied Bionics and Biomechanics* **11**: 13-24.

BRASSEY, C. A. 2014. *Biomechanical modelling of long bones and body mass estimation in modern and fossil species*. Doctor of Philosophy Thesis University of Manchester. London. United Kingdom.

BREKELMANS, W. A., POORT, H. W., and SLOOFF, T. J. 1972. A new method to analyse the mechanical behaviour of skeletal parts. *Acta Orthopaedica Scandinavica*. **43**: 301–307.

BRINK, A. S. 1956. Speculations on some advanced mammalian characteristics in the higher mammal like reptiles. *Palaeontologica Africana* **4:** 77-96.

BRINK, A. S. 1958. Note on a new skeleton of *Thrinaxodon liorhinus*. *Palaeontologica Africana* **6**: 15 -22.

BRIGHT, J. A. and RAYFIELD, E. J. 2011. The response of cranial biomechanical finite element models to variations in mesh density. *The Anatomical Record* **294**: 610-620.

BROOM, R. 1903. On the axis, atlas and proatlas in the higher theriodonts. *Proceedings of the Zoological Society of London* **1**: 177-180.

BUTCHER, M. T., WHITE. B. J., HUDZIK, N. B., GOSNELL, C. W., PARRISH, J. H. A. and BLOB, R. W. 2011. *In vivo* strains in the femur of the Virginia opossum (Didelphis virginiana) during terrestrial locomotion: testing hypotheses of evolutionary shifts in mammalian bone loading and design. *The Journal of Experimental Biology* **214**: 2631-2640.

BUTLER, E. 2009. *The postcranial skeleton of the Early Triassic non-mammalian cynodont Galesaurus planiceps: implications for biology and lifestyle*. MSc Dissertation. University of the Free State. Bloemfontein.

CAMPIONE, N. E. and EVANS, D. 2012. A universal scaling relationship between body mass and proximal limb bone dimensions in quadrupedal terrestrial tetrapods. *Journal of Biology* **10**: 1-21.

CARLSON, K. J. 2014. Linearity in the Real World: An experimental assessment of nonlinearity in terrestrial locomotion. Chapter 14. In: CARLSON, K. J. and MARCHI, D. (eds) *Reconstructing Mobility: Environmental, Behavioural, and Morphological Determinants*. Springer. New York. United States of America.

CARTER, D. R. 1987. Mechanical loading history and skeletal biology. *Journal of Biomechanics* **20**: 1095-1109.

CASINOS, A., QUINTANA, C. and VILADIU, C. 1993. Allometry and adaptation in the long bones of a digging group of rodents (Ctenomyinae). *Zoological Journal of the Linnaean Society* **107**: 107 -115.

CHINSAMY, A. 1997. Assessing the biology of fossil vertebrate through bone histology. *Palaeontologica Africana* **33**: 29-35.

CHRISTIANSEN, P. and PAUL, G. S. 2001. Limb bone scaling, limb proportions and bone strength in Neoceratopsian dinosaurs. *GAIA* 13-29. Lisbon.

CROMPTON, A. W. 1963. Tooth replacement in the cynodont *Thrinaxodon liorhinus* Seeley. *Annuals of the South African Museum* **46**: 479-521.

CROMPTON, A. W. 1968. The enigma of the evolution of mammals. *Optima* **18**: 137-51.

CROMPTON, A. W. and JENKINS, F. A. Jr. 1973. Mammals from reptiles: A review of mammalian origins. *Annual Review of Earth and Planetary Science* **1**: 131-155.

DAMIANI, R., MODESTO, S., YATES, A. and NEVELING, J. 2003. Earliest evidence of cynodont burrowing. *Proceedings of the Royal Society of London: Biological Sciences* **270**: 1747-1751.

DIAL, K. P., GREENE, E. and IRSCHICK, D. J. 2008. Allometry of behaviour. *Trends in Ecology and Evolution* **23**: 394-401.

DOUBE, M., CONROY, A. W., CHRISTIANSEN, P., HUTCHINSON, J. R. and SHEFELBINE,S. J. 2009. Three-dimensional geometric analysis of Felid limb bone allometry. *PLOS One* **4**: 1-10.

DOUBE, M., KLOSOWSKI, M. M., ARGANDA-CARRERAS, I., CORDELIERES, F. P., DOUGHERTY, R. P., JACKSON, J. S., SCHMID, B., HUTCHINSON, J. R. and SHEFELBINE, S. J. 2010. BoneJ: Free and extensible bone image analysis in ImageJ. *Bone* **47**: 1076-1079.

DZIALO, C. M. 2012. *Investigating the relationship between material property axes and strain orientations in Cebus Apella Crania*. MSc Dissertation. University of Massachusetts. Amherst.

EATON, T. H. Jr. 1962. Adaptive features of the fore limb in primitive tetrapods and mammals. *American Zoologist* **2**: 157-160.

ERICKSON, G. M., CATANESE, J. III. and KEAVENY, T. M. 2002. Evolution of the biomechanical material properties of the femur. *The Anatomical Record* **268**: 115-124.

EVANS, F. G. 1939. The morphology and functional evolution of the atlas-axis complex from fish to mammals. *Annals of the New York Academy of Sciences* **39**: 29-104.

FERNANDEZ, V., ABDALA, F., CARLSON, K. J, COOK, D. C., RUBIDGE, B. S., YATES, A. and TAFFOREAU, P. 2013. Synchrotron Reveals Early Triassic Odd Couple: Injured Amphibian and Aestivating Therapsid Share Burrow. *PLOS One* **08**: 01-07.

FARKE, A. and ALICEA, J. Femoral strength and posture in terrestrial birds and non-avian theropods. *The Anatomical Record* **292**:1406–1411.

FORTUNY, J., MARCE-NOGUE, J., HEISS, E., SANCHEZ, M., GIL, L. and GALOBART, A. 2015. 3D bite modelling and feeding mechanics of the largest living amphibian, the Chinese Giant Salamander *Andrias davidianus* (Amphibia: Urodela). *PLOS One* **10**: 1-20.

FOURIE, H. and RUBIDGE, B. S. 2009. The postcranial skeleton of the basal therocephalian *Glanosuchus macrops* (Scylacosauridae) and comparison of morphological and phylogenetic trends amongst the Theriodontia. *Palaeontologica Africana* **44**: 27-39.

FROBISCH, J. 2006. Locomotion in derived dicynodonts (Synapsida, Anomodontia): a functional analysis of the pelvic girdle and hind limb of *Tetragonias njalilus*. *Canadian Journal of Earth Sciences* **43**: 1297-1308.

GAMBARYAN, P. P., ARISTOVE, A. A., DIXON, J. M. and ZUBTSOVA, G. Y. 2002. Peculiarities of the hind limb musculature in monotremes: an anatomical description and functional approach. *Russian Journal of Theriology* **1**: 1-36.

GAMBARYAN, P. P. and KIELAN-JAWOROWSKA, Z. 1997. Sprawling versus parasagittal stance in multituberculate mammals. *Acta Palaeontologica Polonica* **42**: 13-44.

GILLIS, G. B. and BIEWENER, A. A. 2001. Hind limb muscle function in relation to speed and gait: *in vivo* patterns of strain and activation in a hip and knee extensor of the rat (*Rattus norvegicus*). *The Journal of Experimental Biology* **204**: 2717-2731.

GOSNELL, W. C. 2010. *Femoral loading mechanics in Virginia opossums (Didelphis virginiana): torsion and mediolateral bending in mammalian parasagittal locomotion*. MSc Dissertation. Clemson University.

GOW, C. E. 1985. Dentitions of juvenile *Thrinaxodon* (Reptilia: Cynodontia) and the origin of mammalian diphyondonty. *Annuals of the Geological Survey of South Africa* **19**: 1-17.

GOW, C. E. 1997. The importance of Karoo fossils in the search for mammal origins. *Palaeontologica Africana* **33**: 23-27.

GRAND, T. I. and BARBOZA, P. S. 2001. Anatomy and development of the koala, *Phascolarctos cinereus*: an evolutionary perspective on the superfamily Vombatoidea. *Anatomy of Embryology* **203**: 211-223.

HABIB, M. B. and RUFF, C. B. 2008. The effects of locomotion on the structural characteristics of avian limb bones. *Zoological Journal of the Linnaean Society* **153**: 601–624.

HEATH, J. E. 1968. The origins of the thermoregulation. In *Evolution and the Environment*, eds. E. T. Drake. Yale University Press. United States of America.

HODGSON, D. 2015. *Modelling muscles in vitro: a finite element analysis study*. CoMPLEX Mini Project 2. University College London.

HOFFSTETTER, R. and GASC, J. P. 1969. Vertebrae and ribs of modern reptiles. In *Biology of the Reptilia*, eds. Gans, C. Volume. 1. Academic Press. New York. United States of America.

HOHN-SCHULTE. 2010. *Form and function of the shoulder girdle in sauropod dinosaurs a biomechanical investigation with the aid of finite elements*. Doctor of Philosophy Thesis. International Graduate School of Biosciences Ruhr-University Bochum.

HOPSON, J. A. and CROMPTON, A. W. 1969. Origin of mammals. *Evolutionary Biology* **3**: 15-72.

HOWELL, A. B. 1941. The femoral trochanters. *Field Museum of Natural History Zoological Series* **27**: 279-291.

HUISKES, R. and HOLLISTER, S. J. 1993. From structure to process, from organ to cell: recent developments of FE-analysis in orthopaedic biomechanics. *The Journal of Biomechanical Engineering* **115**: 520–27.

HUTTENLOCKER, A. K. and BOTHA-BRINK, J. 2014. Bone microstructure and the evolution of growth patterns in Permo-Triassic therocephalians (Amniota, Therapsida) of South Africa. *PeerJ* **325**: 1-31.

HUTTENLOCKER, A. K. and FARMER, C. G. 2017. Bone microvasculature tracks red blood cell size diminution in Triassic mammal and dinosaur forerunners. *Current Biology Report Cell Press* **27**: 48–54.

IQBAL, S. 2015. *The functional morphology and internal structure of the forelimb of the Early Triassic non-mammaliaform cynodont Thrinaxodon liorhinus*. MSc Dissertation. University of the Witwatersrand, Johannesburg, South Africa.

IQBAL, S., CARLSON, K. J., ABDALA, F. and FERNANDEZ, V. in prep. Fossorial adaptations in the forelimb of the Early Triassic cynodont *Thrinaxodon liorhinus*. Intended for *Journal of Morphology*.

JASINOSKI, S. C., ABDALA, F. and FERNANDEZ, V. 2015. Ontogeny of the Early Triassic cynodont *Thrinaxodon liorhinus* (Therapsid): cranial morphology. *Anatomical Record* **298**: 1440 -1464.

JENKINS, F. A. 1971. The postcranial skeleton of African cynodonts: Problems in the early evolution of the mammalian postcranial skeleton. *Bulletin of the Peabody Museum of Natural History* **36**: 1 -216.

JIANG, Y. 2007. Bone imaging and finite element analysis. *BoneKEy-Osteovision* **12**: 346-351.

KARDONG, K. V. 2009. *Vertebrates: Comparative Anatomy, function, evolution.* Sixth Edition. McGraw-Hill. New York. USA.

KAWANO, S. M., ECONOMY, D. R., KENNEDY, M. S., DEAN, D. and BLOB, R. W. 2016. Comparative limb bone loading in the humerus and femur of the tiger salamander: testing the 'mixed-chain' hypothesis for skeletal safety factors. *Journal of Experimental Biology* **219**: 341 -353.

KEMP, T. S. 1978. Stance and gait in the hind limb of a therocephalian mammal-like reptile. *Journal of Zoology* **186**: 143-161.

KEMP, T. S. 1980. The primitive cynodont *Procynosuchus*: structure, function and evolution of the postcranial skeleton. *Philosophical Transactions of the Royal Society of London Biological Sciences* **288**: 217-258.

KEMP, T. S. 1982. *Mammal-like Reptiles and the Origin of Mammals*. Academic Press. New York. United States of America.

KEMP, T. S. 1986. The skeleton of a Baurioid Therocephalian therapsid from the Lower Triassic (Lystrosaurus Zone) of South Africa. *Journal of Vertebrate Palaeontology* **6**: 215-232.

KEMP, T. S. 2005. *The origin and evolution of mammals*. Oxford University Press. Oxford. New York. United States of America. Pp. 60-74.

KEMP, T. S. 2006. The origin of mammalian endothermy: a paradigm for the evolution of complex biological structure. *Zoological Journal of the Linnaean Society* **147**: 473-488.

KUBO, T. and BENTON, M. J. 2009. Tetrapod postural shift estimated from Permian and Triassic trackways. *Palaeontology* **52:** 1029-1037.

KUPCZIK, K. 2008. Virtual biomechanics: basic concepts and technical aspects of finite element analysis in vertebrate morphology. *Journal of Anthropological Sciences* **86**: 193-198.

LAI, P. H., BIEWENER, A. and PIERCE, S. E. 2017. Three-dimensional mobility and muscle attachments in the pectoral limb of the Triassic cynodont *Massetognathus pascuali*. In press.

LARSON, S. G. 2007. The definition of humeral torsion: a comment on Rhodes (2006). *American Journal of Physical Anthropology* **133**: 819– 820.

LIEBERMAN, D. E., POLK, J. D. and DEMES, B. 2004. Predicting long bone loading from cross sectional geometry. *American Journal of Physical Anthropology* **123**: 156-171.

LUI, J. and OLSEN, P. 2010. The phylogenetic relationships of Eucynodontia (Amniota: Synapsida). *Journal of Mammal Evolution* **17**: 151-176.

LUO, Z. X. 2007. Transformation and diversification in early mammal evolution. *Nature Reviews* **45**: 1011-1019.

MARCE-NOGUE, J., FORTUNY, J., GIL, Ll. and GALOBART, A. 2011. Using reverse engineering to reconstruct tetrapod skulls and analyze its feeding behavior. *Proceedings of the Thirteenth International Conference on Civil, Structural and Environmental Engineering Computing*, Scotland **237**: 01-12.

MARCHI, D. and TARLI, S. M. B. 2004. Cross-sectional geometry of the limb bones of the *Hominoidea* by biplanar radiography and moulding techniques. *Journal of Anthropological Science* **82**: 89 -102.

MARTIN, R. B. 1991. Determinants of mechanical properties of bone. *Journal of Biomechanics* **24**: 79 -88.

MEERS, M. B. 2003. Crocodilian forelimb musculature and its relevance to Archosauria. *The Anatomical Record Part A* **274A**: 891-916.

MORENO, K., CARRANO, T. and SYNDER, R. 2006. Morphological changes in pedal phalanges through Ornithopod Dinosaur Evolution: A biomechanical approach. *Journal of Morphology* **268**: 50-63.

OLESIAK, S. E., OYEN, M., SPONHEIMER, M., EBERLE, J. J. and FERGUSON, V. L. 2007. Ultrastructural mechanical and material characterization of fossilized bone. *Materials Research Society* **975**: 03-09.

OLIVEIRA, T. V. D. and SCHULTZ, C. L. 2015. Functional morphology and biomechanics of the Cynodont Trucidocynodon riograndensis from the Triassic of Southern Brazil: Pectoral girdle and forelimb. *Acta Palaeontologica Polonica* **61**: 377-386.

O' NEILL, M. C. and RUFF. 2004. Estimating human long bone cross-sectional geometric properties: a comparison of non-invasive methods. *Journal of Human Evolution* **47**: 221-235.

PADIAN, K., LI, C. and PCHELNIKOVA, J. 2010. The tracemaker of *Apatopus* (Late Triassic, North America): implications for the evolution of Archosaur stance and gait. *Palaeontology* **53**: 175 -189.

PANAGIOTOPOULOU, O., WILSHIN, S. D., RAYFIELD, E. J., SHEFELBINE, S. J. and HUTCHINSON, J. R. 2012. What makes an accurate and reliable subject-specific finite element model? A case study of an elephant femur. *Journal of The Royal Society Interface* **9**: 351-361.

PARRINGTON, F. R. 1933. On the cynodont reptile *Thrinaxodon liorhinus*. *Seeley. Annals and Magazine of Natural History Series* **10**: 16-24.

PARRINGTON, F. R. 1936. On the tooth-replacement in theriodont reptiles. *Philosophical Transactions of the Royal Society of London* **226**: 121-142.

PETERS, S. E., MULKEY, R., RASMUSSEN, S. A. and GOSLOW, G. E. JR. 1984. Motor units of the primary ankle extensor muscles of the Opossum (*Didelphis virginiana*): Functional properties and fiber types. *Journal of Morphology* **181**: 305-317.

POLLY, P. D. 2007. Limbs in mammalian evolution. Chapter 15 in HALL, B. K. (ed) *Fins into Limb: Evolution, Development, and Transformation*. University of Chicago Press. Chicago. USA.

PRENDERGAST, P. J. and HUISKES, R. 1995. The biomechanics of Wolff's law: recent advances. *International Journal of Molecular Sciences* 152-154.

RAYFIELD, E. J. 2007. Finite element analysis and understanding the biomechanics and evolution of living and fossil organisms. *Annual Review of Earth and Planetary Sciences* **35**: 541-576.

REID, R. E. H. 1996. Bone histology of the Cleveland-Lloyd dinosaurs and of dinosaurs in general, Part I: Introduction to bone tissues. *University of Geology Studies* **41**:25–71.

REILLY, T. D. and BURNSTEIN, A. H. 1975. The elastic and ultimate properties of compact bone tissue. *Journal of Biomechanics* **11**: 393-405.

REILLY, S. M. and DELANCEY, M. J. 1997. Sprawling locomotion in the lizard *Sceloporus clarkia*: quantitative kinetics of a walking trot. *The Journal of Experimental Biology* **200**: 753-765.

REILLY, S. M. and ELIAS, J. A. 1998. Locomotion in *Alligator mississippiensis*: kinetic effects of speed and posture and their relevance of the sprawling-to-erect paradigm. *The Journal of Experimental Biology* **201**: 2559–2574.

REILLY, S. M. and BLOB, R. W. 2003. Motor control of locomotor hind limb posture in the American alligator (*Alligator mississippiensis*). *The Journal of Experimental Biology* **206**: 4327-4340.

REILLY, S. M., McELROY, E. J. and BIKNEVICIUS, A. R. Posture, gait and the ecological relevance of locomotor costs and energy-saving mechanisms in tetrapods. *Zoology* **110**: 271-289.

REMES, K. 2008. Evolution of the pectoral girdle and forelimb in Sauropodomorpha (Dinosauria, Saurischia): osteology, myology and function. PhD Thesis. University of Munich. Germany. Europe.

RHEE, Y., HUR, J. H., WON, Y. Y., LIM, S. K., BEAK, M. H., CUI, W. Q., KIM, K. G. and KIM, Y. E. 2009. Assessment of bone quality using finite element analysis based upon micro-CT images. *Clinics in Orthopaedic Surgery* **01**: 40-47.

RHO, J. Y., KUHN-SPEARING, L. and ZIOUPOS, P. 1998. Mechanical properties and the hierarchical structure of bone. *Medical Engineering and Physics* **20**: 92-102.

RICHMOND, B. G., WRIGHT, B. W., GROSSE, I., DECHOW, P. C., ROSS, C. F., SPENCER, M. A. and STRAIT, D. S. 2005. Finite Element Analysis in Functional Morphology. *The Anatomical Record Part A* **283A**: 259-274.

RISKIN, D. K., KENDALL, C. J. and HERMANSON, J. W. 2016. The crouching of the shrew: Mechanical consequences of limb posture in small mammals. *PeerJ* **2131**: 1-14.

ROMER, A. S. 1922. The locomotor apparatus of certain primitive and mammal-like reptiles. *Bulletin American Museum of Natural History* **81**: 571-604

ROMER, A. S. 1924. The lesser trochanter of the mammalian femur. *Anatomical Record* **28**: 95-102.

ROSE, J. A., SANDEFUR, M., HUSKEY, S., DEMIER, J. L. and BUTCHER, M. T. 2013. Muscle architecture and out-force potential of the thoracic limb in the Eastern Mole (*Scalopus aquaticus*). *Journal of Morphology* **274**: 1277-1287.

ROSS, C. F. 2005. Finite element analysis in vertebrate biomechanics. *The Anatomical Record Part A* **283A**: 253-258.

ROWE, T., MACRINI, T. E. and LUO, Z. X. 2011. Fossil evidence on origin of the mammalian brain. *Supporting Online Materials*. 1-26.

RUFF, C. B., HOLT, B. H. and TRINKAUS, E. 2006. Who's afraid of the big bad Wolff? Wolff's Law and bone functional adaptation. *American Journal of Physical Anthropology* **129**: 484-498.

RUFF, C. B. and LARSON, C. S. 2014. Long bone structural analyses and the reconstruction of Past mobility: a historical review. Chapter 2. In: CARLSON, K. J. and MARCHI, D. (eds) *Reconstructing Mobility: Environmental, Behavioural, and Morphological Determinants*. Springer. New York. United States of America.

RUSSELL, M. B., SURENDRAN, P. N., and PROBERT, S. D. 2002. Quantifying acceptable mesh dependencies for computational investigations of airflows within rooms. *Applied Energy* **72**: 409 -425.

SAHA, S. and HAYES, W. C. 1974. Instrumented tensile-impact tests of bone. *Experimental Mechanics* 473–478.

SCHMIDT-NIELSEN, K. 1975. Scaling in biology: The consequences of size. *Journal of Experimental Zoology* **194**: 287-307.

SHENG, W., JI, A. and CHEN, C. 2017. Biomechanical research of the femur finite element model combined with different material assignment methods. *MATEC Web of Conferences* **104**: 1-6.

SIGURDSEN, T., HUTTENLOCKER, A. K., MODESTO, S. P., ROWE, T. B. and DAMIANI, R. 2012. Reassessment of the morphology and paleobiology of the Therocephalian *Tetracynodon darti* (Therapsida), and the phylogenetic relationships of Baurioid. *Journal of Vertebrate Palaeontology* **32**: 1113-1134.

SMITH, R. and BOTHA, J. 2005. The recovery of terrestrial vertebrate diversity in the South African Karoo Basin after the end-Permian extinction. *Comptes Rendus Palevol* **4**: 623-636.

SOLOMON, E. P., BERG, L. R. and MARTIN, D. W. 2011. *Biology*. Brooks/Cole. Cengage Learning. Canada.

SPIERS, A. D., HELLER, M. O., DUDA, G. N. and TAYLOR, W. R. 2007. Physiologically based boundary conditions in finite element modelling. *Journal of Biomechanics* **40**: 2318-2323.

STRAIT, D. S., WANG, Q., DECHOW, P. C., ROSS, C. F., RICHMOND, B. G., SPENCER, M. A. and PATEL, B. A. 2005. Modelling elastic properties in finite-element analysis: how much precision is needed to produce an accurate model? *The Anatomical Record* **283A**:275–287.

SU, A. 2011. *The functional morphology of subchondral and trabecular bone in the hominoid tibiotalar joint*. PhD Thesis. Stony Brook University. USA.

SUES, H. D. and FRASER, N. C. 2010. *Triassic life on land: the great transition*. Columbia University Press. New York. USA.

SZALAY, F. S. 1994. *Evolutionary history of the marsupials and an analysis of osteological characters.* Cambridge University Press. New York. USA.

SZIVEK, J.A., JOHNSON, E. M. and MAGEE, F. P. 1992. *In vivo* strain analysis of the greyhound femoral diaphysis. *Journal of Investigative Surgery* **5**:91–108.

TAMVADA, K. H. 2014. Femoral mechanics, mobility, and finite element analysis. Chapter 15. In: CARLSON, K. J. and MARCHI, D. (eds) *Reconstructing Mobility: Environmental, Behavioural, and Morphological Determinants*. Springer. New York. United States of America.

TURNBULL, W. D. and REED, C. A. 1967. *Pseudochrysochloris*, a specialised burrowing mammal from the Early Oligocene of Wyoming. *Journal of Palaeontology* **41**: 623-631.

VAN VALKENBURG, B. and JENKINS, I. 2002. Evolutionary patterns in the history of Permo-Triassic and Cenozoic synapsid predators. *Paleontological Society Papers* **8**: 267-288.

VIGNOLI, L. L. and KENEDI, P. P. 2016. Bone Anisotropy – Analytical and Finite Element Analysis. *Latin American Journal of Solids and Structures* **10**: 51-72.

WARBURTON, N. M., GREGOIRE, L., JACQUES, S. and FLANDRIN, C. 2013. Adaptations for digging in the forelimb muscle anatomy of the southern brown bandicoot (*Isoodon obesulus*) and bilby (*Macrotis lagotis*). *Australian Journal of Zoology* **61**: 402-419.

WILLIAMS, S. B., WILSON, A. M., RHODES, L., ANDREWS, J. and PAYNE, R. C. 2008. Functional anatomy and muscle moment arms of the pelvic limb of an elite sprinting athlete: the racing greyhound (*Canis familiaris*). *Journal of Anatomy* **213**: 361-372.

WILLIAMS, S. B., WILSON, A. M., DAYNES, J., PECKHAM, K. and PAYNE, R. C. 2008. Functional anatomy and muscle moment arms of the thoracic limb of an elite sprinting athlete: the racing greyhound (*Canis familiaris*). *Journal of Anatomy* **213**: 373-382.

WILSON, J. A. 2005. Integrating ichnofossil and body fossil records to estimate locomotor posture and spatiotemporal distribution of early sauropod dinosaurs: a stratocladistic approach. *Paleobiology* **31**: 400-423.

WITMER, L. 1995. The extant phylogenetic bracket and the importance of reconstructing soft tissues in fossils. In: THOMASON, J. J. (ed) *Functional morphology in vertebrate paleontology*. Cambridge: Cambridge University Press.

WRIGHT, K. 2008. *Loading mechanics in femora of tiger salamanders (Ambystoma tigrinum) and tegu lizards (Tupinambis merianae): implications for the evolution of limb bone design*. MSc Dissertation. Clemson University.

YOUNG, M. T., RAYFIELD, E. J., HOLLIDAY, C. M., WITMER, L. M., BUTTON, D. J., UPCHURCH, P. and BARRETT, P. M. 2012. Cranial biomechanics of Diplodocus (Dinosauria, Sauropoda): testing hypotheses of feeding behaviour in an extinct megaherbivore. *Naturwissenschaften* **99**: 637-643.

ZYSSET, P. K., DALL' ARA, E., VARGA, P. and PAHR, D. H. 2013. Review: Finite element analysis for prediction of bone strength. *BoneKEy reports* **2**: 386.

Appendix A

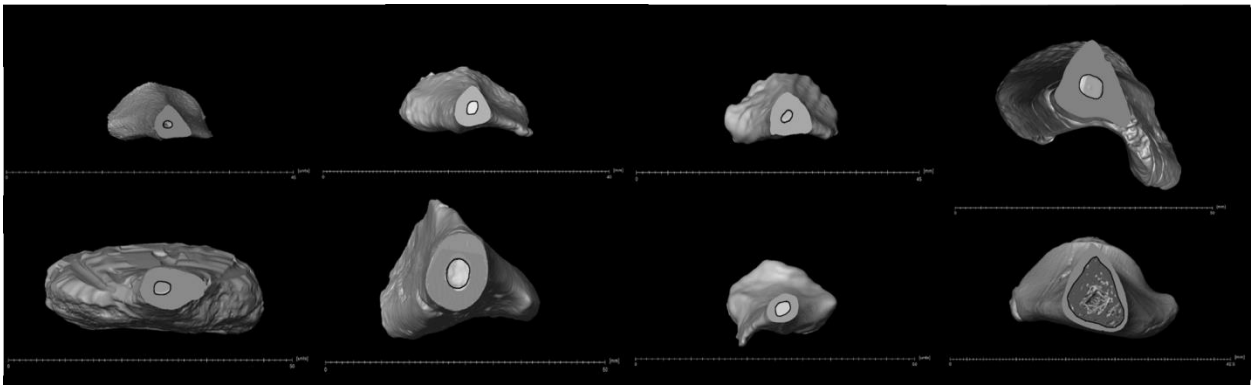


Figure A1: Cross-sections of species humeri at 50% diaphyseal length: 1 – *Thrinaxodon* (BP/1/7199), 2 – *Thrinaxodon* (BP/1/1730), 3 – *Thrinaxodon* (BP/1/1693), 4 – *Cynognathus* (BP/1/1675), 5 – *Galesaurus* (BP/1/4506), 6 – *Glanosuchus* (BP/1/6228), 7 – *Tetracynodon darti* (BP/1/4335), 8 – *Tachyglossus.*

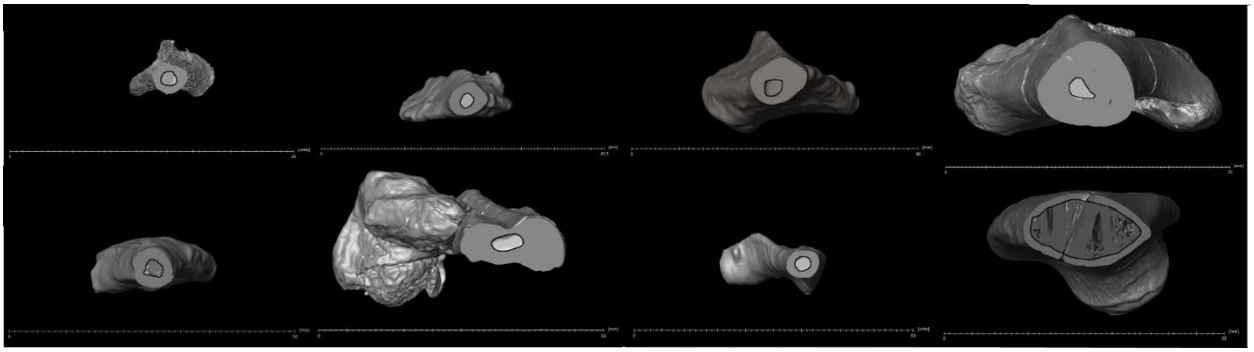


Figure A2: Cross-sections of species femora at 50% diaphyseal length: 1 – *Thrinaxodon* (BP/1/7199), 2 – *Thrinaxodon* (BP/1/1730), 3 – *Thrinaxodon* (BP/1/1693), 4 – *Cynognathus* (BP/1/1675), 5 – *Galesaurus* (BP/1/4506), 6 – *Glanosuchus* (BP/1/6228), 7 – *Tetracynodon darti* (BP/1/4335), 8 – *Tachyglossus.*

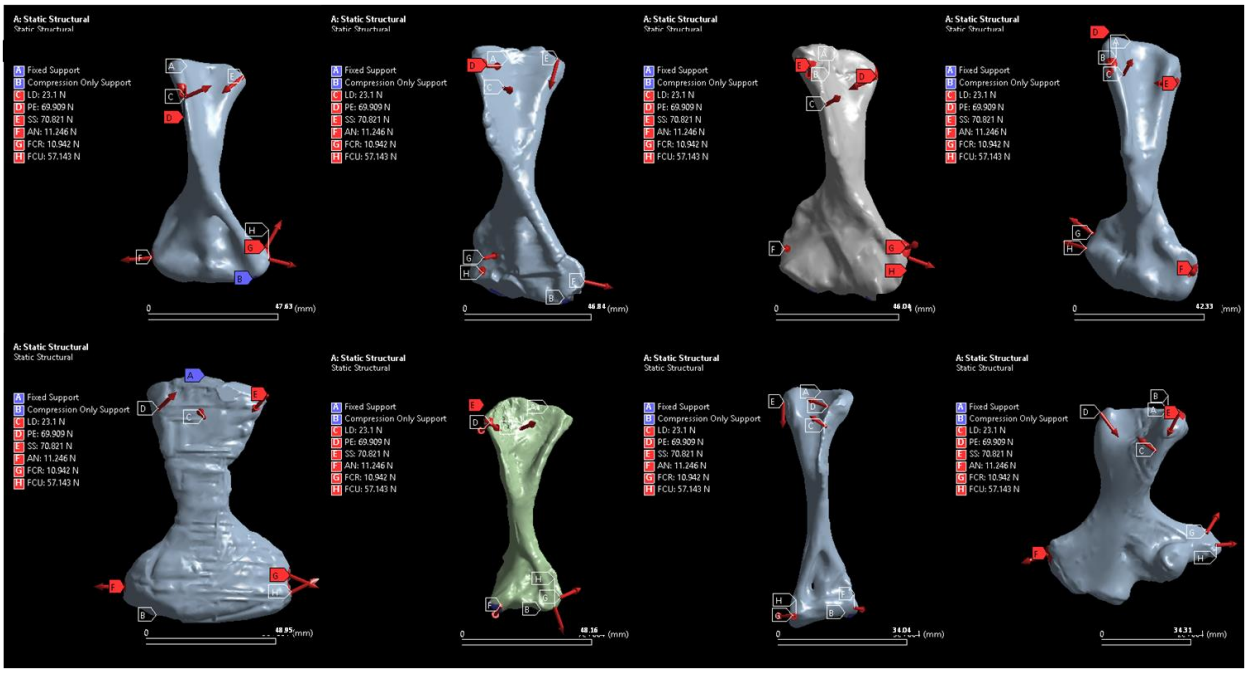


Figure A3: Loading parameters for humeri: 1 – *Thrinaxodon* (BP/1/7199), 2 – *Thrinaxodon* (BP/1/1730), 3 – *Thrinaxodon* (BP/1/1693), 4 – *Cynognathus* (BP/1/1675), 5 – *Galesaurus* (BP/1/4506), 6 – *Glanosuchus* (BP/1/6228), 7 – *Tetracynodon darti* (BP/1/4335), 8 – *Tachyglossus.*

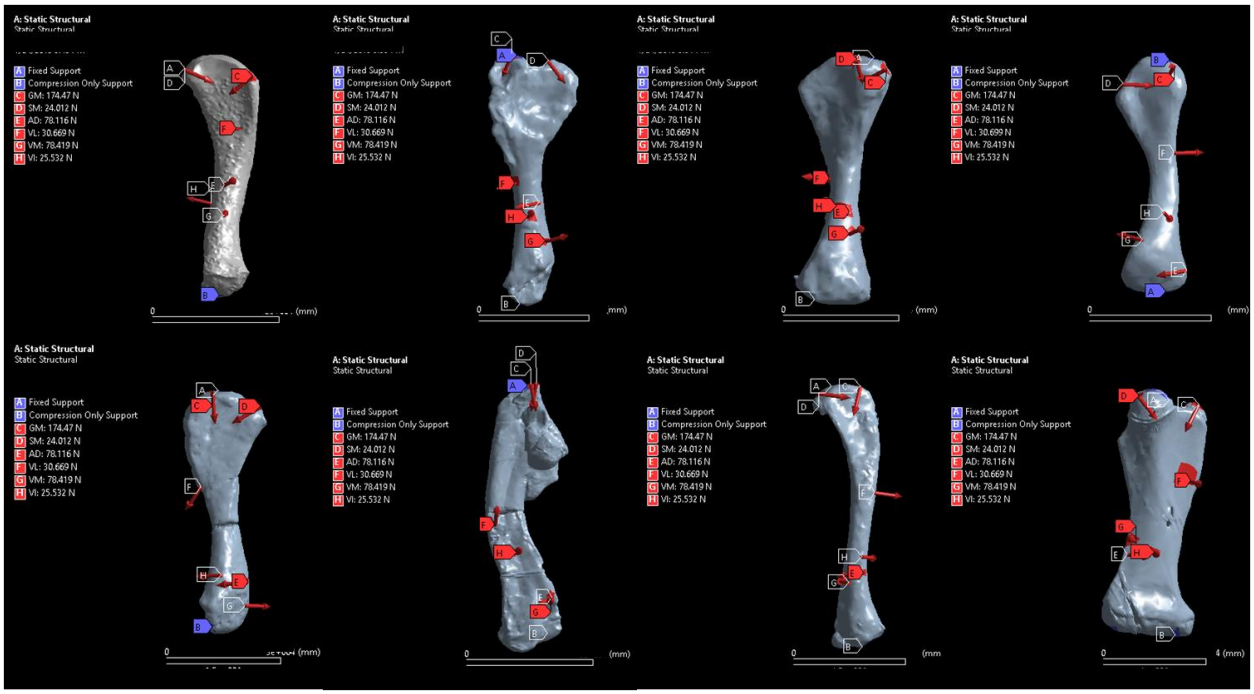


Figure A4: Loading parameters for femora: 1 – *Thrinaxodon* (BP/1/7199), 2 – *Thrinaxodon* (BP/1/1730), 3 – *Thrinaxodon* (BP/1/1693), 4 – *Cynognathus* (BP/1/1675), 5 – *Galesaurus* (BP/1/4506), 6 – *Glanosuchus* (BP/1/6228), 7 – *Tetracynodon darti* (BP/1/4335), 8 – *Tachyglossus.*

Appendix B

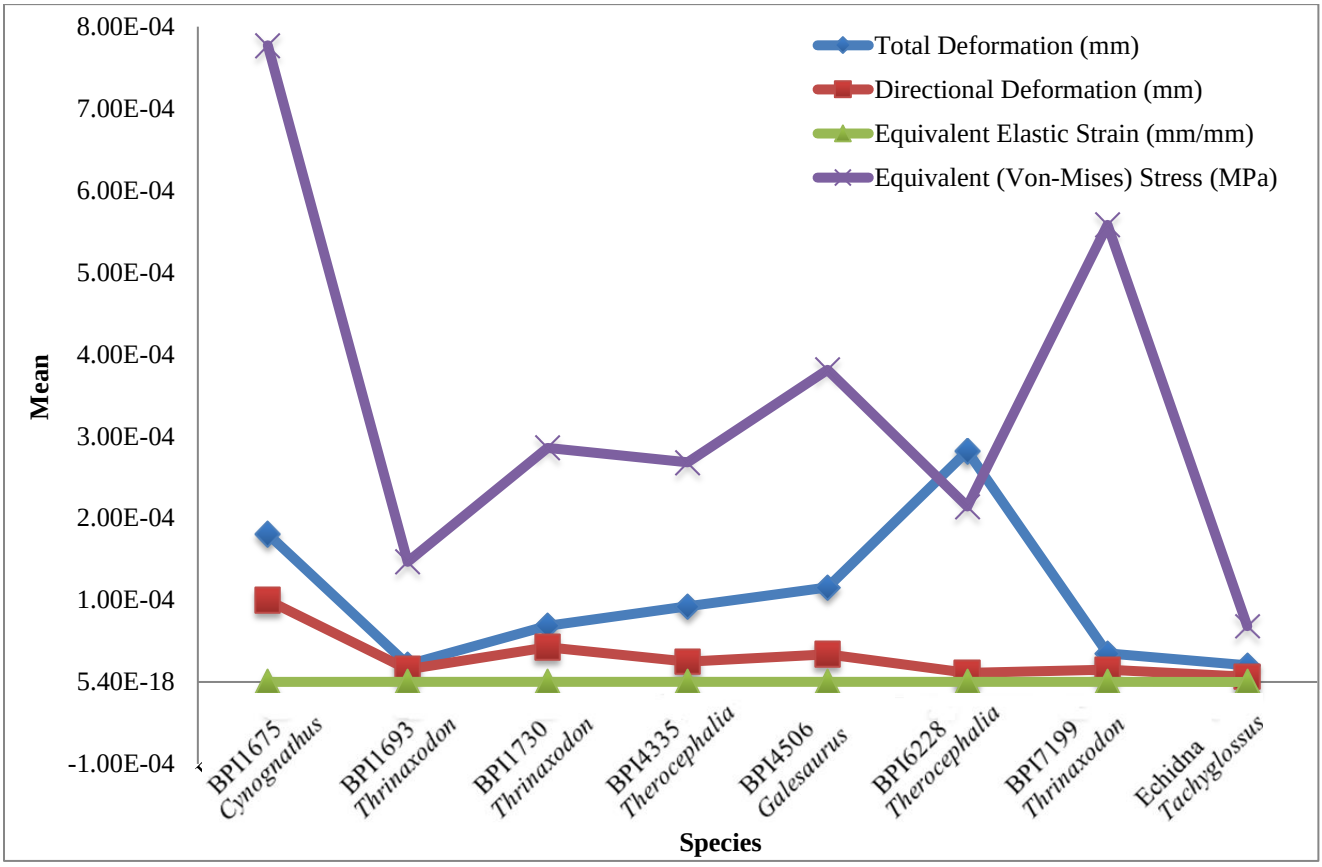


Figure B1: Finite Element Analysis for the comparative taxa humeri for a parasagittal gait.

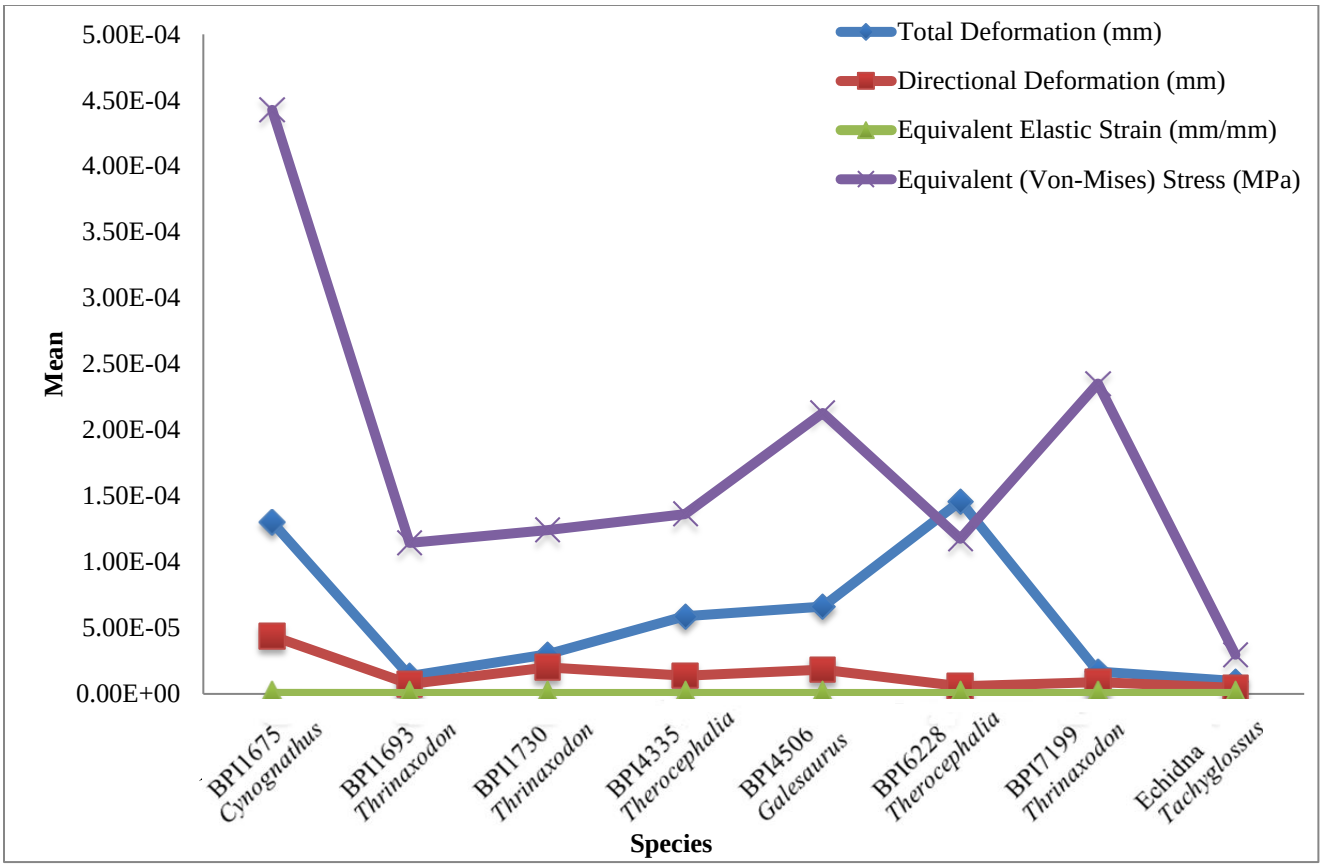


Figure B2: Finite Element Analysis for the comparative taxa humeri for a semi-sprawled gait.

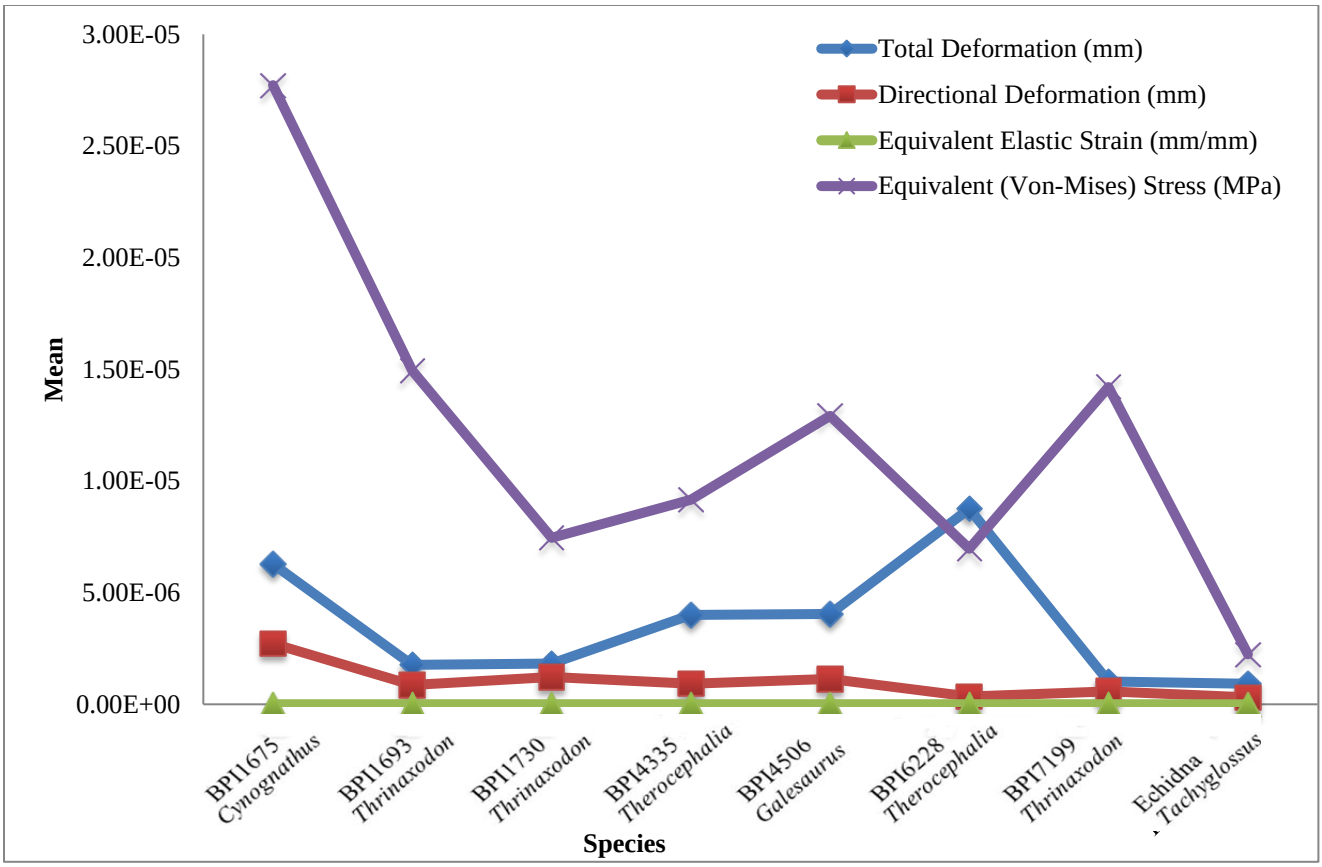


Figure B3: Finite Element Analysis for the comparative taxa humeri for a sprawled gait.

Appendix C

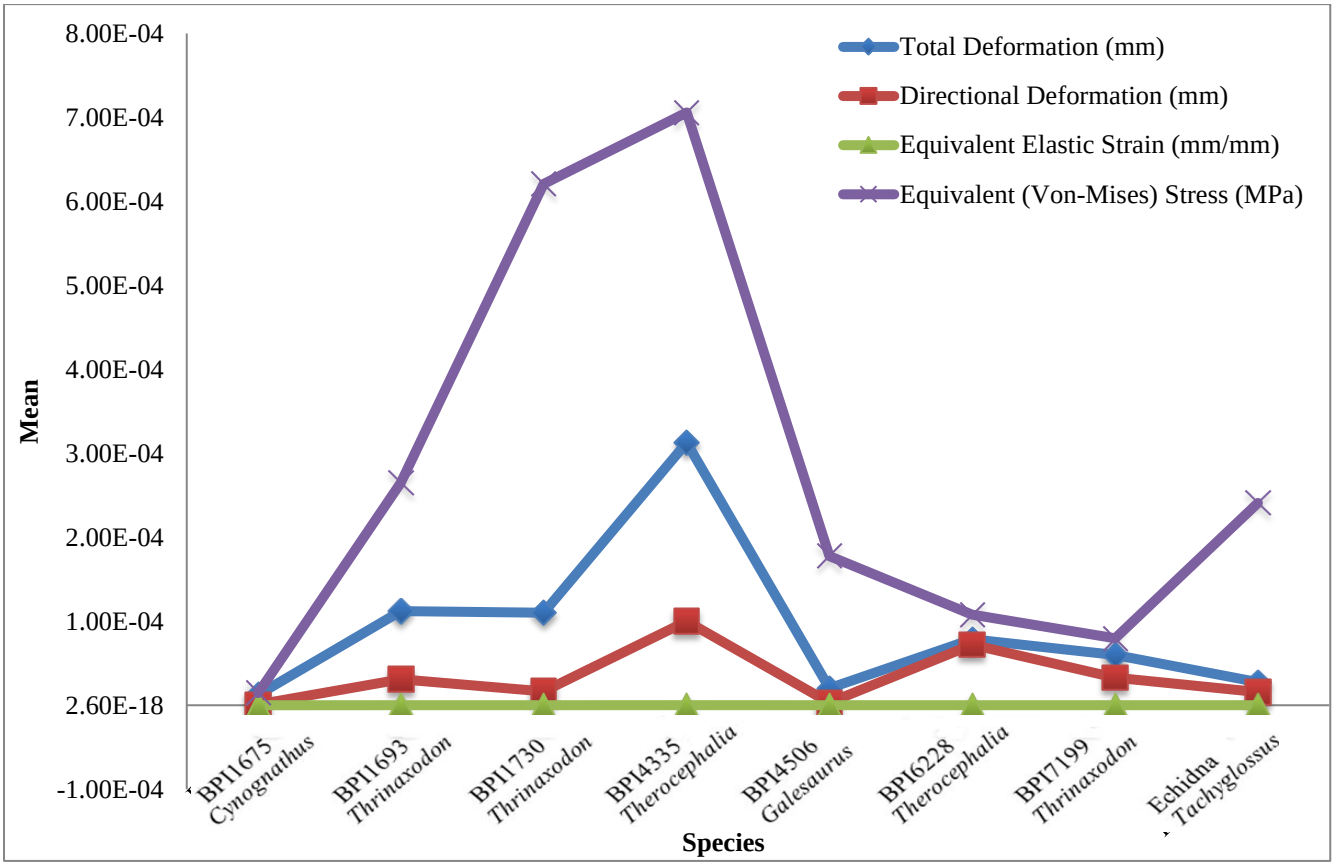


Figure C1: Finite Element Analysis for the comparative taxa femora for a parasagittal gait.

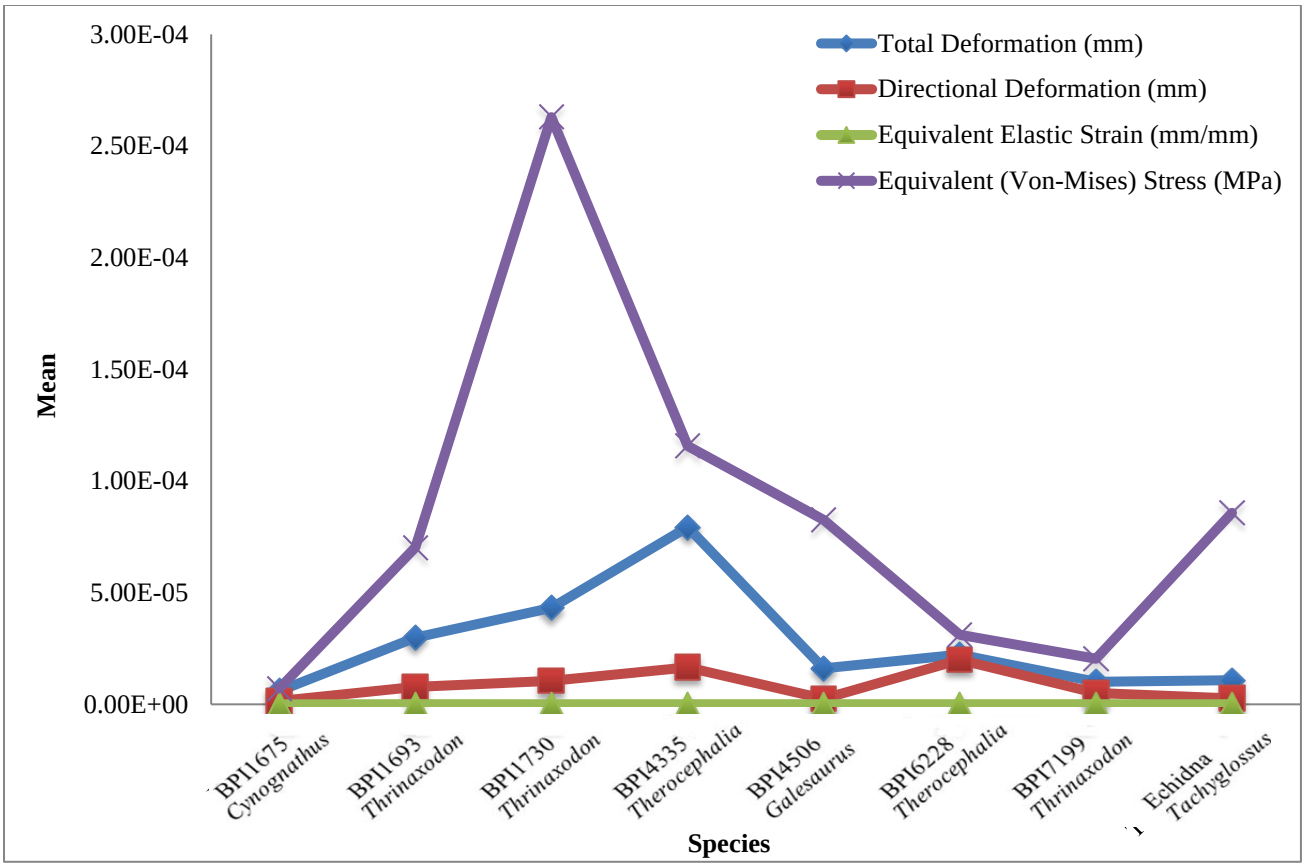


Figure C2: Finite Element Analysis for the comparative taxa femora for a semi-sprawled gait.

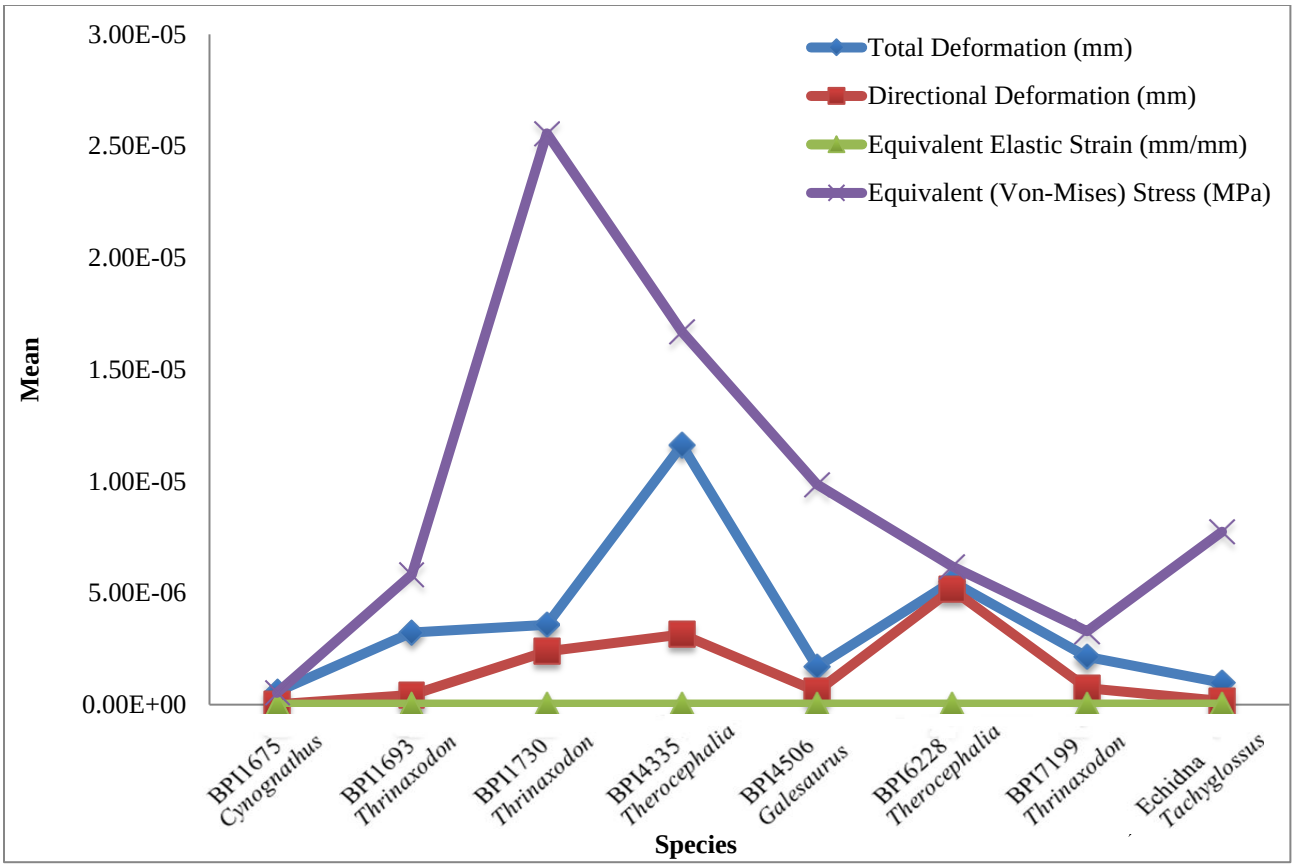


Figure C3: Finite Element Analysis for the comparative taxa femora for a sprawled gait.

Appendix D

Table D1: ANOVA results for parasagittal, semi-sprawled and sprawled gait for each species under investigation.

ANOVA Summary for grouped fossils			
		Humerus	Femur
Bonferroni Correction		0.0167	0.0167
Kruskal-Wallis P-value		<0.0001	0.009
Parameter	Significant Pairwise		
DD	Pa.SS	0.322	0.322
	SS.Sp	0.008*	0.043*
	Pa.Sp	0.000*	0.003*
Kruskal-Wallis P-value		<0.0001	<0.0001
TD	Pa.SS	0.464	0.212
	SS.Sp	0.005*	0.016*
	Pa.Sp	0.000*	0.000*
Kruskal-Wallis P-value		<0.0001	0.000
EES	Pa.SS	0.155	0.228
	SS.Sp	0.014*	0.025*
	Pa.Sp	0.000*	0.001*
Kruskal-Wallis P-value		<0.0001	0.001
ES	Pa.SS	0.168	0.245
	SS.Sp	0.016*	0.028*
	Pa.Sp	0.000*	0.001*

*Statistically significant